Aus dem Institut für Schlaganfall- und Demenzforschung (ISD)

der Ludwig-Maximilians-Universität München

Vorstand: Prof. Dr. Martin Dichgans

MIF proteins and their receptors in atherogenesis:
Structure-activity relationships and novel cellular routes

Dissertation

zum Erwerb des Doktorgrades der Naturwissenschaften (Dr. rer. nat.)

an der Medizinischen Fakultät der

Ludwig-Maximilians-Universität zu München

vorgelegt von

Christine Maria Krammer

aus

München

2021

Mit Genehmigung der Medizinischen Fakultät

der Universität München

Betreuer: Prof. Dr. rer. nat. Jürgen Bernhagen

Zweitgutachterin: Prof. Dr. Dr. Simone Kreth

Dekan: Prof. Dr. med. Thomas Gudermann

Tag der mündlichen Prüfung: 03.11.2021

Affidavit

Krammer, Christine

_____

Name, Vorname

Ich erkläre hiermit an Eides statt, dass ich die vorliegende Dissertation mit dem Titel:

"MIF proteins and their receptors in atherogenesis: Structure-activity relationships and novel cellular routes"

selbständig verfasst, mich außer der angegebenen keiner weiteren Hilfsmittel bedient und alle Erkenntnisse, die aus dem Schrifttum ganz oder annähernd übernommen sind, als solche kenntlich gemacht und nach ihrer Herkunft unter Bezeichnung der Fundstelle einzeln nachgewiesen habe.

Ich erkläre des Weiteren, dass die hier vorgelegte Dissertation nicht in gleicher oder in ähnlicher Form bei einer anderen Stelle zur Erlangung eines akademischen Grades eingereicht wurde.

Holzkirchen, 04.12.2021   Christine Krammer

_____   _____

Ort, Datum   Unterschrift Doktorandin

Table of Contents

Abbreviations

°C	Degree Celsius
μg	Microgram
μM	Micromolar
μm	Micrometer
μl	Microliter
4-IPP	4-iodo-6-phenylpyrimidine
ACK	Atypical chemokine
AIF	Apoptosis-inducing factor
AMPK	AMP-activated protein kinase
APC	Antigen-presenting cell
Apoe	*Apolipoprotein e*
ATLO	Artery tertiary lymphoid organs
ATP	Adenosine triphosphate
BAFF-R	B-cell activating factor receptor
BCA	Brachiocephalic artery
BCR	B-cell receptor
BM	Bone marrow
Breg	Regulatory B cell
BSA	Bovine serum albumin
BTK	Bruton tyrosine kinase
CAA	Coronary artery atherosclerosis
CAD	Coronary artery disease
CD	Cluster of differentiation
cDNA	Complementary DNA
CLP	Common lymphoid progenitor
C-terminal	Carboxy-terminal
CVD	Cardiovascular disease
DC	Dendritic cell
ddH2O	Double-distilled water
D-DT	D-Dopachrome tautomerase
DGE	Differential gene expression
DMR	Dynamic mass redistribution
EC	Endothelial cell
ECL	Extracellular loop
ECM	Extracellular matrix

EDTA	Ethylene diamine tetraacetic acid
EdU	5-Ethynyl-2'-deoxyuridine
e.g.	For example
ERK	Extracellular signal-regulated kinase
FACS	Fluorescence-activated cell sorting
FALC	Fat-associated lymphoid cluster
FDC	Follicular dendritic cell
FOB cell	Follicular B cell
GC	Germinal center
GO	Gene ontology
GPCR	G-protein-coupled receptor
h	Hour
H&E	Hematoxylin and eosin
H-chain	Immunoglobulin heavy chain
HEV	High endothelial venule
HFD	High-fat diet
HIV	Human immunodeficiency virus
HMGB1	High mobility group box protein 1
HRP	Horseradish peroxidase
HSC	Hematopoietic stem cell
ICAM-1	Intercellular adhesion molecule-1
ICL	Intracellular loop
IFN-γ	Interferon-γ
Ig	Immunoglobulin
IHC	Immunohistochemistry
IL	Interleukin
i.p.	Intraperitoneal
IRA	Innate response activator
ISO-1	(S,R)-3-(4-hydroxyphenyl)-4,5-dihydro-5-isoxazole acetic acid methyl ester
JAB1	JUN activation domain-binding protein 1
JNK	c-Jun N-terminal kinase
L-chain	Immunoglobulin light chain
LDL	Low-density lipoprotein
LDLR	Low-density lipoprotein receptor
LN	Lymph node
LPS	Lipopolysaccharide

Lyve-1	Lymphatic vessel endothelial hyaluronic acid receptor
MACS	Magnetic cell separation
MAPK	Mitogen-activated protein kinase
M-CSF	Macrophage colony-stimulating factor
mDC	Monocyte-derived dendritic cell
MFI	Mean fluorescence intensity
mg	Milligram
MHC	Major histocompatibility complex
MI/RI	Myocardial ischemia/reperfusion injury
MIF	Macrophage migration inhibitory factor
min	Minute
ml	Milliliter
mM	Millimolar
mm	Millimeter
MMP	Matrix metalloproteinase
MZB cell	Marginal zone B cell
MZP-B cell	Marginal zone precursor B cell
n	Quantity
Nf-κB	Nuclear factor 'kappa-light-chain-enhancer' of activated B cells
ng	Nanogram
nm	Nanometer
NMR	Nuclear magnetic resonance
Notch2	Neurogenic locus notch homolog protein 2
ns	Non-significant
N-terminal	Amino-terminal
ORO	Oil-red-O
OSE	Oxidation-specific epitopes
oxLDL	Oxidized low-density lipoprotein
PBS	Phosphate-buffered saline
PC	Plasma cell
PFA	Paraformaldehyde
pH	*Potentia hydrogenii*
PI3K	Phosphoinositide 3-kinase
Pnad	Peripheral node addressin
RAG1/2	Recombination-activating enzyme 1/2
RBC	Red blood cell
RNA	Ribonucleic acid

RNAseq	RNA-sequencing
RT	Room temperature
RT-qPCR	Reverse transcription and quantitative real-time PCR
SAR	Structure-activity relationship
scRNAseq	Single cell RNA-sequencing
SD	Standard deviation
SDF-1α	Stromal cell-derived factor-1α
sec	Second
SLE	Systemic lupus erythematosus
SLO	Secondary lymphoid organ
SMC	Smooth muscle cell
SMD	Small molecule drug
T1/2-B	Transitional type 1/2 B cells
t-SNE	t-distributed stochastic neighbor embedding
Th cell	T-helper cell
TNF-α	Tumor necrosis factor-α
Treg	Regulatory T cell
U	Unit
UMAP	Uniform Manifold Approximation and Reduction
VCAM-1	Vascular cell adhesion protein-1
VSMC	Vascular smooth muscle cell
WT	Wild type

List of Figures

Introduction

Appendix A: Publication III

Appendix B: Publication IV

List of Tables

List of Publications

Schindler L, Zwissler L, Krammer C, Hendgen-Cotta U, Rassaf T, Hampton M.B., Dickerhof N, Bernhagen J. Macrophage migration inhibitory factor inhibits neutrophil apoptosis by inducing cytokine release from mononuclear cells. *J Leukoc Biol.* 2021 Feb; online ahead of print.

Kontos C*, El Bounkari O*, Krammer C*, Sinitski D, Hille K, Zan C, Yan G, Wang S, Gao Y, Brandhofer M, Megens RTA, Hoffmann A, Pauli J, Asare Y, Gerra S, Bourilhon P, Leng L, Eckstein HH, Kempf WE, Pelisek J, Gokce O, Maegdefessel L, Bucala R, Dichgans M, Weber C, Kapurniotu A, Bernhagen J. Designed CXCR4 mimic acts as a soluble chemokine receptor that blocks atherogenic inflammation by agonist-specific targeting. *Nat Commun.* 2020 Nov;11(1):5981.

Krammer C, Kontos C, Dewor M, Hille K, Dalla Volta B, El Bounkari O, Taş K, Sinitski D, Brandhofer M, Megens RTA, Weber C, Schultz JR, Bernhagen J, Kapurniotu A. A MIF-derived cyclopeptide that inhibits MIF binding and atherogenic signaling via the chemokine receptor CXCR2. *Chembiochem.* 2020 Oct; online ahead of print.

Sinitski D*, Kontos C*, Krammer C*, Asare Y, Kapurniotu A, Bernhagen J. Macrophage Migration Inhibitory Factor (MIF)-based therapeutic concepts in atherosclerosis and inflammation. *Thromb Haemost.* 2019 Apr;119(4):553-566.

Schmitz C, Noels H, El Bounkari O, Straussfeld E, Megens RTA, Sternkopf M, Alampour-Rajabi S, Krammer C, Tilstam PV, Gerdes N, Bürger C, Kapurniotu A, Bucala R, Jankowski J, Weber C, Bernhagen J. *Mif*-deficiency favors an atheroprotective autoantibody phenotype in atherosclerosis. *FASEB J.* 2018 Aug;32(8):4428-4443.

Lacy M, Kontos C, Brandhofer M, Hille K, Gröning S, Sinitski D, Bourilhon P, Rosenberg E, Krammer C, Thavayogarajah T, Pantouris G, Bakou M, Weber C, Lolis E, Bernhagen J, Kapurniotu A. Identification of an Arg-Leu-Arg tripeptide that contributes to the binding interface between the cytokine MIF and the chemokine receptor CXCR4. *Sci Rep.* 2018 Mar; 8(1):5171.

*Equally contributing first author

1 Introduction

1.1 Epidemiology and risk factors of cardiovascular diseases

Cardiovascular diseases (CVDs) are the most common cause of death representing up to 30% of the global mortality[1,2]. The term CVD is used to describe a group of pathologies affecting the heart, the vasculature or the brain, which becomes apparent in diseases, such as ischemic heart disease, cerebrovascular disease, hypertensive heart disease and others[2]. Among those, acute myocardial infarction and stroke account for most of the CVD-related deaths. Aging and growing populations, as well as lifestyle changes and different risk factors, such as hypertension, smoking, unhealthy diets, alcohol and hyper-lipidemia have been resulting in an increasing number of lethal CVD cases[3-5].

1.2 Atherosclerosis

Atherosclerosis is a chronic inflammatory condition of medium size and large arterial blood vessels and is therefore one of the major drivers of CVDs. Most commonly, atherosclerosis develops progressively over several years involving the infiltration of immune cells and deposition of low-density lipoprotein (LDL) cholesterol inside the vessel wall resulting in plaque formation and decreased luminal volume of the artery. This can contribute to reduced blood flow and plaque rupture might eventually lead to thrombus formation[6,7]. A cascade of inflammatory events has been associated with atherogenesis, which involves lesion initiation and progresses until clinical manifestation[8-11].

1.2.1 Initiation and early phases of atherogenesis

Plaque formation is initiated by spontaneous or induced injury of the endothelium resulting in endothelial dysfunction and enhanced permeability for LDL cholesterol[10]. Consequently, lipids infiltrate the intima, where they are oxidized by enzymes or reactive oxygen species leading to the generation of oxidized LDL (oxLDL). In turn, oxLDL activates endothelial cells (ECs) and leads to the upregulation of chemokines and adhesion molecules, like vascular cell adhesion protein (VCAM)-1 or intracellular cell adhesion molecule (ICAM)-1, promoting the recruitment, adhesion and arterial infiltration of monocytes and T cells. Following endothelial transmigration, macrophage colony-stimulating factor (M-CSF) induces the differentiation of monocytes into macrophages that internalize ox-LDL and form macrophage foam cells (Figure 1)[9,11]. The uptake of oxLDL is mediated by pattern recognition receptors (PRRs), which serve as scavenger receptors for oxLDL,

indicating a role of innate immune functions in atherogenesis[12]. Additionally, infiltrated monocytes and activated T cells produce cytokines and other atherogenic and inflammatory factors that amplify inflammation and contribute to disease progression[8,9]. These early lesions consisting of macrophage-derived foam cells, T cells and accumulated LDL particles are also known as fatty streaks[8].
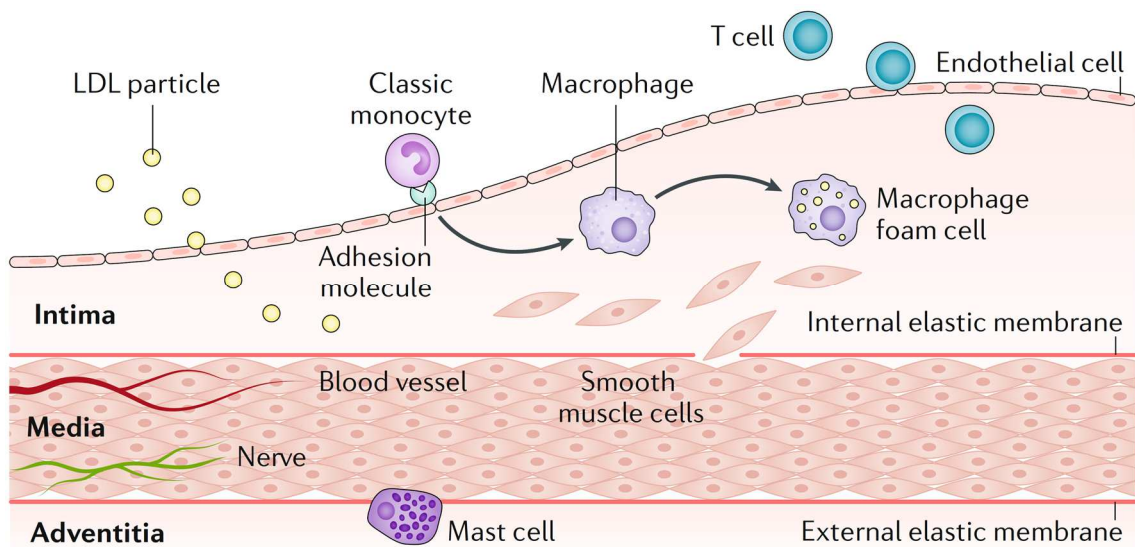
Figure 1: Initiation and early phases of atherogenesis. The layered structure of a healthy blood vessel is composed of the intima, the media and the adventitia. The development of an atherosclerotic lesion in the arterial intima is initiated by endothelial dysfunction and develops progressively involving different processes including the endothelial transmigration of immune cells, such as monocytes and T cells. Inside the intima, monocyte differentiation into macrophages is followed by the engulfment of oxidized low-density lipoprotein (oxLDL) particles leading to foam cell formation. Additionally, smooth muscle cells (SMCs) that reside in the media migrate into the intima contributing to the formation of fatty streaks. Figure from Libby et *al.*, *Nat Rev Dis Primers*, 2019[7].

1.2.2 Disease progression and clinical manifestation

During disease progression, the plaque is getting more complex and develops into an advanced atheroma with dying foam cells and cellular debris constituting a lipid-rich necrotic core. Smooth muscle cells (SMCs) mediate the synthesis of collagen, a extracellular matrix (ECM) constituent, leading to the construction of a fibrous cap overlaying the necrotic core (Figure 2)[9]. The stability of the plaque correlates with the thickness and composition of the fibrous cap[13]. Also the volume and lipid content of the necrotic core has been linked to plaque stability[14]. While vulnerable plaques with sparse ECM/collagen content and prominent cholesterol accumulations are prone to rupture, plaques with a high ECM volume and meager lipid deposition are considered as stable[15]. The proliferation and migration of SMCs into the intima, as well as the rate of the SMC collagen synthesis are main factors contributing to fibrous cap thickening[16].
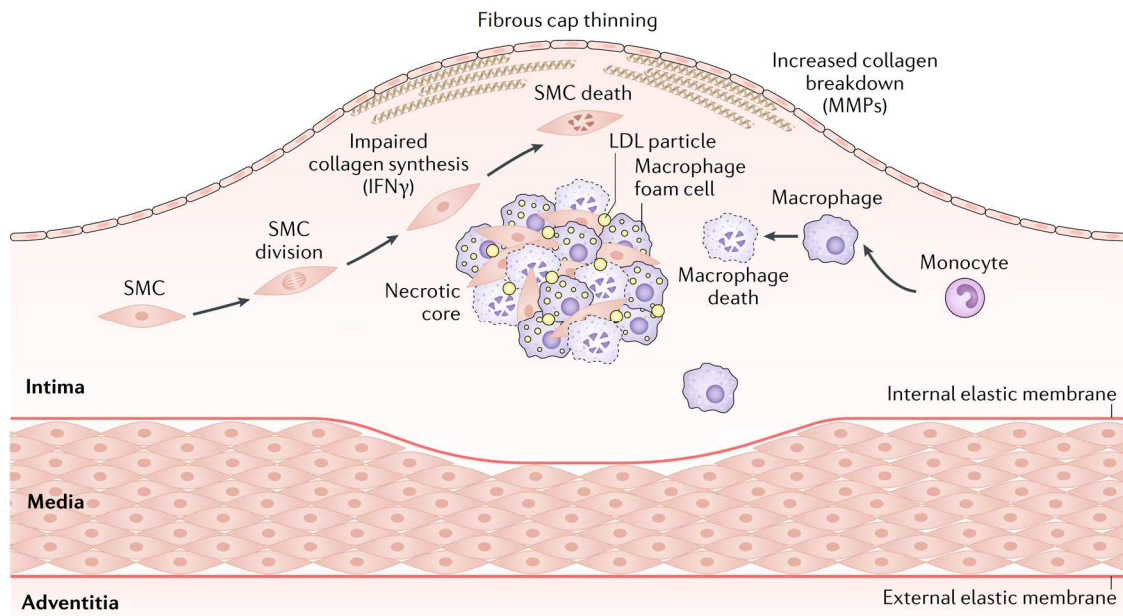
Figure 2: Progression of atherosclerosis and formation of advanced lesions. Progressive inflammation in the intima leads to the formation of an advanced atheroma characterized by a necrotic core comprised of lipids and dying foam cells. The necrotic core is encompassed by a smooth muscle cell (SMC)- and collagen-containing fibrous cap. The expression of matrix metalloproteinases (MMPs) and interferon (IFN)-γ contributes to the destabilization of the fibrous cap. Figure adapted from Libby et *al., Nat Rev Dis Primers,* 2019[7].

ECM-degrading matrix metalloproteinases (MMPs) expressed by mast cells and macrophages residing predominately in the shoulder regions of the plaque contribute to a more rupture-prone phenotype[17,18]. Plaque vulnerability is aggravated by the expression of inflammatory cytokines, such as interferon (IFN)-γ, which inhibit SMC proliferation and collagen production[19]. Eventually, these processes mediate plaque rupture and thrombus formation resulting in clinical manifestations (Figure 3)[8].
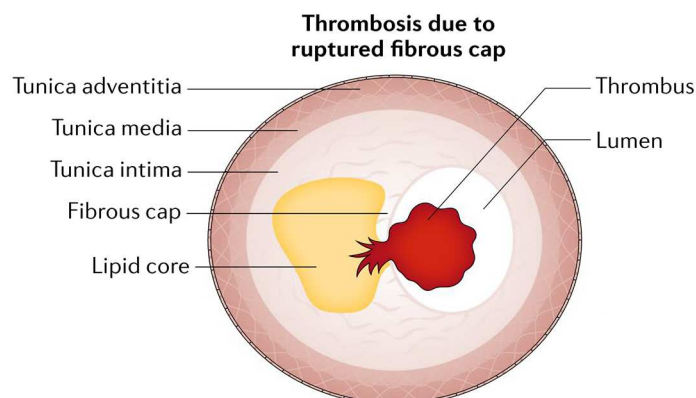
Figure 3: Schematic overview of a ruptured plaque. Atherosclerotic lesions form inside the intima, the inner layer of a blood vessel. Vulnerable plaques with sparse collagen content are prone to break, leading to thrombus formation. This might result in the occlusion of an artery clinically manifesting in cardiovascular events including myocardial infarction or stroke. Figure adapted from Libby et *al.*, Nat Rev Dis Primers, 2019[7].

In addition, the emerging "plaque-erosion" concept has been discussed in the context of atherosclerosis and coronary thrombosis. In contrast to plaque rupture, plaque erosion mainly affects lesions characterized by high SMC and ECM content as well as sparse lipid accumulation. However, the underlying mechanisms are less well understood[20].

1.2.3 Immune cells in the atherosclerotic lesion

Different immune cell subsets executing diverse biological functions have been identified in the atherosclerotic plaque, including mainly macrophages and T cells, but also mast cells and dendritic cells (DCs) (Figure 4)[21]. The lesional macrophage population is divided into pro-atherogenic M1 and anti-atherogenic M2 macrophages, whereat the M1 subset producing pro-inflammatory cytokines, such as interleukin (IL)-6 and tumor necrosis factor (TNF)-α, has been shown to predominate in the shoulder region of the plaque[22]. However, recent advances in single cell RNA sequencing (scRNAseq) and cytometry by time-of-flight mass spectrometry analysis revealed deeper insights to the cellular complexity of murine and human plaques[23-25]. Several macrophage subpopulations with either atheroprotective or atheroprogressive functions have been described in murine aortic lesions[26,27]. For example, Cochain et *al.* detected three distinct macrophage subsets including adventitial resident-like macrophages, pro-inflammatory and anti-inflammatory Trem2-expressing macrophages adding further complexity to the classical M1/2 classification of macrophages[26]. Trem2-expressing macrophages are lipid-laden foamy cells that have been shown to reside in the intima and necrotic core of diseased vessels and are characterized by plaque-resolving functions[27,28]. Anti-inflammatory macrophages with transcriptomic features of foam cells have been also identified in human carotid artery plaques[24]. Of note, foam cells are classically regarded as pro-inflammatory based on the secretion of inflammatory cytokines and chemokines promoting inflammation and disease progression[29]. Various additional subsets have been described, suggesting a vast heterogeneity of human plaque macrophages that affect atherogenesis by diverse pro- or anti-inflammatory mechanisms[23,24]. Similar to macrophages, several T-cell populations including pro-atherogenic CD4^{+} type 1 T-helper (Th) cells, anti-atherogenic regulatory T cells (Tregs) and additional T-helper cell subpopulations, such as Th2 or Th17, reside in the plaque. However, pro-inflammatory Th1-mediated immune responses involving the expression of IFN-γ or TNF-α seem to predominate within the plaque[30]. Also cytotoxic CD8^{+} T cells inhabit murine lesions and have been associated with plaque vulnerability[31]. All the above-mentioned T-cell subsets in murine lesions have been also associated with human atherosclerotic plaques[24]. Mast cells are under-represented in the plaque, but they are discussed in the context of plaque rupture and might

contribute to atherogenesis by the secretion of TNF-α[32]. In contrast to T cells and macrophages, the existence of neutrophils and B cells in atherosclerotic lesions is limited and their function in atherosclerosis is less well understood[33,34].
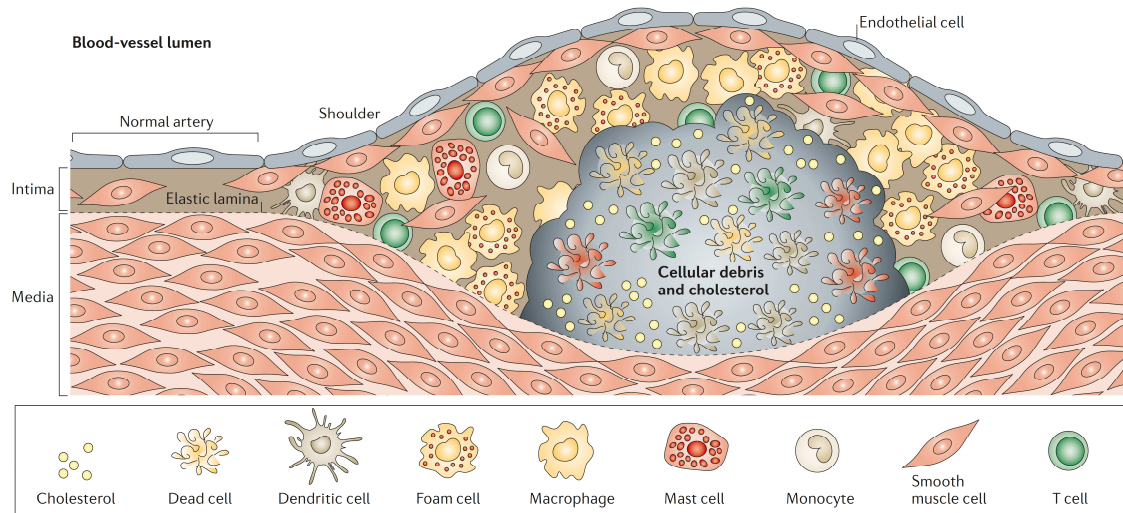
Figure 4: Immune cell infiltrates of atherosclerotic lesions. Different cells of the immune system including T cells, monocytes/macrophages, dendritic cells and mast cells have been identified in atherosclerotic plaques contributing to disease progression. Dying immune cells and lipid deposits constitute the necrotic core of the plaque. Figure from Hansson and Libby, *Nat Rev Immunol,* 2006[12].

1.3   B cells in atherosclerosis

1.3.1 Functional diversity of B1- and B2-cell subsets

The association of B cells and atherosclerosis has gained more attention in the last 8-10 years. Originally, B cells were related to protective roles in atherogenesis. Accordingly, splenectomized *Apoe*^{−/−} mice were shown to display enhanced lesion formation compared to control animals, a phenotype which was reversed by the adoptive transfer of B cells but not T cells. B-cell transplantation also reduced CD4^{+} T-helper cell numbers in atherosclerotic lesions indicating that B cells indirectly affect atherogenesis[35]. Similarly, protective roles for B cells were uncovered in irradiated low-density lipoprotein receptor (*Ldlr)*[−/−] mice after bone marrow (BM) reconstitution[36]. At the same time, other studies investigating the effects of B-cell depletion in atherogenic mouse models revealed pro-atherogenic roles of B cells[37,38]. These divergent results suggest that different B-cell subsets with opposite roles in atherogenesis exist. Indeed, two subsets, namely B1 and B2 cells, with distinct functional features were subsequently described in mice[39,40].

B2 cells are the conventional B-cell subpopulation residing in secondary lymphoid organs (SLOs), like lymph nodes or spleen, and can be further divided into marginal zone (MZB) and follicular (FOB) B cells. FOB cells home to splenic follicles and are also found in the

circulation, whereas MZB cells solely inhabit the splenic marginal zone[41]. Activated MZB cells produce natural IgM antibodies recognizing blood-borne antigens[42]. In humans, IgM-producing memory B cells with characteristics of MZB cells have been identified. These MZB-like cells represent up to 40% of the peripheral B cell pool and are characterized by distinct features compared to the classical memory B cells[43]. FOB cells contribute to germinal center (GC) reactions including immunoglobulin (Ig) class-switching and affinity maturation in lymph nodes and spleen, thereby creating high-affinity antibodies of five isotypes, including IgM, IgD, IgG, IgA and IgE. These processes give rise to long-lived antibody-producing plasma or memory B cells providing an accelerated immune response upon antigen-mediated re-activation[39,40]. Besides, short-lived antibody-producing plasmablasts are generated in a splenic extrafollicular response producing antibodies with a lower affinity compared to plasma cell-derived antibodies as they lack affinity maturation[44].

In contrast to B2 cells, murine B1 cells are rare in SLOs accounting only for up to 5% of the splenic B-cell pool, but they prevail in pleural and peritoneal cavities (40-60% of total B cells)[45]. Based on the expression of CD5, different B1 subpopulations, namely B1a and B1b cells, have been classified[39]. B1 cells have self-renewing capacities and produce polyreactive, low-affinity IgM antibodies, thereby protecting against diverse antigens[42,46]. Cells with similar characteristics as murine B1 cells have been described to exist in human blood and the umbilical cord[47].

1.3.2 Early B-cell maturation in the bone marrow (BM)

B-cell development occurs in the BM and is a complex process including numerous maturation steps that give rise to a highly diverse antibody-producing B-cell repertoire (Figure 5). Immune checkpoints tightly control the developmental cascade at different stages in order to ensure immune homeostasis and to avoid the generation of autoreactive B cells. These processes have been comprehensively discussed in several articles and reviews[48-52]. B cells arise from hematopoietic stem cells (HSCs) that differentiate into early lymphoid progenitors and further into IL-7 receptor (IL-7R)-expressing common lymphoid progenitors. These progenitor cells in turn generate different lymphoid cell lineages in the BM[53]. B-cell fate commitment and development is driven by the regulated expression of transcription factors including Ebf1, PU.1 and Pax5[54]. Different rearrangement events of the Ig heavy chain (H-chain) genes mediated by recombination-activating enzymes (Rag1/2) lead to the formation of the pre-B-cell receptor (pre-BCR), which accompanies the generation of pre-B-cells[51,55]. The proper assembly and signaling through

the pre-BCR is critical for the progression of the B-cell developmental cascade. Accordingly, binding of antigens via the pre-BCR leads to a positive selection and further differentiation[52,56]. After the genes of the Ig light chain (L-chain) have been successfully rearranged, the H-chain combines with the L-chain generating the B-cell receptor (BCR). The functional BCR of immature B cells consists of an IgM isotype and an intracellular domain, while upon further maturation an additional IgD isotype appears on the cell surface[57]. Self-reactive immature B cells that bind self-antigens via their BCR undergo clonal deletion through apoptosis or alternatively adjust the arrangement of the H-chain and L-chain by receptor editing. Thus, the correct assembly of the BCR serves as another important checkpoint in B-cell development[50,52]. After passing the manifold checkpoints and selection steps in the BM, only about 25% of the generated B cells survive and leave the BM for their final maturation in the spleen[52]. During B-cell development in the BM, proliferation and differentiation are mainly controlled by IL-7R- and pre-BCR signaling[48,51]. In this context, the BM microenvironment plays a crucial role as it provides distinct cytokines and chemokines that are needed for the respective developmental program. Early-stage B cells developing from HSCs are found next to the sinusoidal endothelium[58,59]. The endothelium is surrounded by CXCL12-abundant reticular cells, the main producers of local stromal cell-derived factor-1α (SDF-1α)/CXCL12 that serves as a crucial niche factor for the maintenance of HSCs in the BM[59,60], but also signals to pre–pro-B cells[59]. Pro-B cells develop in proximity to IL-7-expressing stromal cells. IL-7R signaling mediates proliferative and survival pathways and blocks differentiation by the downregulation of RAG1/2[51,61]. IL-7R-mediated proliferation is enhanced in large pre-B cells by pre-BCR-mediated signaling. However, an inhibitory loop mediates the reduction of pre-BCR constituents expressed on the cell membrane dampening proliferation and promoting differentiation at the small pre-B-cell stage[62]. In addition, upregulation of CXCR4 is suggested to mediate the migration to CXCL12-rich niches, where the cells evade proliferative signals and exit the cell cycle[63].

1.3.3 Final B-cell maturation in SLOs

During the developmental cascade and prior to the final maturation in the spleen, immature B cells pass a transitional stage. Via the blood stream, these so-called transitional B cells migrate from the BM into SLOs, where they further differentiate into fully mature B cells (Figure 5). Two different transitional B-cell subpopulations (T1-B and T2-B cells) were identified in the spleen. The survival of T1-B cell is regulated by B-cell activating factor receptor (BAFF-R) signaling[64] and gives rise to T2-B cells, which show enhanced potential to develop into a mature B cell[65]. Cell fate determination is controlled by BCR

signaling and several additional signaling pathways involving neurogenic locus notch homolog protein 2 (Notch2), nuclear factor 'kappa-light-chain-enhancer' of activated B-cells (NF-κB) and Bruton tyrosine kinase (BTK)[66]. Strong BCR signaling leading to the induction of BTK has been associated with the development of FOB cells, while weak BCR signaling mediates MZB-cell development[66]. Two distinct FOB-cell populations (FO1-B and FO2-B cells) have been identified. While antigen-mediated BCR and BTK signaling is indispensable for the development of FO1-B cells, it seems negligible for FO2-B-cell maturation[67].
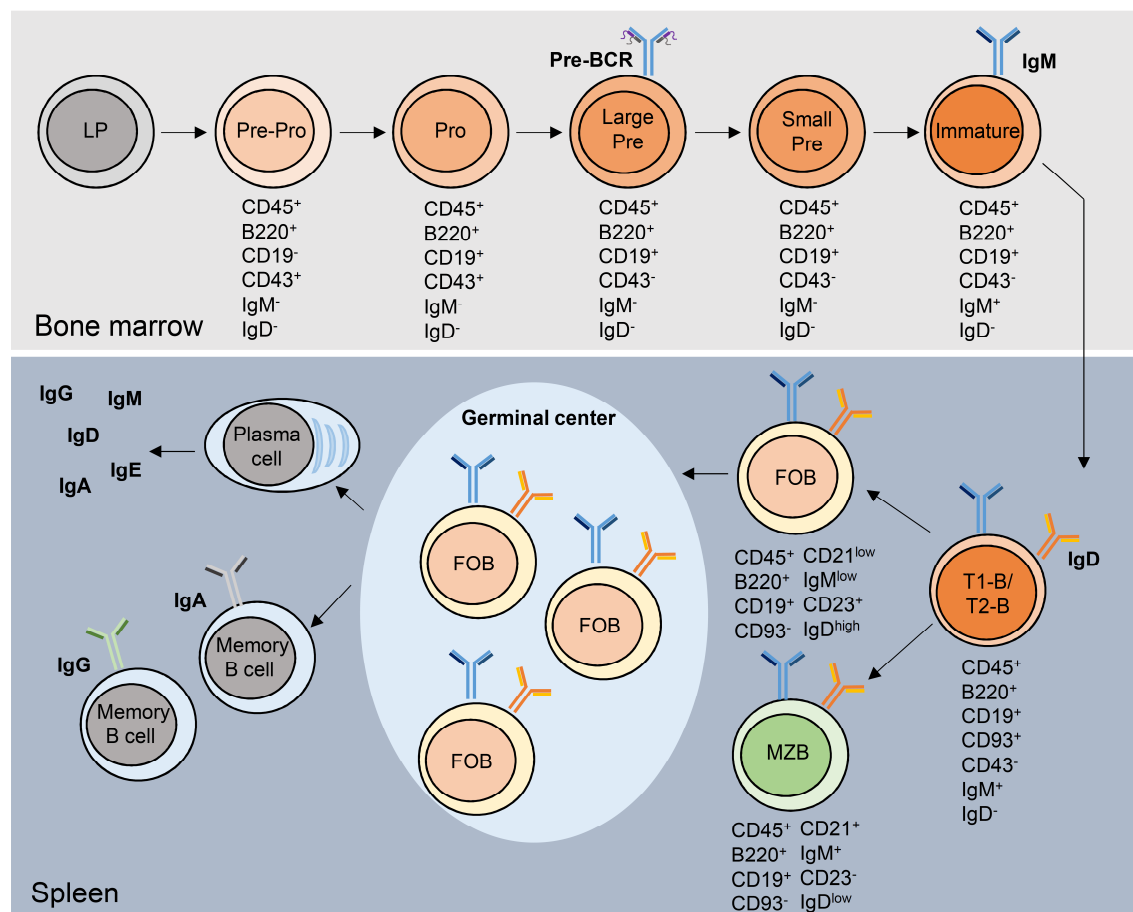
Figure 5: Schematic overview of the B-cell developmental cascade in the bone marrow (BM) and spleen. B cells arise from lymphoid progenitors (LPs) in the BM over several stages including pre–pro-, pro-, large and small pre- as well as immature B cells. Ig rearrangements mediated by recombination-activating enzymes (Rag1/2) of the immunoglobulin heavy chain (H-chain) lead to the formation of a pre-B-cell receptor (pre-BCR) expressed at the surface of large pre-B cells. Further rearrangements of the immunoglobulin light chain (L-chain) and combination with the H-chain generate the BCR expressed by immature B cells, which emigrate from the BM. In the spleen, transitional B cells (T1-B and T2-B) give rise to follicular (FOB) or marginal zone (MZB) B cells. FOB cells contribute to germinal center (GC) reactions resulting in plasma cells and memory B cells producing a heterogeneous repertoire of antibodies. Specific cell surface markers of the individual developmental stages are indicated. Figure designed as a modified version from Pieper et al., *J Allergy Clin Immunol*, 2013[49].

1.3.4 B-cell-mediated humoral immune responses in atherosclerosis

The characteristic feature of B cells is the secretion of antibodies with either protective or exacerbating roles in atherogenesis (Figure 6). While B cells are rare in the atherosclerotic lesion, they have been shown to reside in the adventitia of the abdominal aorta and brachiocephalic artery (BCA)[68,69]. B1 and B2 cells including FOB and MZB cells, as well as plasma cells infiltrate the adventitia, where they form large antibody pools that can enter the plaque[39]. Different Ig functions have been described in the context of atherosclerosis dependent on the respective isotype. For example, IgG has been attributed pro-atherogenic functions by forming immune complexes with oxLDL that promote macrophage activation by Fcγ-receptor interactions[70,71]. IgG has been also shown to be involved in SMC proliferation, thereby regulating size and vulnerability of atherosclerotic lesions[72]. Similarly, IgE is described as a pro-atherogenic antibody as it binds to the IgE receptor FcεRI mediating the activation of macrophages and mast cells[70]. In contrast, IgM binds to oxidation-specific epitopes (OSE), for example on oxLDL, or apoptotic cells in the necrotic core. Thereby, natural IgM reduces foam cell formation, neutralizes additional oxLDL-mediated activities and mediates clearance of apoptotic cells[70]. The role of IgA in disease development is still unclear[39].

FOB cells give rise to a diverse antibody repertoire including IgG, IgA and IgE isotypes. Thus, FOB cells have been associated with atheroprogression[70]. MZB cells mainly produce natural IgM antibodies, but also IgG3 has been shown to be generated[73]. In contrast to FOB cells, recent evidence suggests that MZB cells mediate atheroprotective functions by suppressing the T follicular helper response[74]. B1 B cells are a major source of natural IgM and IgA antibodies[70,71]. Kyaw et *al.* revealed the B1a B-cell subset to protect against atherosclerosis, while the role of B1b cells has long been elusive[75]. However, it was shown lately that, similarly to the B1a subset, B1b cells secrete natural oxLDL-specific IgM and mediate atheroprotection in adoptive transfer experiments[76]. A third B cell population comprising innate response activator (IRA)-B cells represents another player in atherosclerosis with disease-exacerbating roles mediated by the activation of IFN-γ-producing Th1 cells and by triggering the generation of pro-inflammatory Ly6C^{high} monocytes[77,78]. In comparison, the role of regulatory B cells (Bregs) is suggested to be atheroprotective via secretion of IL-10[79].
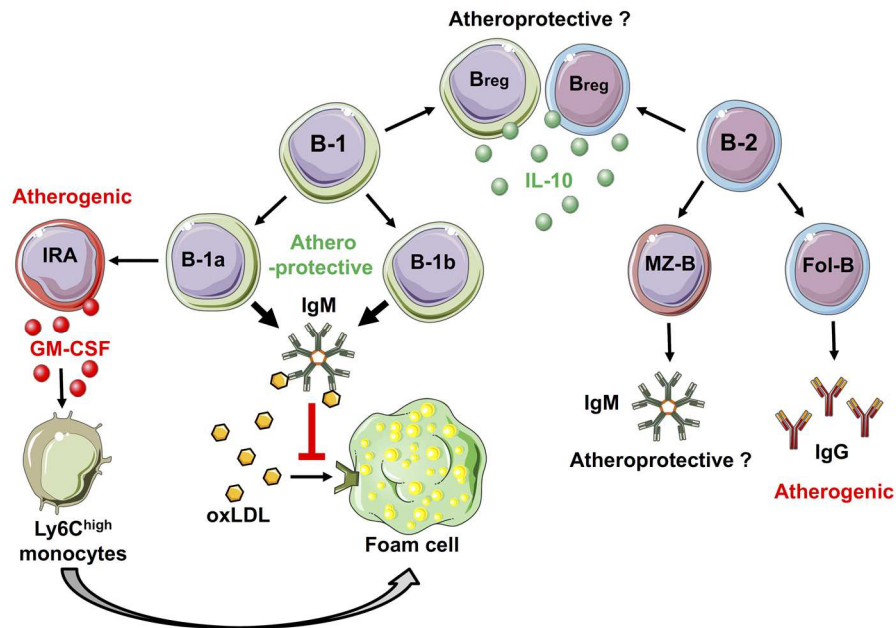
Figure 6: Overview of different murine B-cell subsets involved in immune responses during atherogenesis. B1 cells are associated with atheroprotection by the secretion of natural oxidized low-density lipoprotein (oxLDL)-specific IgM that inhibits foam cell formation. Similarly, marginal zone (MZB) B cells produce IgM and are suggested to be atheroprotective. In contrast, follicular (FOB) B cells produce atheroprogressive IgG antibodies. Additional B-cell subsets involved in atherosclerosis are atherogenic innate response activator (IRA)-B cells and regulatory B cells (Bregs) secreting interleukin (IL)-10. GM-CSF: granulocyte macrophage-colony stimulating factor. Figure from Srikakulapu and McNamara, *Am J Physiol Heart Circ Physiol,* 2017 [40].

In aged *Apoe*^{−/−} mice, B cells have been shown to assemble in artery tertiary lymphoid organs (ATLOs) (Figure 7)[80,81]. ATLOs are lymphoid structures that are formed upon chronic inflammation in the adventitia nearby the developing atherosclerotic lesion orchestrating diverse immune functions. The architecture of ATLOs is well organized comprising distinct T-cell areas, DCs, plasma cell niches and B-cell zones comprising GCs and follicular dendritic cells (FDCs) [81,82]. The existence of GCs suggests the *de novo* development of plasma cells and memory B cells within the ATLO. Additionally, B1 cells, FOB cells and transitional B cells have been identified[83]. Besides, ATLOs are preferential sites of neoangiogenesis and lymphangiogenesis as well as for the formation of high endothelial venules (HEVs) and conduit networks[81]. ATLO-formation is a stepwise process: Stage 1 is characterized by T- and B-cell infiltration mediated by chemokines including CXCL13 and CCL21. At stage 2, infiltrated immune cells organize into separated areas and lymph vessels together with conduit-like structures are formed. Further maturation leads to stage 3 ATLOs that are complex and harbor GCs[82]. Yet, a clear-cut atheroprotective or atheroprogressive role of ATLOs in atherogenesis has not been defined.

ATLO Media Plaque

T Cell Area

B Cell Follicle

Plasma Cell Niche

M1 Macrophage | M2 Macrophage | SMC | T Cell | Treg
cDC | mDC | B Cell | Centrocyte | FDC | Reticular Fibroblast
Plasma Cell | Mantle B Cell | Tissue Macrophage | HEV | Adipocyte
Endothelial Cell | Blood Vessel | Conduit | Lymph Vessel
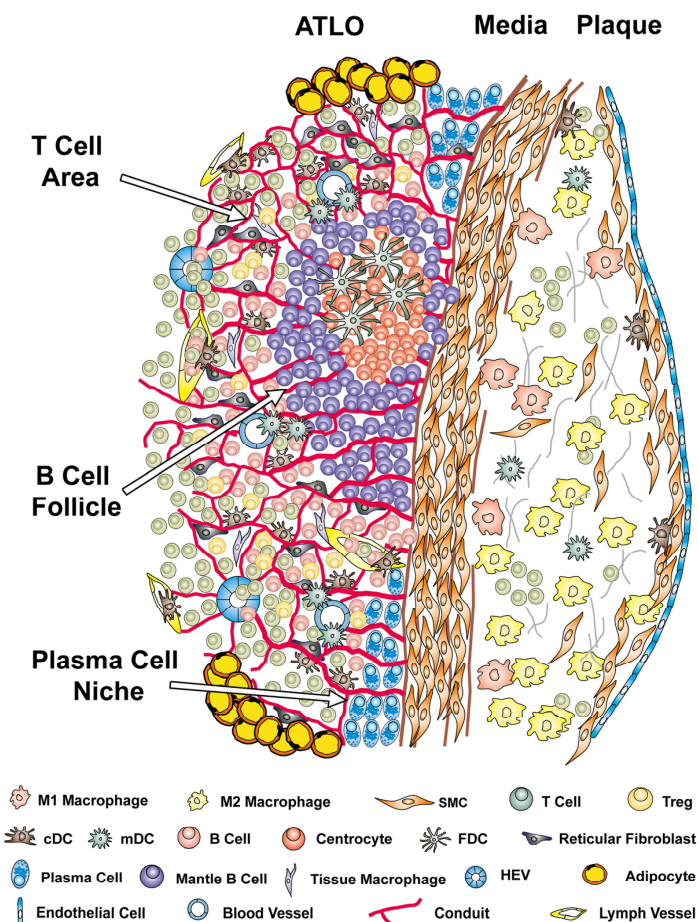
Figure 7: Complexity of artery tertiary lymphoid organs (ATLOs). ATLOs are lymphoid structures in the adventitia nearby the atherosclerotic lesion mediating diverse immune responses during atherosclerosis. A hallmark of ATLOs is the existence of separated T- and B-cell zones as well as plasma cell-rich areas. Diverse additional immune cells as well as conduits, blood and lymph vessels contribute to the complexity of the aggregate. SMC: smooth muscle cell; Treg: regulatory T cell; cDC: conventional dendritic cell; mDC: monocyte-derived DC; FDC: follicular dendritic cell; HEV: high endothelial venule. Figure from Mohanta, Yin et *al.*, *Circ Res,* 2014[81].

The existence of ATLOs in human artery adventitial tissue is still indefinite. However, B-cell-rich cellular aggregates, which contribute to humoral immunity and correlate with lesion formation as well as severity of atherosclerosis-related diseases, have been identified in the adventitia of diseased coronary arteries and aortas [84,85].

1.4 Intervention options in atherosclerosis and cardiovascular diseases

Therapeutic concepts developed to treat atherosclerosis and related CVDs mainly focus on reducing risk factors. One example are lipid-lowering medications like statins that reduce the levels of pro-atherogenic LDL-cholesterol. Additionally, statins lower superoxide levels and reduce the susceptibility of LDL against oxidation[86]. However, the ben-

efits of statins are controversially discussed and side effects, including myopathy or muscle pain, might overweigh the beneficial effects[87,88]. Moreover, statin therapies fail to address the inflammatory aspects of disease development. Despite reduced lipid-levels, individuals might not benefit from the treatment and might remain at high risk of cardiovascular events, which is also known as "residual inflammatory risk"[89]. Accordingly, a clinical study, namely the CANTOS trail, emphasized the role of inflammation in atherosclerosis and showed that treatment with Canakimumab, an anti-IL-1β antibody, reduces the risk for cardiovascular diseases without affecting lipid levels[90]. However, atherosclerosis treatment with Canakimumab has not been approved by the Food and Drug Administration.

Additional strategies for primary prevention include anti-hypertensive and anti-platelet strategies[91]. Secondary prevention strategies involve β-adrenergic blockers and aspirin[92,93]. Besides pharmacological treatment, lifestyle changes are crucial for lowering the disease risk[91]. However, none of the mentioned treatment options is able to reverse the clinical manifestations of atherosclerosis. An improved knowledge of the inflammatory pathways implicated in atherosclerosis development can be of great benefit for the improvement of treatment options and the identification of novel targets. As B2 cells have recently been described as drivers of atherosclerosis, they might represent an attractive target for therapeutic intervention. Existing B-cell depletion strategies focus on the reduction of atheroprogressive B2 cells mostly by monoclonal antibodies directed against the surface protein CD20. In mouse models, this strategy has been shown to reduce atherosclerotic burden, but clinical studies are missing so far[38,94].

1.5 Chemokines in atherosclerosis

1.5.1 Classes and functions of classical chemokines and chemokine receptors

Chemokines have been attributed major functions in atherogenesis and other inflammatory diseases. The classification of chemokines into C-, CC-, CXC- and CX$_3$C-chemokines is owing to the amount and position of *N*-terminal cysteine-residues. Dependent on the existence of the ELR (Glu-Leu-Arg)-motif located *N*-terminal to the conserved cysteine, CXC-chemokines are divided into ELR-positive and ELR-negative chemokines[95]. The common characteristic of all chemokines is their chemoattractant properties, which for example mediate leukocyte recruitment and arrest. Constitutively expressed chemokines are important in developmental and homeostatic cell migration processes, while the expression of inflammatory chemokines is triggered by infectious and inflammatory processes leading to the recruitment of immune cells to damaged and inflamed

tissue[96]. All chemokines share a conserved 3D-structure, described as the *chemokine-fold*, comprising the *N*-terminal N-loop, the 3_{10} helix, a three-stranded anti-parallel β-sheet and an α-helix at the *C*-terminus[97]. Chemokines mediate their functions by binding to chemokine receptors representing a subgroup of G protein-coupled receptors (GPCRs). The structural elucidation of chemokine receptors is difficult. However, as an example, the structure of CXCR4 was successfully solved via X-ray crystallography in association with a virus-derived chemokine analogue or cyclic peptide antagonists[98,99]. Chemokine receptors consist of an extracellular *N*-domain, 7-transmembrane spanning helices, three extracellular loops (ECL), three intracellular loops (ICL) and an intracellular *C*-domain[100]. The nomenclature of the receptors is based on the chemokine subclass that interacts with the receptor[95]. Signaling via chemokine receptors is facilitated by G-proteins consisting of an α-, β- and γ-subunit. Upon ligand/receptor engagement, the G-protein trimer separates into a G_α-monomer and a $G_{\beta\gamma}$-dimer that activate different signaling cascades[101].

1.5.2 Promiscuity of the chemokine/receptor

Currently, approximately 50 chemokines and 20 chemokine receptors have been identified. Chemokine receptors are often bound by multiple chemokines of a certain subclass, while many chemokines are able to recognize more than one receptor indicating high promiscuity and redundancy in the chemokine/receptor network. In contrast, some chemokine receptors are specific for a particular ligand (Figure 8)[102]. Binding of chemokines to their receptors requires two binding sites. Site 1 contains the receptor *N*-domain and the chemokine N-loop, while site 2 involves *N*-terminal residues of the chemokine and receptor ECLs as well as a portion of the transmembrane binding cavity. Site 1 and site 2 affect binding affinity, selectivity and receptor activation in a distinct manner, with site 1 being involved in binding affinity and selectivity and site 2 playing a role in binding affinity and receptor activation. It is suggested that both sites are not independent, but may enable ligand binding in a sequential manner, with chemokine binding to site 1 inducing conformational changes in the receptor that in turn mediate site 2 interaction[100]. Additionally, chemokines as well as their receptors can form homo- and hetero-oligomers that might affect binding characteristics and signaling properties[103].
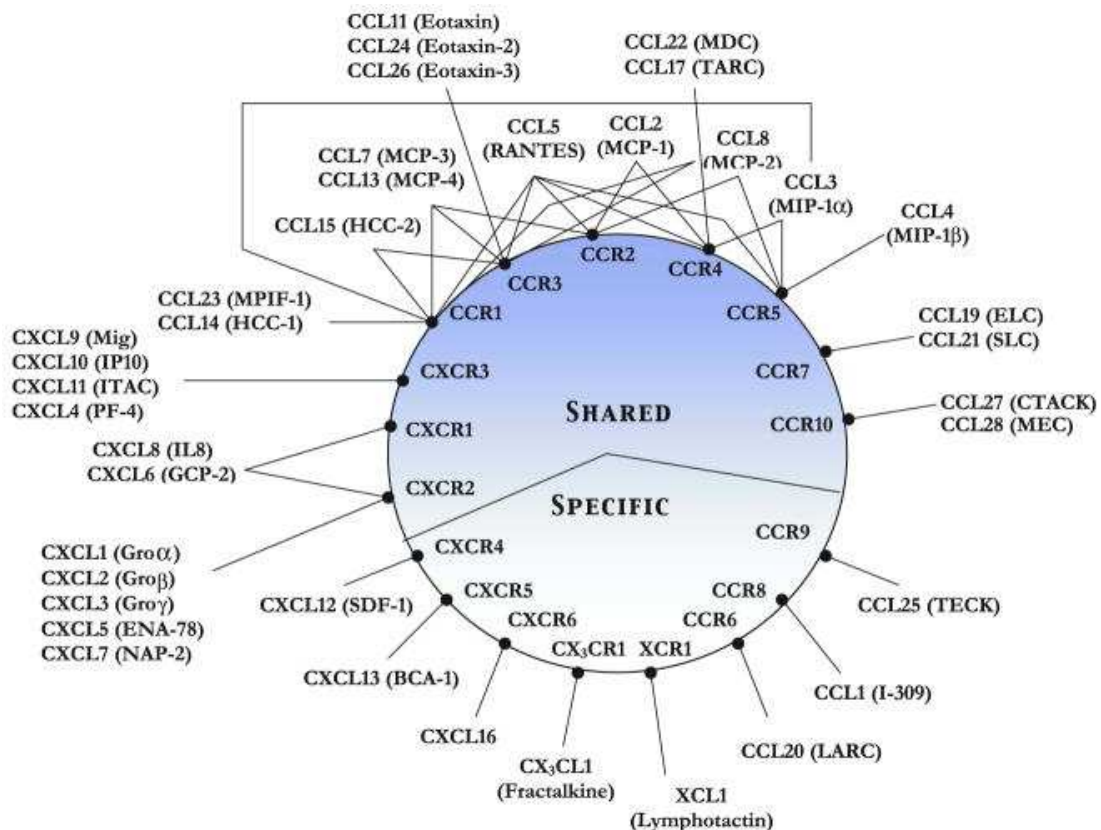
Figure 8: Promiscuity of the chemokine/chemokine receptor network. Classical chemokines include C-, CC-, CXC- and CX3C-chemokines and they mediate signaling by binding to chemokine receptors. While some chemokines bind several chemokine receptors, others are restricted to a certain receptor. At the same time, chemokine receptors can be used by several chemokines (shared), while others are highly specific, suggesting a high degree of redundancy and promiscuity in the chemokine/receptor network. Figure from Rajagopalan and Rajarathnam, *Biosci Rep,* 2006 [100]

1.5.3 Atherogenic cell recruitment is mediated by chemokines

Expressed by different cell types including SMCs, ECs and leukocytes chemokines play fundamental roles in atherogenesis as they are inducing the directed migration of immune cells towards the developing lesion. The functions of chemokines and their receptors in atherogenic cell recruitment are complex and in part controversially discussed[104-106]. For example, it has been shown that the chemokine receptors CCR2, CX3CR1 and CCR5 are involved in monocyte recruitment[107]. However, this data has been revised revealing that CCR5 and CCR1 are responsible for monocyte infiltration into the developing lesion[108], while CX3CR1 plays a role in monocyte survival[109]. Additionally, the CXCL1-CXCR2 axis has been associated with monocyte and neutrophil mobilization and recruitment to the vascular endothelium covering the developing lesion[110,111]. Even if neutrophils are rare in atherosclerotic lesions, they have been implicated in disease pathology recently. Thus, blockade of the CXCL12-CXCR4 axis mediated the egress of

neutrophils from the BM and the recruitment to the atherosclerotic lesion leading to enhanced lesion formation and plaque instability, suggesting a protective role for the CXCL12-CXCR4 axis in atherosclerosis[112]. At the same time, CXCL12 has been linked to platelet aggregation during thrombus formation[113].

1.5.4 Atypical chemokines

The identification of atypical chemokines (ACKs) has added further complexity to the chemokine/receptor network in atherosclerosis. ACKs are not considered as members of the well-known chemokine subclasses owing to the absence of the typical cysteine motif at the protein *N*-terminus. Unlike classical chemokines, ACKs have been attributed *bona fide* intracellular functions in addition to their extracellular, receptor-mediated functions. ACKs function as non-cognate ligands of classical chemokine receptors, thereby inducing the migration of immune cells[114]. Thus, this class of proteins is also referred to as chemokine-like function cytokines including alarmins, like high mobility group protein 1 (HMGB1), human β-defensins, aminoacyl-t-RNA synthetases and macrophage migration inhibitory factor (MIF), the latter described in more detail below (see 1.6)[114-117].

1.6   Macrophage migration inhibitory factor (MIF)

1.6.1 Structure and biological functions of MIF

MIF was identified over 50 years ago as a soluble factor in the supernatant of lymphocytes inhibiting macrophage migration during tuberculin-induced delayed-type hypersensitivity[118,119]. Today, MIF is described as a pleiotropic pro-inflammatory cytokine and is classified as an ACK. Mouse and human MIF share about 90% sequence identity and contain 114 amino acids with a molecular weight of 12.345 kDa[120]. The MIF monomer features high structural similarity to the CXCL8 dimer including two antiparallel α-helices, and a four-stranded β-sheet. Additional structural features of MIF are the N-like loop and the pseudo-(E)LR motif (Asp44-X-Arg11)[121]. In addition to the monomer, MIF forms dimers and trimers as revealed by nuclear magnetic resonance and X-ray analysis (Figure 9)[122,123]. Complex formation in the trimer involves two accessory β-strands connecting different monomers[121]. However, the oligomerization state of the active MIF is still elusive. Cross-linking analysis revealed that all MIF oligomers are present in solution with a preference of the monomeric and dimeric state[124]. At the same time, recent findings suggest that MIF might lead to receptor activation as a trimer[125].
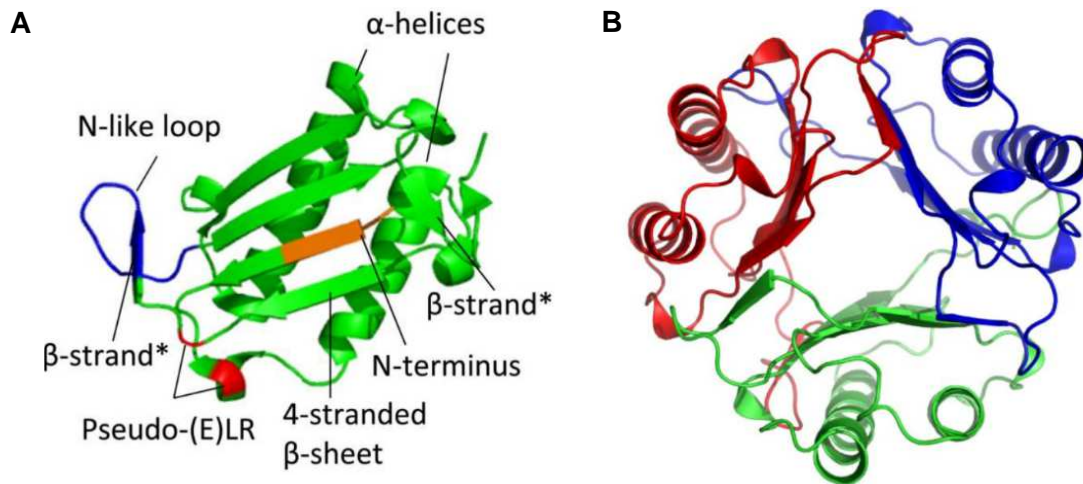
Figure 9: Crystal structure of the monomeric and trimeric state of MIF. A) The MIF monomer contains two anti-parallel α-helices and a four-stranded β-sheet together with two additional β-strands that are involved in oligomerization. Important structural moieties including the *N*-terminus (orange), the N-like loop (blue) and the pseudo-(E)LR motif (red) are highlighted. Figure from Pawig, Klasen et *al.*, *Front Immunol*, 2015[121]. **B)** Crystal structure of the MIF trimer (subunits are indicated by different colors). Figure from Merk et *al.*, *Cytokine,* 2012[126].

Unlike classical pro-inflammatory chemokines, MIF is constitutively expressed by immune cells, ECs and SMCs, where it is stored in intracellular pools[127-129]. The stimulation with different inflammatory stressors like lipopolysaccharide (LPS), hypoxia or oxLDL triggers the secretion of MIF. As a typical signaling peptide that mediates the release of MIF is structurally missing, it is exported by an alternative pathway that is independent from the endoplasmic reticulum but depends on an ATP-binding cassette transporter[130]. Once secreted, MIF exerts its functions by receptor binding. Different MIF receptors including CXCR2, CXCR4, CXCR7 and CD74 have been identified, through which MIF mediates the activation of signaling cascades involving extracellular signal-regulated kinase (ERK)/mitogen-activated protein kinase (MAPK) or phosphoinositide 3-kinase (PI3K)/AKT, and promotes the recruitment and arrest of immune cells (see 1.6.3)[131]. Moreover, MIF triggers the secretion of cytokines, chemokines and adhesion molecules, thereby further enhancing cell recruitment[132]. Besides immune cells, endothelial progenitor cells and tumor cells are recruited owing to the chemotactic properties of MIF[133,134].

In addition, MIF has been shown to mediate intracellular functions through interaction with different molecules, such as JUN-activation domain-binding protein 1 (JAB1)/CSN5, the subunit 5 of the COP9 signalosome. Thereby MIF inhibits JAB1-mediated activities and affects cell-cycle regulation by JAB1[135]. MIF was also attributed a nuclease function that is dependent on the release of apoptosis inducing factor (AIF) guiding MIF to the

nucleus[136]. Additionally, MIF displays enzymatic activity as an oxidoreductase and tautomerase[137,138]. The CALC (Cys57-Ala-Leu-Cys60) motif of MIF has been associated with its oxidoreductase activity contributing to redox homeostasis[139], while the tautomerase activity depends on the *N*-terminal proline (Pro-1)[140]. As a tautomerase, MIF mediates the conversion of D-dopachrome and 4-hydroxyphenyl pyruvate[138]. However, a physiological substrate has not been identified yet.

D-dopachrome tautomerase (D-DT/MIF-2) is a structural homologue of MIF, which can be classified into the MIF protein family. MIF-2 and MIF share some functions including the tautomerase activity mediated by Pro-1 and the induction of ERK-MAPK signaling. However, MIF-2 lacks other characteristic structural elements of MIF such as the CALC or pseudo-(E)LR motif[141].

1.6.2 Role of MIF in atherosclerosis and related cardiovascular diseases

Dysregulated expression of MIF has been linked to different pathophysiological conditions, like cancer and inflammatory conditions including sepsis, rheumatoid arthritis and atherosclerosis[142-146]. MIF is strongly expressed in human atherosclerotic plaques and enhanced peripheral amounts of MIF have been determined in coronary artery disease (CAD) patients[147,148]. Moreover, CATT-repeat polymorphisms in the MIF promotor affect the severity of carotid artery atherosclerosis (CAA) in ischemic stroke patients. The amounts of CATT-repeats (5, 6, 7, or 8 CATT-repeats) decide upon the separation of patients into MIF-low and -high expressors with (CATT)5 and (CATT)6 carriers displaying lowest basal MIF levels[149].

Antibody-mediated blockade and genetic deletion of MIF in various atherogenic mouse models including *Apoe*$^{-/-}$ and *Ldlr*$^{-/-}$ mice have revealed that MIF is a pivotal driver of atherosclerosis[150-153]. MIF is involved in atherosclerotic disease development and progression by different mechanisms. For example, it drives the expression of adhesion molecules and the production of diverse pro-inflammatory cytokines including TNF-α or IL-1β[154,155]. Moreover, MIF triggers the uptake of oxLDL by macrophages leading to enhanced foam cell formation[156] and mediates the expression of MMPs, thereby contributing to plaque destabilization[157]. Via non-cognate engagement with chemokine receptors CXCR2 and CXCR4, MIF recruits immune cells into the developing lesion, thereby amplifying inflammatory responses[145].

1.6.3 Complexity of the MIF/receptor network in atherosclerosis

The first MIF receptor that was identified is CD74, previously described as the invariant chain of major histocompatibility complex (MHC) class II, a chaperon facilitating antigen presentation via MHC class II[158]. Signal transduction is mediated only in complex with additional molecules as CD74 is lacking respective signaling modalities. MIF binding to CD74 in complex with CD44 has been shown to activate ERK-MAPK and PI3K/AKT pathways resulting in cell proliferation and survival[159,160]. Besides, MIF signaling via the CD74/CD44 complex is associated with AMP-activating protein kinase (AMPK) activation and phase-dependent cardioprotection during myocardial ischemia/reperfusion injury (MI/RI) (Figure 10)[161]. CD74 also forms complexes with chemokine receptors CXCR2 or CXCR4. For example, MIF activates the c-Jun *N*-terminal kinase (JNK)-MAPK pathway via the CD74-CXCR4 axis leading to the upregulation of the pro-inflammatory chemokine CXCL8[162].

As mentioned before (see 1.6.2), MIF's pro-atherogenic effects are mediated through engagement with the chemokine receptors CXCR2 and CXCR4 triggering the recruitment of monocytes/neutrophils and T cells, respectively (Figure 10)[145]. CD74 was also implicated in monocyte recruitment based on its ability to form complexes with CXCR2[145]. The network gets even more complex when considering the functions mediated by the cognate ligands of CXCR2/4. Binding of IL-8 (CXCL8) to CXCR2 has been shown to induce endothelial cell migration and neovascularization and is thus implicated in angiogenesis an important process during vascular development, inflammation and cancer progression[163,164]. The role of the CXCL12-CXCR4 signaling cascade is diverse and has been associated with atheroprotective and homeostatic functions. Atheroprotective functions of this axis are mainly mediated by controlling neutrophil mobilization and infiltration into the plaque[112]. Besides, CXCL12 has been shown to contribute to plaque stability by promoting SMC-chemotaxis[165]. Additionally, the CXCL12-CXCR4 axis induces anti-apoptotic pathways in cardiomyocytes during MI/RI, suggesting a role in cardioprotection[166]. Moreover, CXCL12 binding to CXCR4 promotes vascular integrity and endothelial barrier function accompanied by the maintenance of the contractile vascular smooth muscle cell (VSMC) phenotype[167]. More recently, CXCR7 has been described as a fourth MIF receptor[168]. As CXCR7 is not associated with G-proteins it has been believed that CXCR7 solely acts as a scavenger receptor. However, CXCR7 was shown to mediate signaling via β-arrestin leading to MAPK activation and migration of VSMCs *in vitro*[169]. Recent findings demonstrate that MIF binding to CXCR7 initiates receptor internalization, ERK activation as well as B-cell migration (Figure 10)[170].

If and how MIF-2 interacts with chemokine receptors is still elusive and needs further investigation. As MIF-2 does not feature a pseudo-(E)LR motif, which is involved in the binding of MIF to CXCR2, it is likely that MIF-2 interacts with CXCR4 but not with CXCR2. Until now, CD74 is the only receptor that has been described for MIF-2 (Figure 10)[141].
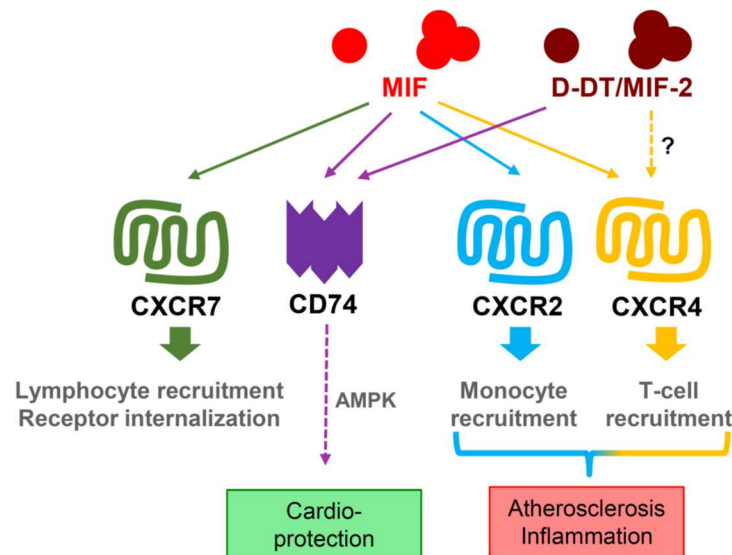
Figure 10: Complexity of the MIF ligand/receptor network in atherosclerosis. MIF is binding and signaling through different receptors including CD74 promoting cardioprotection via AMP-activating protein kinase (AMPK) and chemokine receptors CXCR2/4 mediating atherogenic immune cell recruitment. Besides, MIF binds to CXCR7, which has been associated with B-cell recruitment and receptor internalization. D-DT/MIF-2, a member of the MIF protein family and structural homologue of MIF, also signals through CD74 but potential interactions with classical chemokine receptors have not been verified. Figure designed based on Alampour-Rajabi and El Bounkari et *al.*, *FASEB J*, 2015[170]; Bernhagen et *al.*, *Nat Med*, 2007[161]; Miller et *al.*, *Nature*, 2008[145], Merk et *al.*, *Cytokine*, 2012[126].

1.6.4 Structural moieties of the interaction interfaces between MIF and chemokine receptors CXCR2/4

MIF engages chemokine receptors CXCR2 and CXCR4 involving two interaction sites, similarly to classical chemokines (see 1.5.2). For example, the cognate ligand CXCL8 binds to CXCR2 involving an *N*-terminal loop (site 1) and the ELR motif (Glu3-Leu4-Arg5) (site 2). The MIF monomer shares structural similarities with the CXCL8 dimer including the pseudo-(E)LR motif with an identical arrangement in MIF's 3D structure compared to the ELR motif in CXCL8. This motif is not only necessary for MIF function but has been shown to be directly involved in the interaction with CXCR2[171,172]. In the two-site binding model the pseudo-(E)LR motif interacts with parts of ECL2 and ECL3 (residues 286-290) of CXCR2 constituting site 2 interaction. Site 1 interaction involves the MIF N-like loop (residues 47-56) and the receptor *N*-domain (residues 19-33) as well as ECL1 (residues 108-120) and parts of ECL2 (residues 184-198) (Figure 11a)[173]. More recently, efforts

have been made to also elucidate the structural elements of the MIF/CXCR4 interface[174,175]. Rajasekaran et *al.*[175] uncovered a large region in MIF, termed extended N-like loop comprising residues 43 to 98, to be involved in the interaction with *N*-terminal segments of CXCR4 (residues 1-27). Peptide arrays showed strongest interaction of CXCR4 with peptide MIF(67-81). Additionally, the *N*-terminal Pro-1 residue was suggested to be an important residue within MIF involved in site 1 binding[174,175]. Structure-activity studies provided further insights into the binding interface revealing the RLR motif (Arg87-Leu88-Arg89) as a crucial determinant of site 1 interaction (Figure 11b)[174]. Structural elements involved in site 2 interaction of MIF and CXCR4 include parts of ECL1 and ECL2, whilst ECL3 seems not to be contributing to the interaction[175].
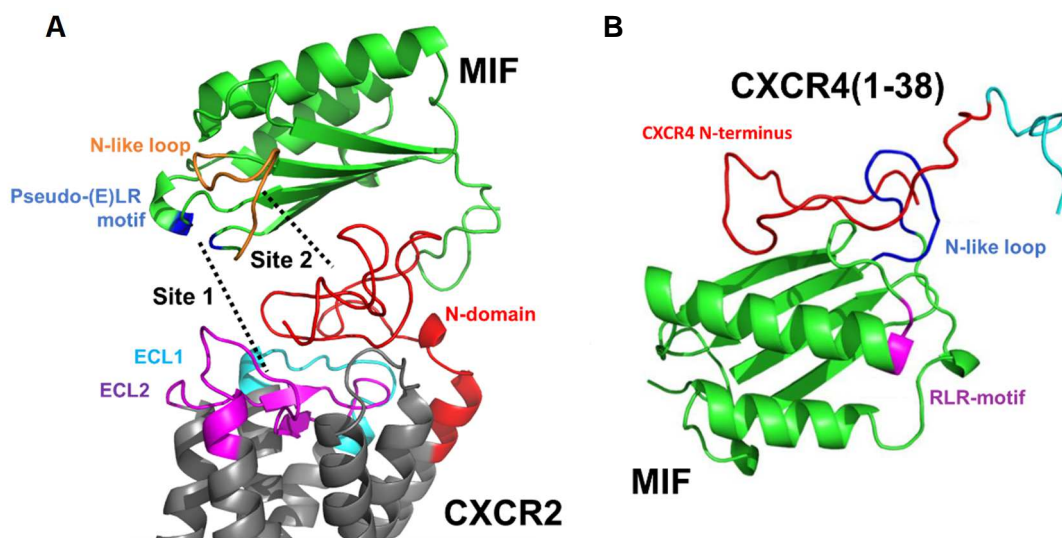
Figure 11: Model of the interaction of human MIF with chemokine receptors CXCR2/4. A) The interaction of MIF with CXCR2 involves the pseudo-(E)LR motif (Asp44-X-Arg11) of MIF and segments of the receptor extracellular loops (ECL)1/2 (site 1) together with the MIF N-like loop (residues 47-56) and the receptor *N*-domain (site 2). The crucial determinants involved in the interaction are highlighted: N-like loop (orange), pseudo-(E)LR motif (blue), ECL1 (cyan), ECL2 (magenta), *N*-domain (red). Figure modified from Krammer et *al.*, *Chembiochem,* 2020[176] (Publication I). **B)** Structural determinants of site 1 interaction of MIF and CXCR4 include the *N*-terminus (residues 1-27) on the site of CXCR4 and the extended N-like loop (residues 43-98) together with the RLR-motif (Arg87-Leu88-Arg89) and residue Pro-1 at the site of MIF. The crucial moieties involved in the binding are highlighted: CXCR4 *N*-terminus (red), RLR-motif (magenta), residues 28-38 of CXCR4 (cyan). The N-like loop comprising residues 47-56 (blue) as part of the extended N-like loop is depicted. Figure modified from Lacy, Kontos, Brandhofer et *al.*, *Sci Rep*, 2018[174]. Models in A and B were predicted using the PatchDock/FireDock algorithm.

1.6.5 Link between MIF and B cells

A first link between B cells and MIF has been described by Gore et *al.* in 2008 providing evidence for the involvement of MIF/CD74/CD44 signaling in B-cell survival[160]. CD74 has been originally identified as MHC class II chaperon, but its role has been expanded to cell proliferation/survival and B-cell maturation[177,178]. In this context, it was shown that cleavage of the cytosolic domain of CD74 activates Nf-κB in the nucleus. The Nf-κB p65

(RelA) homodimer and its coactivator TAFII105 subsequently initiate a transcriptional program regulating B-cell development from immature to mature B cells and mediate the survival of mature B cells[179,180]. An additional study showed that these pathways were activated by the treatment with an anti-CD74 antibody *in vitro*. More importantly, similar effects were obtained by stimulation with MIF[177]. Later it was shown that the described MIF-induced signaling via CD74 in B cells was only feasible in complex with CD44 (Figure 12)[160]. Pro-inflammatory stimuli, like TNF-α or LPS, triggered the upregulation of CD74 on the B-cell surface, thereby augmenting MIF-mediated B-cell proliferation. As this observation emphasizes the involvement of MIF-triggered B-cell responses during inflammation, MIF/CD74 signaling pathways in B cells have become targets in the treatment of inflammatory pathologies[181]. Accordingly, treatment of systemic lupus erythematosus (SLE) with a tolerogenic peptide mediated the downregulation of factors involved in MIF/CD74 signaling, while pro-apoptotic molecules were upregulated in B cells[182].

Besides CD74, MIF receptor CXCR4 is expressed by B cells. Via interaction with a CXCR4/CD74 complex MIF induces B-cell chemotaxis through the induction of a ZAP-70-dependent signaling pathway (Figure 12)[183].

While MIF has been related to B cells in the context of inflammation and autoimmune diseases [181,182,184], a functional connection in atherosclerosis is still elusive. Recently, we scrutinized the potential link in more detail and showed that *Mif*-gene deletion causes a maturation defect of BM B cells accompanied by an atheroprotective antibody-repertoire and reduced splenic and peripheral B-cell numbers[152]. However, the molecular functions and mechanisms of MIF as a mediator of B-cell development remained elusive (related to publication IV, in preparation, appendix B). Moreover, *Mif*-deficiency was associated with the formation of (peri-)adventitial B-cell-rich clusters in atherogenic mice that received a cholesterol-rich diet (HFD) for 24 weeks, while these clusters were absent in age-matched control mice[152]. However, the detailed cellular and molecular composition of the clusters as well as age-dependent effects of *Mif*-deficiency on B-cell cluster formation were unknown (related to publication III, in preparation, appendix A).
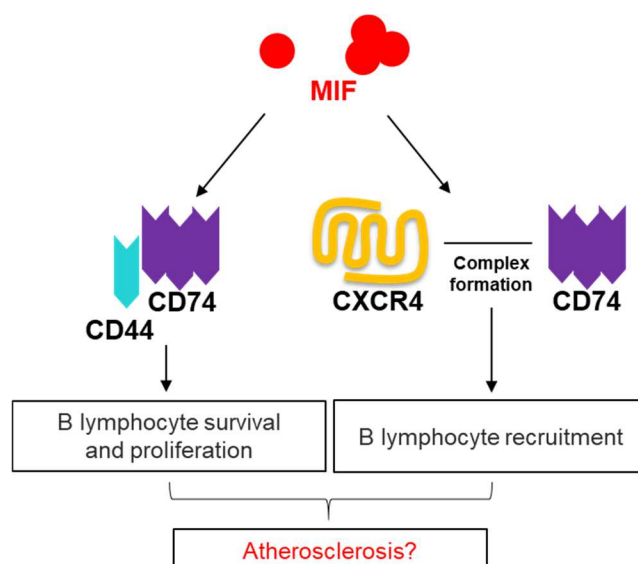
Figure 12: MIF-mediated responses in B cells involving CD74 and chemokine receptor CXCR4. MIF receptors CD74 and CXCR4 are expressed on the B-cell membrane. MIF binding to CD74/CD44 triggers B-cell survival and proliferation, while MIF signaling via CXCR4/CD74 leads to B-cell recruitment. If these signaling pathways in B cells are involved in atherogenesis and how they affect disease development is still elusive. Figure designed based on Klasen et *al.*, *J Immunol*, 2014[183] and Gore et *al., J Biol Chem,* 2008[160].

1.7 MIF-directed therapeutic intervention strategies in atherosclerosis and cardiovascular diseases

1.7.1 Targeting of MIF and its receptors by small molecule drugs or antibodies

Due to MIF's diverse biological activities together with its role in tumorigenesis[185,186] and various inflammatory diseases including atherosclerosis[145], it represents an interesting target for drug development. As discussed in a wealth of research articles, several MIF-directed therapeutic strategies including antibodies and small molecule inhibitors have been developed over the past years (Figure 13)[187-191]. For example, the monoclonal antibody Imalumab (Bax69) binds MIF after redox-specific oxidation of a cysteine at position 81[192] and has been investigated in phase1/2a clinical studies (NCT02448810, NCT01765790) in individuals suffering from ovarian and metastatic colorectal cancer[193]. In the context of inflammation, the small molecule inhibitor (S,R)-3-(4-hydroxyphenyl)-4,5-dihydro-5-isoxazole acetic acid methyl ester (ISO-1) targeting MIF's tautomerase site has been extensively studied and it has been shown that it blocks inflammatory functions of MIF in a mouse model of endotoxaemia[194,195]. An additional small molecule inhibitor targeting the catalytic pocket is 4-iodo-6-phenylpyrimidine (4-IPP) that covalently binds to Pro-1[196]. As this residue is also involved in the MIF-CXCR4/CD74 interaction, approaches targeting the tautomerase site of MIF need to be implemented with caution[175,194,197]. Besides, the small molecule Ebselen was found to block MIF's catalytic activities by introducing cysteine modifications that inhibit MIF trimer formation, while it

enhances MIF-mediated monocyte migration *in vitro* suggesting bioactivity of the monomer[190]. As the blockade of MIF's catalytic functions might not fully inhibit its pro-inflammatory and atheroprogressive activities, the applicability of the discussed MIF-targeting strategies in cardiovascular diseases remains uncertain[189]. In addition, interference with MIF-mediated cardioprotective functions through CD74 might occur as a result of MIF-targeted therapeutical intervention[187].

Thus, other approaches focus on targeting MIF-receptors (Figure 13). For example, Milatuzumab is a CD74-directed antibody developed for the treatment of patients with cancer pathologies including chronic lymphocytic leukemia[198]. So far, targeting of CXCR2/4 mainly focuses on small molecules, like Plerixafor (AMD3100) directed against CXCR4 and Reparixin against CXCR2[187]. Plerixafor was initially developed for the treatment of AIDS as it might block infection by human immunodeficiency virus (HIV) and more recently, its role in stem cell mobilization has gained attention[199]. However, targeting MIF receptors in atherosclerosis might have certain limitations as it might affect the angiogenic and homeostatic functions of cognate ligands[187].

1.7.2 Peptide-based therapeutic strategies

Alternative treatment options focus on peptides, mainly because of their enhanced selectivity and potency in comparison to small molecule inhibitors and antibodies and their low production costs. Additionally, peptides better cover the relatively large interaction interface between chemokines and their receptors than small molecule inhibitors (Figure 13)[187,200]. Recently, some peptides blocking the MIF/CD74 interaction have been investigated including a MIF-derived peptide spanning residues 79-86 and a human recombinant T-cell receptor ligand (RTL1000)[201,202]. A more attractive target for the drug development in atherosclerosis might be the atherogenic MIF/CXCR2 or MIF/CXCR4 axis. Peptides targeting CXCR4 have been designed to cure cancer pathologies and to protect against HIV infection[203]. However, those might not be suitable for the treatment of atherosclerosis-related diseases as they might also block CXCL12-mediated atheroprotective effects. Additionally, the discontinuous structure of chemokine receptors challenges the generation of chemokine receptor-based drugs[204]. Despite recent progress in the design of peptide-based drugs, approaches that specifically block the pro-inflammatory and atherogenic interaction between MIF and its chemokine receptors CXCR2 and CXCR4 have not been developed[187]. These would avoid interference with the action of cognate ligands and would not affect MIF's cardioprotective or homeostatic functions[187] (related to publication I and II).
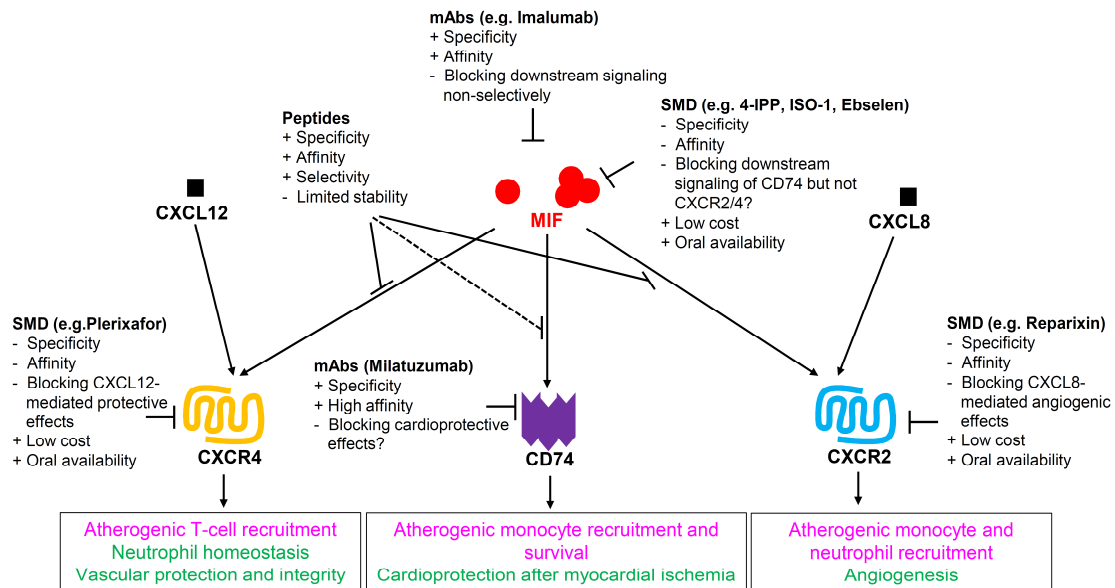
Figure 13: Inhibitory strategies targeting MIF and its receptors in atherosclerosis. Different therapeutic approaches targeting MIF or its receptors including peptides, small molecule drugs (SMDs) and monoclonal antibodies (mAbs) are discussed in the context of atherosclerosis and related cardiovascular diseases. While MIF-mediated signaling through CXCR2/4 mainly mediates atheroprogressive functions (magenta), binding of cognate ligands CXCL8 and CXCL12 to the respective receptors was associated with atheroprotective and homeostatic effects (green). Besides, MIF mediates cardioprotection via CD74, which should be considered when developing therapeutic approaches in the treatment of atherosclerosis. Peptides can be used to specifically target MIF-receptor axes and have several additional advantages over antibodies and small molecules such as high affinity and selectivity. Advantages (indicated by "+") and disadvantages (indicated by "-") of each therapeutical approach are depicted. Figure modified from Sinitski, Kontos, Krammer et *al.*, *Thromb Haemost,* 2019[187].

1.8   Research rationale and aims

Despite continuously improving cardiologic and surgical intervention options, the incidence of CVDs has dramatically increased over the past years mainly owing to an aging population and increased risk factors[1]. Thus, the development of treatment options for related pathologies has become more important. Atherosclerosis has been defined as the main underlying cause of CVDs and the role of MIF in atherogenesis is well established[205]. MIF has been also implicated in diverse additional acute and chronic inflammatory conditions, metabolic disorders as well as cancer[206]. Different treatment strategies targeting MIF have been proposed. However, these approaches lack selectivity, are mainly focusing on small-molecule drugs and monoclonal antibodies and have mainly been targeted to cancer pathologies[187,207,208]. MIF also plays crucial roles in immune homeostasis and cardioprotection[161] and we proposed a so far unknown connection between MIF and B cells in the atherosclerotic cascade indicating that MIF impacts B-cell development, B-cell clustering and atheroprotective antibody production[152]. Thus, suggesting a complex and multifaceted role of MIF in health and disease that is challenging when considering the development of applicable inhibitors targeting MIF or its receptors.

Based on this background, my thesis focuses on the following aims that are part of different projects and publications:

- To elucidate the structural determinants of the MIF/CXCR interface and to develop anti-atherogenic peptides that specifically target the engagement of MIF with its receptors CXCR2/4 (related to publication I and publication II).

- To explore the impact of *Mif*-gene deletion over the course of aging in advanced atherosclerosis with a focus on (peri-)adventitial B-cell cluster formation (related to publication III, in preparation, appendix A).

- To scrutinize the role of MIF as a mediator in B-cell development (related to publication IV, in preparation, appendix B).

A more detailed description of these aims follows in the subsequent chapters.

1.8.1 Investigation of structural moieties of the MIF/CXCR2 interface for the development of anti-atherogenic MIF-derived peptides

MIF mediates the atherogenic recruitment of immune cells including monocytes and T cells by non-cognate interactions with the chemokine receptors CXCR2 and CXCR4, respectively[145]. An in-depth knowledge of the structural features of the interaction interfaces between MIF and its receptors is obligatory when considering the design of novel MIF-derived inhibitors in atherosclerosis. The molecular moieties of the interaction interface of MIF and CXCR2 have been previously explored, revealing a role for the MIF N-like loop. Peptide MIF(47-56) derived from the MIF N-like loop inhibited MIF binding to CXCR2 and blocked MIF-mediated leukocyte adhesion *in vivo* and *in vitro*[173]. However, it was not clear if the inhibitory effects were a result of a direct interaction of MIF(47-56) and CXCR2 or due to MIF's property to form homocomplexes. The aim of this thesis project was to explore the fundamental mechanisms of the inhibitory effects of MIF(47-56) and to determine critical residues for a inhibitory peptide activity. In this context, I planned to analyze binding properties of MIF(47-56) by receptor binding assays and to screen peptide-derived alanine-variants for their inhibitory potential *in vitro*. Structure-activity studies should not only be able to identify critical residues in MIF(47-56), but also dispensable residues that could be exchanged by other residues for stability and function improvements necessary for *in vivo* applications. Improved MIF(47-56)-derived analogues could serve as a potential therapeutic anti-MIF agent that specifically target the MIF/CXCR2 interaction without interfering with the angiogenic activities of the cognate CXCR2-ligand CXCL8. Conformational restriction through cyclization by disulfide-

bridging was considered to improve pharmacokinetics and binding capacities of MIF(47-56). I aimed to test the inhibitory potential of different cyclized peptide variants *in vitro* and identified candidate peptides with improved or similar functions as the linear peptide that were then subjected to *ex vivo/in vivo* applications. These studies have been published and are part of this thesis (related to publication I).

1.8.2 Development of a CXCR4-ectodomain peptide that specifically blocks atherogenic MIF/CXCR4-mediated signaling

Besides targeting the MIF/CXCR2 axis, the development of therapeutic peptides to distinctively inhibit the engagement of MIF with CXCR4 without affecting CXCL12-mediated pro-atherogenic and homeostatic effects seems to be another promising approach for the treatment of atherosclerosis. Based on novel insights into the interaction interface revealing parts of ECL1 and ECL2 of CXCR4 to be involved in the interaction with MIF[175], the objective of this project was to generate soluble CXCR4-ectodomain mimics (msR4Ms) that selectively target the MIF/CXCR4 interaction and block MIF-mediated atherogenic functions. Together with my colleagues, I aimed at testing the binding affinity of these peptides towards MIF and to prove their selectivity for MIF sparing CXCL12. Candidate peptides with high affinity, such as peptide msR4M-L1 consisting of ECL1(97-110) and ECL2(182-196) connected by a synthetic linker, were tested for their inhibitory potential in different *in vitro* applications. Moreover, I wanted to identify critical determinants of the msR4M-L1/MIF interface and to precisely map the binding region by applying peptide array analysis and competition experiments. Additionally, the peptide was administered as a potential atherosclerosis-blocker *in vivo*. In this context, the therapeutic effectiveness of the peptide regarding atherogenic plaque formation, lesional immune cell infiltration and synthesis of inflammatory cytokines was estimated. The results of this study have been published and are part of this thesis (related to publication II).

1.8.3 Analysis of age-dependent effects of *Mif*-deficiency in atherosclerosis

Besides T cells and monocytes, also B cells are involved in the development of atherosclerosis with subset-dependent pro- and anti-atherogenic effects[39]. Only few B cells reside in the plaque, but they are more pronounced in adventitial sites of the BCA and the abdominal aorta[68,69]. In aged *Apoe*^{-/-} mice (>52 weeks), B cells concentrate in ATLOs, where they contribute to adaptive immune responses in atherosclerosis[81]. We recently revealed enhanced formation of B-cell-rich clusters in *Mif*-deficient mice after 24 weeks of HFD, while total vascular B-cell numbers were unchanged compared to the *Apoe*^{-/-}

controls[152]. However, the nature of these clusters had remained elusive. Based on these findings, I asked whether the detected clusters might be early ATLOs, ATLO-like or other related structures. I planned to stain the clusters for B cells, T cells and diverse ATLO-specific markers including CD35 (FDCs), PNAd (HEVs) and LYVE-1 (lymph vessels), among others. As the formation of ATLOs is stage-specific and progresses during aging, I wanted to implement an aging mouse model of atherosclerosis in combination with HFD. The effects of global *Mif*-deficiency were investigated in 30-, 42-, and 48-week-old *Apoe*^−/− mice on HFD for 24, 36, or 42 weeks, respectively, and in 52-week-old mice on a 6-week HFD. Indeed, aging has been described as a major risk factor in atherosclerosis[4]. However, so far atherogenic mouse models focus on young to middle-aged mice and therefore do not fully address the aged disease phenotype in humans[151-153]. Thus, I aimed at scrutinizing the effects of *Mif*-deficiency on B-cell clustering, plaque formation and lesional immune cell infiltration in different parts of the aorta and the BCA during the course of aging focusing on advanced disease stages. Previously, we described a site-specific atheroprotective phenotype of *Mif*-deficient *Apoe*^−/− mice, specifically in the abdominal aorta and BCA[152]. To clarify, whether this phenotype is maintained during aging was subject of this study. The phenotypical analyses of aged *Mif*-deficient *Apoe*^−/− mice were complemented by fluorescence-activated cell sorting (FACS)-based immune cell profiling of different organs and the periphery. Moreover, I aimed to investigate MIF- and age-dependent changes in levels of soluble atherosclerosis-relevant mediators including ox-LDL-specific antibodies. The results of this study are presented and discussed as part of this thesis (related to publication III, in preparation, appendix A).

1.8.4 Investigation of MIF's role in B-cell development by transcriptome analysis via RNAseq

Recently, we showed that *Mif*-gene deletion impedes B-cell development in the BM of *Apoe*^−/− mice accompanied by reduced splenic and peripheral B-cell numbers[152]. These results suggested that MIF might act as crucial mediator of B-cell maturation, but the precise fundamental functional and molecular mechanisms were not investigated so far. In this project, I aimed for deeper insights into the role of MIF in the B-cell developmental cascade and to elucidate the impact of *Mif*-deficiency on B-cell phenotypes in BM and spleen. For this reason, I wanted to conduct an extensive transcriptome analysis of distinct B-cell developmental subpopulations via RNAseq. RNAseq is an emerging and powerful tool to unbiasedly analyze the entire transcriptome either of a single-cell (scRNAseq) or cell populations (bulk RNAseq)[209,210]. A lot of effort has been recently

made to enlighten the complexity and heterogeneity of genome-wide transcriptomes and to identify the cellular composition of individual tissues and organs[211,212]. Moreover, RNAseq can give functional insights into human disease pathologies and altered biologically processes[213]. In this work, small bulk RNAseq (50 cells) was applied to compare the transcriptomic signature of developmental B-cell stages between *Mif*-deficient mice and wild type (WT) controls and to evaluate how these changes could affect B-cell maturation. I further aimed at the functional verification of the RNAseq results by different *in vitro* and *in vivo* approaches. The outcome of this study is presented and discussed as part of this thesis (related to publication IV, in preparation, appendix B).

2 Personal Contributions to the Publications

Within the scope of my thesis, I contributed to different projects resulting in various publications including research papers and review articles.

2.1 Publication I

Krammer C, Kontos C, Dewor M, Hille K, Dalla Volta B, El Bounkari O, Taş K, Sinitski D, Brandhofer M, Megens RTA, Weber C, Schultz JR, Bernhagen J, Kapurniotu A. *A MIF-derived cyclopeptide that inhibits MIF binding and atherogenic signaling via the chemokine receptor CXCR2*. **Chembiochem.** 2020 Oct 30; online ahead of print.

As the sole first author of this publication, I performed the majority of the experiments, analyzed the data and was partly responsible for the overall study design. Moreover, I prepared the manuscript together with the corresponding authors Prof. Bernhagen and Prof. Kapurniotu (TUM). My personal contributions to the experimental section include receptor binding assays and dynamic mass redistribution (DMR) experiments in order to verify the direct interaction of MIF(47-56) and CXCR2 (Figure 1e-f). In addition, I applied DMR measurements in order to screen MIF(47-56)-derived mutant peptides for potential interactions with CXCR2 (Table 1, Figure 2a, Supplementary figure 1). Moreover; I was involved in performing transwell migration assays in order to evaluate if MIF(47-56) peptide variants and cyclic analogues inhibit MIF-mediated chemotaxis (Figure 2b and Figure 3a-b). Additionally, I assisted in conducting monocyte adhesion assays to test the anti-atherogenic activity of the cyclized peptide variant MIF(cyclo10) in an atherosclerosis-related setting (Figure 4b-d).

2.2 Publication II

Kontos C*, El Bounkari O*, Krammer C*, Sinitski D, Hille K, Zan C, Yan G, Wang S, Gao Y, Brandhofer M, Megens RTA, Hoffmann A, Pauli J, Asare Y, Gerra S, Bourilhon P, Leng L, Eckstein HH, Kempf WE, Pelisek J, Gokce O, Maegdefessel L, Bucala R, Dichgans M, Weber C, Kapurniotu A, Bernhagen J. Designed CXCR4 mimic acts as a soluble chemokine receptor that blocks atherogenic inflammation by agonist-specific targeting. ***Nat Commun.*** 2020 Nov 25;11(1):5981

As a co-first author of this publication I planned, performed and analyzed a great number of the experiments, designed figures and was involved in comprehensive discussions of the results with the co-authors. Moreover, I wrote parts of the materials and methods section and revised the manuscript. Regarding the experimental part, I was mainly involved in the analysis of properties of the msR4M-L1/MIF interaction. For example, I performed dot blot experiments in order to verify the specific interaction of msR4M-L1 and MIF, while omitting CXCL12 (Figure 1j, Supplementary figure 8). Due to the sequence similarities of human and mouse MIF, I was able to detect equal binding affinities of msR4M-L1 to recombinant MIF of both species (Supplementary figure 14). Based on this result, I showed that msR4M-L1 interacts with MIF expressed in atherosclerotic lesions in the aorta of $Ldlr^{-/-}$ mice and the BCA of $Apoe^{-/-}$ mice by immunohistochemistry (IHC) (Figure 5d-e, Supplementary figure 21). IHC was also applied to detect and quantify msR4M-L1 binding to MIF in stable and unstable plaques of human carotid endarterectomy samples compared to healthy controls (Figure 6n-p, Supplementary figure 6a-b). Besides, I was able to significantly block the binding of msR4M-L1 to MIF expressed in stable plaques by the treatment with the MIF-derived peptide MIF(54-80) (Supplementary figure 28c-d). Similarly, I blocked the binding to MIF in the dot blot setup (Figure 2h). In addition, I performed peptide array experiments in combination with alanine-scanning in order to detect positions that are involved in the interface between msR4M-L1 and MIF (Supplementary figure 12).

2.3 Publication III (in preparation, appendix A)

Krammer C, Yang B, Reichl S, Bolini V, Schmitz S, Noels H, Kapurniotu A, Weber C, Mohanta S, Bernhagen J. Aging leads to loss of atheroprotection in *Mif*-deficient atherosclerotic mice. Manuscript in final preparation for submission to the cardiovascular journal ***Basic Res Cardiol***.

As the sole first author of this publication, I was substantially involved in the conception and experimental design of this study. Briefly, we scrutinized the impact of *Mif*-deficiency in an $Apoe^{-/-}$ mouse model during the course of aging focusing on advanced lesions. More precisely, we analyzed 30-, 42-, and 48-week-old $Mif^{-/-}Apoe^{-/-}$ mice and the gender-matched $Apoe^{-/-}$ control mice on HFD for 24, 36, or 42 weeks, respectively, as well as 52-week-old mice on a 6-week HFD. I planned and conducted the animal experiments and collected the samples for further investigations. In this context, I monitored the weight of the animals during aging (Table A.1) and measured different blood parameters (Table A.3). Moreover, I conducted the majority of the experiments and analyzed the

data. These include lesion quantification across the vascular tree (Figure A.1a-i, Supplementary figure A.1e-h), FACS-based immune cell profiling (Figure A.2a-d, Supplementary figure A.1i-j, Supplementary figure A.4a-d) and IHC stainings for lesional immune cells in *Mif*-deficient $Apoe^{-/-}$ mice and $Apoe^{-/-}$ controls (Figure A.3a-f). Moreover, I investigated the formation of (peri-)adventitial B-cell clusters in the BCA (Figure A.4a-b) and evaluated the nature of the clusters by IHC (Figure A.4c). Additionally, I measured the levels of atheroprotective and -progressive antibody titers in murine plasma (Figure A.5a-b) as well as plasma cholesterol and triglyceride levels (Table A.2). I complemented the study by evaluating mRNA levels in the spleen and liver by qPCR (Supplementary figure A.2a-b) and in the plasma by ELISA (Supplementary figure A.2c). Besides, I prepared the figures including a summary scheme (Figure A.6) and wrote the manuscript together with Prof. Bernhagen.

2.4   Publication IV (in preparation, appendix B)

Krammer C*, Besson-Girard S*, Usifo F, Reichl S, Bolini V, Bernhagen J, Gokce O. Macrophage migration inhibitory factor (MIF) alters the transcriptomic program of bone marrow B-cell subsets to control B-cell development and function. Manuscript in preparation for submission to the developmental biology journal ***Development***.

This project was conducted in cooperation with Simon Besson-Girard and Ozgun Gokce (Systems Neuroscience group, ISD, University Hospital Munich) and combines computational biology and "wet-lab"-based research. The data obtained in this context is not published yet but will be part of a manuscript that is already in preparation and will be submitted soon. The first authorship will be shared between Simon Besson-Girard and myself. I was partly responsible for the experimental design and conception of this study and prepared the figures in collaboration with the co-first author. The manuscript included in the appendix of this thesis was written by myself. Moreover, I established a FACS-based sorting strategy of different developmental B-cell stages from BM and spleen based on the expression of subset-specific markers (Figure B.2a, Supplementary figure B.1a-b). I also used FACS analysis to estimate the number of distinct splenic and BM-derived B-cell subsets from $Mif^{-/-}$ and WT mice (Figure B.4a-b, Supplementary figure B.2a-b). S. Besson-Girard was responsible for the preparation of the libraries and the computational part including the analysis of the RNAseq data. Together, we interpreted the RNAseq data and on this basis, I performed various experiments for the functional verification of the results. More precisely, I performed B-cell migration assays using BM-derived cells in combination with the FACS-based determination and quantification of

migrated B-cell subsets (Figure B.1a-d). Additionally, I conducted a VCAM-1 adhesion assay to scrutinize the effect of *Mif*-deficiency on the adhesion potential of B cells in response to different cytokines/chemokines (Figure B.3a-d). Besides, I estimated the proliferative capacity of B-cell subsets by intraperitoneal (i.p.) application of 5-ethynyl-2'deoxyuridine (EdU) that was detected in a click chemistry reaction (Figure B.4d, Supplementary figure B.3a-e, k). Moreover, I performed apoptosis assays using Annexin V (Figure B.4e, Supplementary figure B.3f-j,l).

3 Summary and Outlook

MIF has been described as an inflammatory cytokine and ACK that is engaged in innate immunity and drives the clinical course of different acute and chronic inflammatory conditions. As evidenced by genetic deletion and antibody-mediated neutralization of MIF in different atherogenic mouse models, MIF is a pivotal driver of atherogenesis. Data from observational studies support this notion. MIF predominately mediates pro-atherogenic functions through binding to chemokine receptors CXCR2/4, thereby promoting lesional monocyte/neutrophil and T-cell recruitment, respectively, but also displays additional pro-atherogenic activities. The interaction interfaces between MIF and its receptors have been comprehensively studied within the last years. The precise determination of contributing binding moieties at the ligand- and receptor-site are crucial for the development of MIF-based therapeutic strategies in atherosclerosis and related CVDs and will add important structure-activity information for the more general development of chemokine-directed strategies.

In this thesis, antagonistic peptides were used as molecular tools to analyze the mechanisms at the interfaces and as potential anti-MIF or anti-MIF-receptor agents interfering with specific MIF/CXCR interactions. The MIF N-like loop including residues 47-56 has been previously shown to be involved in the interaction with CXCR2 and MIF-derived peptide MIF(47-56) successfully blocked atherogenic functions of MIF. This work uncovered that MIF(47-56) competed with the MIF/CXCR2 interaction by binding directly to CXCR2. Moreover, structure-activity studies of different alanine-variants of the peptide revealed that residues at position 47 and 48 are crucial for receptor binding and inhibitory peptide activity and should be spared when considering the substitution of residues to generate improved peptide variants. In addition, a cyclic peptide derivate of MIF(47-56), namely MIF(cyclo10), with improved proteolytic stability, inhibited MIF-triggered monocyte migration similar to the linear peptide *in vitro* and effectively blocked MIF-mediated leukocyte recruitment to carotid arteries in an *ex vivo/in vivo* setting, suggesting that MIF-derived cyclic peptide variants might be promising leads for the development of anti-atherosclerotic drugs. Further functional and stability improvements by stepwise extension or shortening as well as the introduction of artificial residues are needed to develop the peptide into peptidomimetics suitable for *in vivo* application. Candidate peptides will be applied in accelerated and chronic mouse models of atherosclerosis in the future (related to publication I).

Moreover, I contributed to the development of a peptide-based CXCR4 ectodomain mimic (msR4M-L1) that specifically blocks the MIF/CXCR4 interaction. While msR4M-L1

did not interact with CXCL12, the cognate ligand of CXCR4, it displayed remarkable affinity for MIF. This study revealed the crucial determinants of the binding region on the site of the peptide (aromatic residues F104 and F107) as well as on the site of MIF (residues 54-80). Importantly, msR4M-L1 blocked MIF-mediated atherogenic activities in different *in vitro* applications, inhibited leukocyte adhesion to carotid arteries *ex vivo* and was shown to reduce atherosclerosis in atherogenic mouse models. In contrast, atheroprotective CXCL12/CXCR4 and cardioprotective MIF/CD74 signaling was not affected. Besides, msR4M-L1 was shown to bind MIF in human carotid endarterectomy plaques providing a translation to the pathology of atherosclerosis in humans. Together, this study indicates that CXCR4 ectodomain mimics, especially msR4M-L1, could serve as proof-of-concept atherosclerosis blocker that could be further developed into advanced next generation mimics applicable to the treatment of human atherosclerosis (related to publication II).

Lately, B cells were described as emerging contributors to the atherogenic progress with subset-dependent atheroprotective and -progressive effects. However, a connection between B cells and MIF in the atherosclerotic pathology has been elusive. While only a minor amount of B cells resides in the atherosclerotic plaque, they accumulate in periadventitial ATLOs in aged *Apoe*$^{-/-}$ mice (>52 weeks). Previously, we identified B-cell-rich clusters in *Mif*-deficient *Apoe*$^{-/-}$ mice after 24 weeks of HFD (corresponds to an age of 30 weeks), but these structures were absent in the respective *Apoe*$^{-/-}$ controls. This work revealed that the structures resemble to early stage-2 ATLOs, suggesting that *Mif*-deficiency accelerates ATLO-like cluster formation in *Apoe*$^{-/-}$ mice. Based on these results, I investigated the role of global *Mif*-deficiency during the course of aging in 30-, 42-, and 48-week-old *Apoe*$^{-/-}$ mice on HFD for 24, 36, or 42 weeks, as well as in 52-week-old mice on a 6-week HFD in more depth focusing on B-cell clustering, site-specific atheroprotection and the secretion of inflammatory mediators. Importantly, the atheroprotective effects of *Mif*-deficiency that were seen in younger mice (30/24-week-old group) were lost at advanced ages (48/42-week-old group). This result was accompanied by changes in lesional immune cell infiltration and atheroprotective plasma anti-oxLDL antibody level, suggesting a multifactorial cause of the observed phenotype (related to publication III, in preparation, appendix A).

Moreover, this work demonstrated the involvement of MIF as a mediator in the B-cell developmental cascade. Previous data has shown that *Mif*-gene deletion is associated with a maturation defect of BM B cells in *Apoe*$^{-/-}$ mice, but fundamental molecular processes and the functional basis of the developmental block have not been investigated. To get deeper insights to the function of MIF in the B-cell developmental cascade, the

transcriptome of different B-cell developmental stages derived from the BM and spleen of healthy, non-atherogenic mice was analyzed by RNAseq analysis accompanied by several functional studies. The results demonstrated significant differences in the transcriptomic signature of all analyzed B-cell stages from *Mif*-deficient mice compared to the WT controls. These changes were accompanied by functional alterations, especially related to pathways associated with cell migration, adhesion, and proliferation. As these mechanisms are connected to the B-cell developmental program, this study indicated a crucial role of MIF in B-cell maturation (related to publication IV, in preparation, appendix B). The functional consequences of *Mif*-gene deletion for the development of B cells in an atherogenic background are subject of further investigations that are ongoing, but not part of this thesis.

Together, this work emphasizes the complex and multifaceted role of MIF in homeostasis, B-cell development, and progression of a chronic vascular inflammatory disease, namely atherosclerosis. The design of therapeutic strategies targeting MIF in atherosclerosis is therefore not trivial and needs a profound knowledge of MIF's disease exacerbating as well as protective functions and the underlying MIF-interaction networks. Moreover, the effectiveness of MIF-based treatment strategies seems to be age-dependent and must be therefore considered with caution.

4 Zusammenfassung und Perspektiven

MIF ist ein inflammatorisches Zytokin und atypisches Chemokin, welches in Prozesse der angeborenen Immunabwehr und der Pathogenese von verschiedenen akuten und chronischen Entzündungskrankheiten involviert ist. Mittels genetischer *Mif*-Deletion und Antikörper-vermittelter MIF-Blockade, konnte gezeigt werden, dass MIF eine entscheidende Rolle in der Entwicklung von Atherosklerose spielt. Diese Auffassung wird durch klinische Beobachtungsstudien unterstützt. Durch die Interaktion mit den Chemokin-rezeptoren CXCR2/4 vermittelt MIF hauptsächlich Atherosklerose-fördernde Funktionen, einschließlich der Rekrutierung von Monozyten/Neutrophilen und T-Zellen in die Läsionen. Die Interaktionsdomänen zwischen MIF und MIF-Rezeptoren wurde in den letzten Jahren bereits umfangreich untersucht. Die präzise Bestimmung von beteiligten Bindestellen, sowohl auf Seiten des Liganden als auch des Rezeptors, sind Grundlage für die Entwicklung von MIF-basierten therapeutischen Strategien in der Behandlung von Atherosklerose und damit verbundenen kardiovaskulären Erkrankungen. Zudem liefert diese Vorgehensweise wichtige Struktur-Aktivitätsinformationen für die allgemeine Entwicklung Chemokin-gerichteter Strategien.

Im Rahmen dieser Dissertation wurden antagonistische Peptide eingesetzt, um die Mechanismen an den Bindungsstellen näher zu untersuchen und spezifische MIF/CXCR Interaktionen zu blockieren. Der MIF N-like loop einschließlich Aminosäurepositionen 47-56 ist an der Interaktion mit CXCR2 beteiligt. Vorausgehende Arbeiten haben gezeigt, dass mittels des abgeleiteten Peptides MIF(47-56) MIF-vermittelte Atherosklerose-fördernde Mechanismen unterbunden werden. In dieser Arbeit konnte dargelegt werden, dass dieses Peptid direkt an CXCR2 bindet und dadurch MIF vom Rezeptor verdrängt. Struktur-Aktivitäts-Untersuchungen verschiedener Alanin-Varianten des Peptides haben gezeigt, dass die Aminosäurepositionen 47 und 48 unerlässlich für Rezeptorbindung und die inhibitorische Funktion des Peptides sind. Bei der Erstellung optimierter Peptidvarianten durch den Austausch bestimmter Aminosäuren, sollten diese beiden Positionen folglich unberührt bleiben. Ähnlich zum linearen Peptid, konnte durch eine zyklisierte Variante des Peptides, MIF(cyclo10), die MIF-vermittelte gerichtete Migration von Monozyten *in vitro* inhibiert werden. Außerdem konnte durch Einsatz dieses Peptides in einem *ex vivo/in vivo* Versuchsaufbau die MIF-vermittelte Rekrutierung von Leukozyten an die Endothelschicht von Karotiden blockiert werden. Diese Ergebnisse deuten darauf hin, dass MIF-basierte zyklisierte Peptid-Derivate künftig als vielversprechende Leitstrukturen für die Entwicklung therapeutischer Peptide in der Behandlung von Athero-

sklerose dienen könnten. Für die Applikation *in vivo* sind weitere Verbesserungen hinsichtlich Funktion und Stabilität, beispielsweise durch schrittweise Verlängerung oder Verkürzung und die Einführung künstlicher Aminosäuren, nötig. Entsprechende Peptid-Kandidaten könnten in Mausmodellen der beschleunigten und chronischen Atherosklerose eingesetzt werden (Zusammenhang mit Publikation I).

Des Weiteren habe ich an der Entwicklung eines Peptidmimetikums der extrazellulären Domänen des Chemokinrezeptors CXCR4 (msR4M-L1) mitgewirkt, durch dessen Einsatz eine spezifische Blockade der MIF/CXCR4 Interaktion erzielt werden konnte. Während msR4M-L1 nicht mit dem CXCR4-Liganden CXCL12 interagierte, zeigte das Peptid eine hohe Affinität für MIF. Im Rahmen dieser Arbeit wurden entsprechende Determinanten der Binderegion, sowohl Seitens des Peptides (aromatische Aminosäuren F104 und F107), als auch Seitens MIFs (Aminosäuren 54-80) nachgewiesen. Außerdem konnten mittels msR4M-L1 MIF-vermittelte Atherosklerose-fördernde Mechanismen in unterschiedlichen *in vitro* Anwendungen inhibiert und die *ex vivo* Adhäsion von Leukozyten an Karotiden gehemmt werden. Zudem führte die Behandlung Atherosklerose-erkrankter Mäuse mit msR4M-L1 zu einer reduzierten Läsionsbildung. Im Gegensatz dazu, wirkte sich das Peptid nicht auf die Atherosklerose-hemmenden Signale der CXCL12/CXCR4-Interaktion, sowie auf kardioprotektive Mechanismen der MIF/CD74-vermittelten Signalweiterleitung aus. Um einen Bezug zur Pathogenese im Menschen herzustellen, wurde die Bindung von msR4M-L1 an MIF in humanen Läsionen (gewonnen aus Karotisendarteriektomien) nachgewiesen. Zusammengefasst zeigte diese Studie, dass Peptidmimetika der extrazellulären Domänen des Chemokinrezeptors CXCR4, vor allem msR4M-L1, als *Proof-of-Concept Atherosklerose-Inhibitoren* dienen könnten, die nach Weiterentwicklung als *Peptidmimetika der nächsten Generation* in der Behandlung von Atherosklerose am Menschen eingesetzt werden könnten (Zusammenhang mit Publikation II).

Kürzlich wurde gezeigt, dass B-Zellen in der Entwicklung von Atherosklerose eine Rolle spielen, wobei Subtypen mit Atherosklerose-fördernden und -hemmenden Eigenschaften unterschieden werden. Ein Zusammenhang zwischen MIF und B-Zellen in der Pathogenese von Atherosklerose wurde bisher jedoch nicht im Detail untersucht. Während B-Zellen in den atherosklerotischen Läsionen nur in geringer Menge auffindbar sind, akkumulieren diese in sogenannten tertiären lymphatischen Organen (ATLOs) in der Adventitia gealterter *Apoe*$^{-/-}$ Mäuse (>52 Wochen). In vorausgehende Arbeiten wurden solche B-Zell-Cluster in *Mif*-defizienten *Apoe*$^{-/-}$ Mäusen bereits nach der Fütterung einer fettreichen Diät über einen Zeitraum von 24 Wochen (entspricht einem Alter von 30 Wochen) nachgewiesen. In den entsprechenden Kontrolltieren konnten ähnliche Cluster nicht belegt werden. In dieser Arbeit wurde gezeigt, dass die identifizierten Strukturen

einem frühen ATLO-Stadium 2 entsprechen. Dieses Ergebnis deutet darauf hin, dass die *Mif*-Defizienz die Bildung ATLO-ähnlicher Cluster in *Apoe*$^{-/-}$ Mäusen beschleunigt. Darauf basierend, wurde im Rahmen dieser Arbeit der Effekt einer globalen *Mif*-Defizienz während des Alterungsprozesses näher untersucht. Dabei wurden 30, 42 und 48 Wochen alte Mäuse analysiert, die jeweils über einen Zeitraum von 24, 36, oder 42 Wochen mit einer HFD gefüttert wurden, sowie 52 Wochen alte Mäuse, denen eine 6-wöchige HFD verabreicht wurde. Im Fokus sollten dabei die Analyse der Bildung von B-Zell-Clustern, die Läsionsbildung in verschiedenen Teilen der Aorta und der BCA, sowie die Sekretion von inflammatorischen Mediatoren stehen. Im Vergleich zu jüngeren Mäusen (30/24 Wochen alte Gruppe), konnte in gealterten Mäusen (48/42 Wochen alte Gruppe) keine Reduktion der Läsionsbildung als Folge der *Mif*-Defizienz nachgewiesen werden. Zusätzlich zeigten sich im Alter Veränderungen in der Akkumulation von Immunzellen in den atherosklerotischen Läsionen, sowie hinsichtlich der Plasma-Titer Atherosklerose-hemmender anti-oxLDL Antikörper (Zusammenhang mit Publikation III, Manuskript in Vorbereitung, Anhang A).

Des Weiteren zeigte diese Arbeit, dass MIF als Mediator der B-Zellentwicklung eine wichtige Rolle spielt. Vorausgehende Daten haben gezeigt, dass die *Mif*-Defizienz mit einem Defekt in der Reifung von B-Zellen im Knochenmark (KM) von *Apoe*$^{-/-}$ Mäusen assoziiert ist. Bisher blieben die fundamentalen molekularen Prozesse und die funktionale Grundlage der Entwicklungsblockade jedoch ungeklärt. Um tiefere Einblicke in die Rolle von MIF in der Entwicklung von B-Zellen zu erlangen, wurde das Transkriptom verschiedener B-Zell-Entwicklungsstufen aus KM und Milz gesunder Mäuse mittels RNA-Sequenzierung in Kombination mit funktionalen Tests analysiert. Die Ergebnisse weisen auf signifikante Unterschiede im Transkriptom aller analysierten zellulären Subtypen aus *Mif*-defizienten Mäusen im Vergleich zu den Kontrollmäusen hin. Neben den Unterschieden im Transkriptom, ergaben sich auch funktionale Veränderungen, vor allem im Hinblick auf Migrations-, Adhäsions- und Proliferationseigenschaften. Da diese Mechanismen eng mit der Entwicklung von B-Zellen verknüpft sind, kann MIF tatsächlich eine wichtige Funktion als Mediator der Reifung von B-Zellen im Knochenmark zugeschrieben werden. Die funktionalen Effekte der *Mif*-Defizienz auf die B-Zellreifung in Maus-Modellen der Atherosklerose werden derzeit untersucht, sind jedoch nicht Teil dieser Arbeit (Zusammenhang mit Publikation IV, Manuskript in Vorbereitung, Anhang B).

Zusammengefasst unterstreichen die Ergebnisse dieser Arbeit die komplexen und vielfältigen Wirkungsweisen von MIF, sowohl in der Reifung von B-Zellen im KM, als auch hinsichtlich der vaskulären chronisch-entzündlichen Erkrankung Atherosklerose. Deshalb ist die Entwicklung MIF-basierter therapeutischer Strategien zur Behandlung von

Atherosklerose nicht trivial, sondern verlangt ein grundlegendes Wissen über die Krankheits-fördernden, sowie -hemmenden Mechanismen von MIF und entsprechende komplexe Interaktionsnetzwerke, in welche MIF eingebunden ist. Zudem scheint die Effizienz MIF-basierter Behandlungsmethoden altersabhängig, was ebenfalls bei der Medikamenten-Entwicklung berücksichtigt werden muss.

5   Publication I

6   Publication II

References

1.   Barquera, S., Pedroza-Tobías, A., Medina, C., Hernández-Barrera, L., Bibbins-Domingo, K., Lozano, R. & Moran, A.E. Global Overview of the Epidemiology of Atherosclerotic Cardiovascular Disease. *Arch Med Res* **46**, 328-338 (2015).
2.   World Health Organization. Cardiovascular Diseases (CVDs) Fact Sheet. Vol. 2020 (2017).
3.   Virani, S.S., Alonso, A., Benjamin, E.J., Bittencourt, M.S., Callaway, C.W., Carson, A.P., Chamberlain, A.M., Chang, A.R., Cheng, S., Delling, F.N., Djousse, L., Elkind, M.S.V., Ferguson, J.F., Fornage, M., Khan, S.S., Kissela, B.M., Knutson, K.L., Kwan, T.W., Lackland, D.T., Lewis, T.T., Lichtman, J.H., Longenecker, C.T., Loop, M.S., Lutsey, P.L., Martin, S.S., Matsushita, K., Moran, A.E., Mussolino, M.E., Perak, A.M., Rosamond, W.D., Roth, G.A., Sampson, U.K.A., Satou, G.M., Schroeder, E.B., Shah, S.H., Shay, C.M., Spartano, N.L., Stokes, A., Tirschwell, D.L., VanWagner, L.B. & Tsao, C.W. Heart Disease and Stroke Statistics-2020 Update: A Report From the American Heart Association. *Circulation* **141**, e139-e596 (2020).
4.   Dahlöf, B. Cardiovascular disease risk factors: epidemiology and risk assessment. *Am J Cardiol* **105**, 3a-9a (2010).
5.   Joseph, P., Leong, D., McKee, M., Anand, S.S., Schwalm, J.D., Teo, K., Mente, A. & Yusuf, S. Reducing the Global Burden of Cardiovascular Disease, Part 1: The Epidemiology and Risk Factors. *Circ Res* **121**, 677-694 (2017).
6.   Lusis, A.J. Atherosclerosis. *Nature* **407**, 233-241 (2000).
7.   Libby, P., Buring, J.E., Badimon, L., Hansson, G.K., Deanfield, J., Bittencourt, M.S., Tokgözoğlu, L. & Lewis, E.F. Atherosclerosis. *Nat Rev Dis Primers* **5**, 56 (2019).
8.   Libby, P. Inflammation in atherosclerosis. *Nature* **420**, 868-874 (2002).
9.   Hansson, G.K. & Hermansson, A. The immune system in atherosclerosis. *Nat Immunol* **12**, 204-212 (2011).
10.   Ross, R. Atherosclerosis-an inflammatory disease. *N Engl J Med* **340**, 115-126 (1999).
11.   Hansson, G.K. Inflammation, atherosclerosis, and coronary artery disease. *N Engl J Med* **352**, 1685-1695 (2005).
12.   Hansson, G.K. & Libby, P. The immune response in atherosclerosis: a double-edged sword. *Nat Rev Immunol* **6**, 508-519 (2006).
13.   Falk, E., Shah, P.K. & Fuster, V. Coronary plaque disruption. *Circulation* **92**, 657-671 (1995).
14.   Davies, M.J., Richardson, P.D., Woolf, N., Katz, D.R. & Mann, J. Risk of thrombosis in human atherosclerotic plaques: role of extracellular lipid, macrophage, and smooth muscle cell content. *Br Heart J* **69**, 377-381 (1993).
15.   Lee, R.T. & Libby, P. The unstable atheroma. *Arterioscler Thromb Vasc Biol* **17**, 1859-1867 (1997).
16.   Ross, R. & Klebanoff, S.J. The smooth muscle cell. I. In vivo synthesis of connective tissue proteins. *J Cell Biol* **50**, 159-171 (1971).
17.   Moreno, P.R., Falk, E., Palacios, I.F., Newell, J.B., Fuster, V. & Fallon, J.T. Macrophage infiltration in acute coronary syndromes. Implications for plaque rupture. *Circulation* **90**, 775-778 (1994).
18.   Constantinides, P. Infiltrates of activated mast cells at the site of coronary atheromatous erosion or rupture in myocardial infarction. *Circulation* **92**, 1083 (1995).
19.   Amento, E.P., Ehsani, N., Palmer, H. & Libby, P. Cytokines and growth factors positively and negatively regulate interstitial collagen gene expression in human vascular smooth muscle cells. *Arterioscler Thromb* **11**, 1223-1230 (1991).
20.   Quillard, T., Franck, G., Mawson, T., Folco, E. & Libby, P. Mechanisms of erosion of atherosclerotic plaques. *Curr Opin Lipidol* **28**, 434-441 (2017).

21. Hansson, G.K. Immune mechanisms in atherosclerosis. *Arterioscler Thromb Vasc Biol* **21**, 1876-1890 (2001).

22. Stöger, J.L., Gijbels, M.J., van der Velden, S., Manca, M., van der Loos, C.M., Biessen, E.A., Daemen, M.J., Lutgens, E. & de Winther, M.P. Distribution of macrophage polarization markers in human atherosclerosis. *Atherosclerosis* **225**, 461-468 (2012).

23. Winkels, H., Ehinger, E., Vassallo, M., Buscher, K., Dinh, H.Q., Kobiyama, K., Hamers, A.A.J., Cochain, C., Vafadarnejad, E., Saliba, A.E., Zernecke, A., Pramod, A.B., Ghosh, A.K., Anto Michel, N., Hoppe, N., Hilgendorf, I., Zirlik, A., Hedrick, C.C., Ley, K. & Wolf, D. Atlas of the Immune Cell Repertoire in Mouse Atherosclerosis Defined by Single-Cell RNA-Sequencing and Mass Cytometry. *Circ Res* **122**, 1675-1688 (2018).

24. Fernandez, D.M., Rahman, A.H., Fernandez, N.F., Chudnovskiy, A., Amir, E.D., Amadori, L., Khan, N.S., Wong, C.K., Shamailova, R., Hill, C.A., Wang, Z., Remark, R., Li, J.R., Pina, C., Faries, C., Awad, A.J., Moss, N., Bjorkegren, J.L.M., Kim-Schulze, S., Gnjatic, S., Ma'ayan, A., Mocco, J., Faries, P., Merad, M. & Giannarelli, C. Single-cell immune landscape of human atherosclerotic plaques. *Nat Med* **25**, 1576-1588 (2019).

25. Depuydt, M.A., Prange, K.H., Slenders, L., Örd, T., Elbersen, D., Boltjes, A., de Jager, S.C., Asselbergs, F.W., de Borst, G.J., Aavik, E., Lönnberg, T., Lutgens, E., Glass, C.K., den Ruijter, H.M., Kaikkonen, M.U., Bot, I., Slütter, B., van der Laan, S.W., Yla-Herttuala, S., Mokry, M., Kuiper, J., de Winther, M.P. & Pasterkamp, G. Microanatomy of the Human Atherosclerotic Plaque by Single-Cell Transcriptomics. *Circ Res* (2020).

26. Cochain, C., Vafadarnejad, E., Arampatzi, P., Pelisek, J., Winkels, H., Ley, K., Wolf, D., Saliba, A.E. & Zernecke, A. Single-Cell RNA-Seq Reveals the Transcriptional Landscape and Heterogeneity of Aortic Macrophages in Murine Atherosclerosis. *Circ Res* **122**, 1661-1674 (2018).

27. Willemsen, L. & de Winther, M.P. Macrophage subsets in atherosclerosis as defined by single-cell technologies. *J Pathol* **250**, 705-714 (2020).

28. Kim, K., Shim, D., Lee, J.S., Zaitsev, K., Williams, J.W., Kim, K.W., Jang, M.Y., Seok Jang, H., Yun, T.J., Lee, S.H., Yoon, W.K., Prat, A., Seidah, N.G., Choi, J., Lee, S.P., Yoon, S.H., Nam, J.W., Seong, J.K., Oh, G.T., Randolph, G.J., Artyomov, M.N., Cheong, C. & Choi, J.H. Transcriptome Analysis Reveals Nonfoamy Rather Than Foamy Plaque Macrophages Are Proinflammatory in Atherosclerotic Murine Models. *Circ Res* **123**, 1127-1142 (2018).

29. Moore, K.J., Sheedy, F.J. & Fisher, E.A. Macrophages in atherosclerosis: a dynamic balance. *Nat Rev Immunol* **13**, 709-721 (2013).

30. Frostegård, J., Ulfgren, A.K., Nyberg, P., Hedin, U., Swedenborg, J., Andersson, U. & Hansson, G.K. Cytokine expression in advanced human atherosclerotic plaques: dominance of pro-inflammatory (Th1) and macrophage-stimulating cytokines. *Atherosclerosis* **145**, 33-43 (1999).

31. Saigusa, R., Winkels, H. & Ley, K. T cell subsets and functions in atherosclerosis. *Nat Rev Cardiol* **17**, 387-401 (2020).

32. Kaartinen, M., Penttilä, A. & Kovanen, P.T. Mast cells in rupture-prone areas of human coronary atheromas produce and store TNF-alpha. *Circulation* **94**, 2787-2792 (1996).

33. Wolf, D. & Ley, K. Immunity and Inflammation in Atherosclerosis. *Circ Res* **124**, 315-327 (2019).

34. Hartwig, H., Silvestre Roig, C., Daemen, M., Lutgens, E. & Soehnlein, O. Neutrophils in atherosclerosis. A brief overview. *Hamostaseologie* **35**, 121-127 (2015).

35.   Caligiuri, G., Nicoletti, A., Poirier, B. & Hansson, G.K. Protective immunity against atherosclerosis carried by B cells of hypercholesterolemic mice. *J Clin Invest* **109**, 745-753 (2002).

36.   Major, A.S., Fazio, S. & Linton, M.F. B-lymphocyte deficiency increases atherosclerosis in LDL receptor-null mice. *Arterioscler Thromb Vasc Biol* **22**, 1892-1898 (2002).

37.   Kyaw, T., Tay, C., Khan, A., Dumouchel, V., Cao, A., To, K., Kehry, M., Dunn, R., Agrotis, A., Tipping, P., Bobik, A. & Toh, B.H. Conventional B2 B cell depletion ameliorates whereas its adoptive transfer aggravates atherosclerosis. *J Immunol* **185**, 4410-4419 (2010).

38.   Ait-Oufella, H., Herbin, O., Bouaziz, J.D., Binder, C.J., Uyttenhove, C., Laurans, L., Taleb, S., Van Vre, E., Esposito, B., Vilar, J., Sirvent, J., Van Snick, J., Tedgui, A., Tedder, T.F. & Mallat, Z. B cell depletion reduces the development of atherosclerosis in mice. *J Exp Med* **207**, 1579-1587 (2010).

39.   Sage, A.P., Tsiantoulas, D., Binder, C.J. & Mallat, Z. The role of B cells in atherosclerosis. *Nat Rev Cardiol* **16**, 180-196 (2019).

40.   Srikakulapu, P. & McNamara, C.A. B cells and atherosclerosis. *Am J Physiol Heart Circ Physiol* **312**, H1060-h1067 (2017).

41.   Muppidi, J.R., Arnon, T.I., Bronevetsky, Y., Veerapen, N., Tanaka, M., Besra, G.S. & Cyster, J.G. Cannabinoid receptor 2 positions and retains marginal zone B cells within the splenic marginal zone. *J Exp Med* **208**, 1941-1948 (2011).

42.   Hoffman, W., Lakkis, F.G. & Chalasani, G. B Cells, Antibodies, and More. *Clin J Am Soc Nephrol* **11**, 137-154 (2016).

43.   Weller, S., Braun, M.C., Tan, B.K., Rosenwald, A., Cordier, C., Conley, M.E., Plebani, A., Kumararatne, D.S., Bonnet, D., Tournilhac, O., Tchernia, G., Steiniger, B., Staudt, L.M., Casanova, J.L., Reynaud, C.A. & Weill, J.C. Human blood IgM "memory" B cells are circulating splenic marginal zone B cells harboring a prediversified immunoglobulin repertoire. *Blood* **104**, 3647-3654 (2004).

44.   Smith, K.G., Hewitson, T.D., Nossal, G.J. & Tarlinton, D.M. The phenotype and fate of the antibody-forming cells of the splenic foci. *Eur J Immunol* **26**, 444-448 (1996).

45.   Hayakawa, K., Hardy, R.R., Herzenberg, L.A. & Herzenberg, L.A. Progenitors for Ly-1 B cells are distinct from progenitors for other B cells. *J Exp Med* **161**, 1554-1568 (1985).

46.   Baumgarth, N. The double life of a B-1 cell: self-reactivity selects for protective effector functions. *Nat Rev Immunol* **11**, 34-46 (2011).

47.   Griffin, D.O., Holodick, N.E. & Rothstein, T.L. Human B1 cells in umbilical cord and adult peripheral blood express the novel phenotype CD20+ CD27+ CD43+ CD70. *J Exp Med* **208**, 67-80 (2011).

48.   Clark, M.R., Mandal, M., Ochiai, K. & Singh, H. Orchestrating B cell lymphopoiesis through interplay of IL-7 receptor and pre-B cell receptor signalling. *Nat Rev Immunol* **14**, 69-80 (2014).

49.   Pieper, K., Grimbacher, B. & Eibel, H. B-cell biology and development. *J Allergy Clin Immunol* **131**, 959-971 (2013).

50.   Hardy, R.R. & Hayakawa, K. B cell development pathways. *Annu Rev Immunol* **19**, 595-621 (2001).

51.   McLean, K.C. & Mandal, M. It Takes Three Receptors to Raise a B Cell. *Trends Immunol* **41**, 629-642 (2020).

52.   Melchers, F. Checkpoints that control B cell development. *J Clin Invest* **125**, 2203-2210 (2015).

53.   Hardy, R.R., Kincade, P.W. & Dorshkind, K. The protean nature of cells in the B lymphocyte lineage. *Immunity* **26**, 703-714 (2007).

54. Mandel, E.M. & Grosschedl, R. Transcription control of early B cell differentiation. *Curr Opin Immunol* **22**, 161-167 (2010).

55. Karasuyama, H., Kudo, A. & Melchers, F. The proteins encoded by the VpreB and lambda 5 pre-B cell-specific genes can associate with each other and with mu heavy chain. *J Exp Med* **172**, 969-972 (1990).

56. Winkler, T.H. & Mårtensson, I.L. The Role of the Pre-B Cell Receptor in B Cell Development, Repertoire Selection, and Tolerance. *Front Immunol* **9**, 2423 (2018).

57. Geisberger, R., Lamers, M. & Achatz, G. The riddle of the dual expression of IgM and IgD. *Immunology* **118**, 429-437 (2006).

58. Kiel, M.J., Yilmaz, O.H., Iwashita, T., Yilmaz, O.H., Terhorst, C. & Morrison, S.J. SLAM family receptors distinguish hematopoietic stem and progenitor cells and reveal endothelial niches for stem cells. *Cell* **121**, 1109-1121 (2005).

59. Pinho, S. & Frenette, P.S. Haematopoietic stem cell activity and interactions with the niche. *Nat Rev Mol Cell Biol* **20**, 303-320 (2019).

60. Sugiyama, T., Kohara, H., Noda, M. & Nagasawa, T. Maintenance of the hematopoietic stem cell pool by CXCL12-CXCR4 chemokine signaling in bone marrow stromal cell niches. *Immunity* **25**, 977-988 (2006).

61. Herzog, S., Hug, E., Meixlsperger, S., Paik, J.H., DePinho, R.A., Reth, M. & Jumaa, H. SLP-65 regulates immunoglobulin light chain gene recombination through the PI(3)K-PKB-Foxo pathway. *Nat Immunol* **9**, 623-631 (2008).

62. Herzog, S., Reth, M. & Jumaa, H. Regulation of B-cell proliferation and differentiation by pre-B-cell receptor signalling. *Nat Rev Immunol* **9**, 195-205 (2009).

63. Mandal, M., Okoreeh, M.K., Kennedy, D.E., Maienschein-Cline, M., Ai, J., McLean, K.C., Kaverina, N., Veselits, M., Aifantis, I., Gounari, F. & Clark, M.R. CXCR4 signaling directs Igk recombination and the molecular mechanisms of late B lymphopoiesis. *Nat Immunol* **20**, 1393-1403 (2019).

64. Batten, M., Groom, J., Cachero, T.G., Qian, F., Schneider, P., Tschopp, J., Browning, J.L. & Mackay, F. BAFF mediates survival of peripheral immature B lymphocytes. *J Exp Med* **192**, 1453-1466 (2000).

65. Petro, J.B., Gerstein, R.M., Lowe, J., Carter, R.S., Shinners, N. & Khan, W.N. Transitional type 1 and 2 B lymphocyte subsets are differentially responsive to antigen receptor signaling. *J Biol Chem* **277**, 48009-48019 (2002).

66. Pillai, S. & Cariappa, A. The follicular versus marginal zone B lymphocyte cell fate decision. *Nat Rev Immunol* **9**, 767-777 (2009).

67. Cariappa, A., Boboila, C., Moran, S.T., Liu, H., Shi, H.N. & Pillai, S. The recirculating B cell pool contains two functionally distinct, long-lived, posttransitional, follicular B cell populations. *J Immunol* **179**, 2270-2281 (2007).

68. Zhou, X. & Hansson, G.K. Detection of B cells and proinflammatory cytokines in atherosclerotic plaques of hypercholesterolaemic apolipoprotein E knockout mice. *Scand J Immunol* **50**, 25-30 (1999).

69. Moos, M.P., John, N., Gräbner, R., Nossmann, S., Günther, B., Vollandt, R., Funk, C.D., Kaiser, B. & Habenicht, A.J. The lamina adventitia is the major site of immune cell accumulation in standard chow-fed apolipoprotein E-deficient mice. *Arterioscler Thromb Vasc Biol* **25**, 2386-2391 (2005).

70. Tsiantoulas, D., Diehl, C.J., Witztum, J.L. & Binder, C.J. B cells and humoral immunity in atherosclerosis. *Circ Res* **114**, 1743-1756 (2014).

71. Tsiantoulas, D., Sage, A.P., Mallat, Z. & Binder, C.J. Targeting B cells in atherosclerosis: closing the gap from bench to bedside. *Arterioscler Thromb Vasc Biol* **35**, 296-302 (2015).

72. Centa, M., Jin, H., Hofste, L., Hellberg, S., Busch, A., Baumgartner, R., Verzaal, N.J., Lind Enoksson, S., Perisic Matic, L., Boddul, S.V., Atzler, D., Li, D.Y., Sun, C., Hansson, G.K., Ketelhuth, D.F.J., Hedin, U., Wermeling, F., Lutgens, E., Binder, C.J., Maegdesfessel, L. & Malin, S.G. Germinal Center-Derived Antibodies Promote Atherosclerosis Plaque Size and Stability. *Circulation* **139**, 2466-2482 (2019).

73. Oliver, A.M., Martin, F., Gartland, G.L., Carter, R.H. & Kearney, J.F. Marginal zone B cells exhibit unique activation, proliferative and immunoglobulin secretory responses. *Eur J Immunol* **27**, 2366-2374 (1997).

74. Nus, M., Sage, A.P., Lu, Y., Masters, L., Lam, B.Y.H., Newland, S., Weller, S., Tsiantoulas, D., Raffort, J., Marcus, D., Finigan, A., Kitt, L., Figg, N., Schirmbeck, R., Kneilling, M., Yeo, G.S.H., Binder, C.J., de la Pompa, J.L. & Mallat, Z. Marginal zone B cells control the response of follicular helper T cells to a high-cholesterol diet. *Nat Med* **23**, 601-610 (2017).

75. Kyaw, T., Tay, C., Krishnamurthi, S., Kanellakis, P., Agrotis, A., Tipping, P., Bobik, A. & Toh, B.H. B1a B lymphocytes are atheroprotective by secreting natural IgM that increases IgM deposits and reduces necrotic cores in atherosclerotic lesions. *Circ Res* **109**, 830-840 (2011).

76. Rosenfeld, S.M., Perry, H.M., Gonen, A., Prohaska, T.A., Srikakulapu, P., Grewal, S., Das, D., McSkimming, C., Taylor, A.M., Tsimikas, S., Bender, T.P., Witztum, J.L. & McNamara, C.A. B-1b Cells Secrete Atheroprotective IgM and Attenuate Atherosclerosis. *Circ Res* **117**, e28-39 (2015).

77. Hilgendorf, I., Theurl, I., Gerhardt, L.M., Robbins, C.S., Weber, G.F., Gonen, A., Iwamoto, Y., Degousee, N., Holderried, T.A., Winter, C., Zirlik, A., Lin, H.Y., Sukhova, G.K., Butany, J., Rubin, B.B., Witztum, J.L., Libby, P., Nahrendorf, M., Weissleder, R. & Swirski, F.K. Innate response activator B cells aggravate atherosclerosis by stimulating T helper-1 adaptive immunity. *Circulation* **129**, 1677-1687 (2014).

78. Robbins, C.S., Chudnovskiy, A., Rauch, P.J., Figueiredo, J.L., Iwamoto, Y., Gorbatov, R., Etzrodt, M., Weber, G.F., Ueno, T., van Rooijen, N., Mulligan-Kehoe, M.J., Libby, P., Nahrendorf, M., Pittet, M.J., Weissleder, R. & Swirski, F.K. Extramedullary hematopoiesis generates Ly-6C(high) monocytes that infiltrate atherosclerotic lesions. *Circulation* **125**, 364-374 (2012).

79. Strom, A.C., Cross, A.J., Cole, J.E., Blair, P.A., Leib, C., Goddard, M.E., Rosser, E.C., Park, I., Hultgårdh Nilsson, A., Nilsson, J., Mauri, C. & Monaco, C. B regulatory cells are increased in hypercholesterolaemic mice and protect from lesion development via IL-10. *Thromb Haemost* **114**, 835-847 (2015).

80. Weih, F., Gräbner, R., Hu, D., Beer, M. & Habenicht, A.J. Control of dichotomic innate and adaptive immune responses by artery tertiary lymphoid organs in atherosclerosis. *Front Physiol* **3**, 226 (2012).

81. Mohanta, S.K., Yin, C., Peng, L., Srikakulapu, P., Bontha, V., Hu, D., Weih, F., Weber, C., Gerdes, N. & Habenicht, A.J. Artery tertiary lymphoid organs contribute to innate and adaptive immune responses in advanced mouse atherosclerosis. *Circ Res* **114**, 1772-1787 (2014).

82. Yin, C., Mohanta, S.K., Srikakulapu, P., Weber, C. & Habenicht, A.J. Artery Tertiary Lymphoid Organs: Powerhouses of Atherosclerosis Immunity. *Front Immunol* **7**, 387 (2016).

83. Srikakulapu, P., Hu, D., Yin, C., Mohanta, S.K., Bontha, S.V., Peng, L., Beer, M., Weber, C., McNamara, C.A., Grassia, G., Maffia, P., Manz, R.A. & Habenicht, A.J. Artery Tertiary Lymphoid Organs Control Multilayered Territorialized Atherosclerosis B-Cell Responses in Aged ApoE-/- Mice. *Arterioscler Thromb Vasc Biol* **36**, 1174-1185 (2016).

84. Schwartz, C.J. & Mitchell, J.R. Cellular infiltration of the human arterial adventitia associated with atheromatous plaques. *Circulation* **26**, 73-78 (1962).

85. Houtkamp, M.A., de Boer, O.J., van der Loos, C.M., van der Wal, A.C. & Becker, A.E. Adventitial infiltrates associated with advanced atherosclerotic plaques: structural organization suggests generation of local humoral immune responses. *J Pathol* **193**, 263-269 (2001).

86. Rosenson, R.S. Statins in atherosclerosis: lipid-lowering agents with antioxidant capabilities. *Atherosclerosis* **173**, 1-12 (2004).

87. Abramson, J.D., Rosenberg, H.G., Jewell, N. & Wright, J.M. Should people at low risk of cardiovascular disease take a statin? *Bmj* **347**, f6123 (2013).

88. Collins, R., Reith, C., Emberson, J., Armitage, J., Baigent, C., Blackwell, L., Blumenthal, R., Danesh, J., Smith, G.D., DeMets, D., Evans, S., Law, M., MacMahon, S., Martin, S., Neal, B., Poulter, N., Preiss, D., Ridker, P., Roberts, I., Rodgers, A., Sandercock, P., Schulz, K., Sever, P., Simes, J., Smeeth, L., Wald, N., Yusuf, S. & Peto, R. Interpretation of the evidence for the efficacy and safety of statin therapy. *Lancet* **388**, 2532-2561 (2016).

89. Aday, A.W. & Ridker, P.M. Targeting Residual Inflammatory Risk: A Shifting Paradigm for Atherosclerotic Disease. *Front Cardiovasc Med* **6**, 16 (2019).

90. Ridker, P.M., Everett, B.M., Thuren, T., MacFadyen, J.G., Chang, W.H., Ballantyne, C., Fonseca, F., Nicolau, J., Koenig, W., Anker, S.D., Kastelein, J.J.P., Cornel, J.H., Pais, P., Pella, D., Genest, J., Cifkova, R., Lorenzatti, A., Forster, T., Kobalava, Z., Vida-Simiti, L., Flather, M., Shimokawa, H., Ogawa, H., Dellborg, M., Rossi, P.R.F., Troquay, R.P.T., Libby, P. & Glynn, R.J. Antiinflammatory Therapy with Canakinumab for Atherosclerotic Disease. *N Engl J Med* **377**, 1119-1131 (2017).

91. Stewart, J., Addy, K., Campbell, S. & Wilkinson, P. Primary prevention of cardiovascular disease: Updated review of contemporary guidance and literature. *JRSM Cardiovasc Dis* **9**, 2048004020949326 (2020).

92. Sipahi, I., Tuzcu, E.M., Wolski, K.E., Nicholls, S.J., Schoenhagen, P., Hu, B., Balog, C., Shishehbor, M., Magyar, W.A., Crowe, T.D., Kapadia, S. & Nissen, S.E. Beta-blockers and progression of coronary atherosclerosis: pooled analysis of 4 intravascular ultrasonography trials. *Ann Intern Med* **147**, 10-18 (2007).

93. Ittaman, S.V., VanWormer, J.J. & Rezkalla, S.H. The role of aspirin in the prevention of cardiovascular disease. *Clin Med Res* **12**, 147-154 (2014).

94. Porsch, F. & Binder, C.J. Impact of B-Cell-Targeted Therapies on Cardiovascular Disease. *Arterioscler Thromb Vasc Biol* **39**, 1705-1714 (2019).

95. Murphy, P.M., Baggiolini, M., Charo, I.F., Hébert, C.A., Horuk, R., Matsushima, K., Miller, L.H., Oppenheim, J.J. & Power, C.A. International union of pharmacology. XXII. Nomenclature for chemokine receptors. *Pharmacol Rev* **52**, 145-176 (2000).

96. Blanchet, X., Langer, M., Weber, C., Koenen, R.R. & von Hundelshausen, P. Touch of chemokines. *Front Immunol* **3**, 175 (2012).

97. Fernandez, E.J. & Lolis, E. Structure, function, and inhibition of chemokines. *Annu Rev Pharmacol Toxicol* **42**, 469-499 (2002).

98. Qin, L., Kufareva, I., Holden, L.G., Wang, C., Zheng, Y., Zhao, C., Fenalti, G., Wu, H., Han, G.W., Cherezov, V., Abagyan, R., Stevens, R.C. & Handel, T.M. Structural biology. Crystal structure of the chemokine receptor CXCR4 in complex with a viral chemokine. *Science* **347**, 1117-1122 (2015).

99. Wu, B., Chien, E.Y., Mol, C.D., Fenalti, G., Liu, W., Katritch, V., Abagyan, R., Brooun, A., Wells, P., Bi, F.C., Hamel, D.J., Kuhn, P., Handel, T.M., Cherezov, V. & Stevens, R.C. Structures of the CXCR4 chemokine GPCR with small-molecule and cyclic peptide antagonists. *Science* **330**, 1066-1071 (2010).

100. Rajagopalan, L. & Rajarathnam, K. Structural basis of chemokine receptor function--a model for binding affinity and ligand selectivity. *Biosci Rep* **26**, 325-339 (2006).

101. Thelen, M. Dancing to the tune of chemokines. *Nat Immunol* **2**, 129-134 (2001).

102. Stone, M.J., Hayward, J.A., Huang, C., Z, E.H. & Sanchez, J. Mechanisms of Regulation of the Chemokine-Receptor Network. *Int J Mol Sci* **18**(2017).

103. Muñoz, L.M., Lucas, P., Holgado, B.L., Barroso, R., Vega, B., Rodríguez-Frade, J.M. & Mellado, M. Receptor oligomerization: a pivotal mechanism for regulating chemokine function. *Pharmacol Ther* **131**, 351-358 (2011).

104. Wan, W. & Murphy, P.M. Regulation of atherogenesis by chemokines and chemokine receptors. *Arch Immunol Ther Exp (Warsz)* **61**, 1-14 (2013).

105. van der Vorst, E.P., Döring, Y. & Weber, C. Chemokines and their receptors in Atherosclerosis. *J Mol Med (Berl)* **93**, 963-971 (2015).

106. Zernecke, A. & Weber, C. Chemokines in atherosclerosis: proceedings resumed. *Arterioscler Thromb Vasc Biol* **34**, 742-750 (2014).

107. Tacke, F., Alvarez, D., Kaplan, T.J., Jakubzick, C., Spanbroek, R., Llodra, J., Garin, A., Liu, J., Mack, M., van Rooijen, N., Lira, S.A., Habenicht, A.J. & Randolph, G.J. Monocyte subsets differentially employ CCR2, CCR5, and CX3CR1 to accumulate within atherosclerotic plaques. *J Clin Invest* **117**, 185-194 (2007).

108. Soehnlein, O., Drechsler, M., Döring, Y., Lievens, D., Hartwig, H., Kemmerich, K., Ortega-Gómez, A., Mandl, M., Vijayan, S., Projahn, D., Garlichs, C.D., Koenen, R.R., Hristov, M., Lutgens, E., Zernecke, A. & Weber, C. Distinct functions of chemokine receptor axes in the atherogenic mobilization and recruitment of classical monocytes. *EMBO Mol Med* **5**, 471-481 (2013).

109. Landsman, L., Bar-On, L., Zernecke, A., Kim, K.W., Krauthgamer, R., Shagdarsuren, E., Lira, S.A., Weissman, I.L., Weber, C. & Jung, S. CX3CR1 is required for monocyte homeostasis and atherogenesis by promoting cell survival. *Blood* **113**, 963-972 (2009).

110. Huo, Y., Weber, C., Forlow, S.B., Sperandio, M., Thatte, J., Mack, M., Jung, S., Littman, D.R. & Ley, K. The chemokine KC, but not monocyte chemoattractant protein-1, triggers monocyte arrest on early atherosclerotic endothelium. *J Clin Invest* **108**, 1307-1314 (2001).

111. Drechsler, M., Megens, R.T., van Zandvoort, M., Weber, C. & Soehnlein, O. Hyperlipidemia-triggered neutrophilia promotes early atherosclerosis. *Circulation* **122**, 1837-1845 (2010).

112. Zernecke, A., Bot, I., Djalali-Talab, Y., Shagdarsuren, E., Bidzhekov, K., Meiler, S., Krohn, R., Schober, A., Sperandio, M., Soehnlein, O., Bornemann, J., Tacke, F., Biessen, E.A. & Weber, C. Protective role of CXC receptor 4/CXC ligand 12 unveils the importance of neutrophils in atherosclerosis. *Circ Res* **102**, 209-217 (2008).

113. Weber, C. Platelets and chemokines in atherosclerosis: partners in crime. *Circ Res* **96**, 612-616 (2005).

114. Kapurniotu, A., Gokce, O. & Bernhagen, J. The Multitasking Potential of Alarmins and Atypical Chemokines. *Front Med (Lausanne)* **6**, 3 (2019).

115. Degryse, B. & de Virgilio, M. The nuclear protein HMGB1, a new kind of chemokine? *FEBS Lett* **553**, 11-17 (2003).

116. Röhrl, J., Yang, D., Oppenheim, J.J. & Hehlgans, T. Human beta-defensin 2 and 3 and their mouse orthologs induce chemotaxis through interaction with CCR2. *J Immunol* **184**, 6688-6694 (2010).

117. Wakasugi, K. & Schimmel, P. Two distinct cytokines released from a human aminoacyl-tRNA synthetase. *Science* **284**, 147-151 (1999).

118. David, J.R. Delayed hypersensitivity in vitro: its mediation by cell-free substances formed by lymphoid cell-antigen interaction. *Proc Natl Acad Sci U S A* **56**, 72-77 (1966).

119. Bloom, B.R. & Bennett, B. Mechanism of a reaction in vitro associated with delayed-type hypersensitivity. *Science* **153**, 80-82 (1966).

120. Bernhagen, J., Mitchell, R.A., Calandra, T., Voelter, W., Cerami, A. & Bucala, R. Purification, bioactivity, and secondary structure analysis of mouse and human macrophage migration inhibitory factor (MIF). *Biochemistry* **33**, 14144-14155 (1994).

121. Pawig, L., Klasen, C., Weber, C., Bernhagen, J. & Noels, H. Diversity and Inter-Connections in the CXCR4 Chemokine Receptor/Ligand Family: Molecular Perspectives. *Front Immunol* **6**, 429 (2015).

122. Mühlhahn, P., Bernhagen, J., Czisch, M., Georgescu, J., Renner, C., Ross, A., Bucala, R. & Holak, T.A. NMR characterization of structure, backbone dynamics, and glutathione binding of the human macrophage migration inhibitory factor (MIF). *Protein Sci* **5**, 2095-2103 (1996).

123. Sun, H.W., Swope, M., Cinquina, C., Bedarkar, S., Bernhagen, J., Bucala, R. & Lolis, E. The subunit structure of human macrophage migration inhibitory factor: evidence for a trimer. *Protein Eng* **9**, 631-635 (1996).

124. Mischke, R., Kleemann, R., Brunner, H. & Bernhagen, J. Cross-linking and mutational analysis of the oligomerization state of the cytokine macrophage migration inhibitory factor (MIF). *FEBS Lett* **427**, 85-90 (1998).

125. Fan, C., Rajasekaran, D., Syed, M.A., Leng, L., Loria, J.P., Bhandari, V., Bucala, R. & Lolis, E.J. MIF intersubunit disulfide mutant antagonist supports activation of CD74 by endogenous MIF trimer at physiologic concentrations. *Proc Natl Acad Sci U S A* **110**, 10994-10999 (2013).

126. Merk, M., Mitchell, R.A., Endres, S. & Bucala, R. D-dopachrome tautomerase (D-DT or MIF-2): doubling the MIF cytokine family. *Cytokine* **59**, 10-17 (2012).

127. Calandra, T., Bernhagen, J., Mitchell, R.A. & Bucala, R. The macrophage is an important and previously unrecognized source of macrophage migration inhibitory factor. *J Exp Med* **179**, 1895-1902 (1994).

128. Nishihira, J., Koyama, Y. & Mizue, Y. Identification of macrophage migration inhibitory factor (MIF) in human vascular endothelial cells and its induction by lipopolysaccharide. *Cytokine* **10**, 199-205 (1998).

129. Chen, L., Yang, G., Zhang, X., Wu, J., Gu, Q., Wei, M., Yang, J., Zhu, Y., Wang, N. & Guan, Y. Induction of MIF expression by oxidized LDL via activation of NF-kappaB in vascular smooth muscle cells. *Atherosclerosis* **207**, 428-433 (2009).

130. Flieger, O., Engling, A., Bucala, R., Lue, H., Nickel, W. & Bernhagen, J. Regulated secretion of macrophage migration inhibitory factor is mediated by a non-classical pathway involving an ABC transporter. *FEBS Lett* **551**, 78-86 (2003).

131. Jankauskas, S.S., Wong, D.W.L., Bucala, R., Djudjaj, S. & Boor, P. Evolving complexity of MIF signaling. *Cell Signal* **57**, 76-88 (2019).

132. Tillmann, S., Bernhagen, J. & Noels, H. Arrest Functions of the MIF Ligand/Receptor Axes in Atherogenesis. *Front Immunol* **4**, 115 (2013).

133. Simons, D., Grieb, G., Hristov, M., Pallua, N., Weber, C., Bernhagen, J. & Steffens, G. Hypoxia-induced endothelial secretion of macrophage migration inhibitory factor and role in endothelial progenitor cell recruitment. *J Cell Mol Med* **15**, 668-678 (2011).

134. Ren, Y., Tsui, H.T., Poon, R.T., Ng, I.O., Li, Z., Chen, Y., Jiang, G., Lau, C., Yu, W.C., Bacher, M. & Fan, S.T. Macrophage migration inhibitory factor: roles in regulating tumor cell migration and expression of angiogenic factors in hepatocellular carcinoma. *Int J Cancer* **107**, 22-29 (2003).

135. Kleemann, R., Hausser, A., Geiger, G., Mischke, R., Burger-Kentischer, A., Flieger, O., Johannes, F.J., Roger, T., Calandra, T., Kapurniotu, A., Grell, M., Finkelmeier, D., Brunner, H. & Bernhagen, J. Intracellular action of the cytokine MIF to modulate AP-1 activity and the cell cycle through Jab1. *Nature* **408**, 211-216 (2000).

136. Wang, Y., An, R., Umanah, G.K., Park, H., Nambiar, K., Eacker, S.M., Kim, B., Bao, L., Harraz, M.M., Chang, C., Chen, R., Wang, J.E., Kam, T.I., Jeong, J.S., Xie, Z., Neifert, S., Qian, J., Andrabi, S.A., Blackshaw, S., Zhu, H., Song, H., Ming, G.L., Dawson, V.L. & Dawson, T.M. A nuclease that mediates cell death induced by DNA damage and poly(ADP-ribose) polymerase-1. *Science* **354**(2016).

137. Kleemann, R., Kapurniotu, A., Frank, R.W., Gessner, A., Mischke, R., Flieger, O., Jüttner, S., Brunner, H. & Bernhagen, J. Disulfide analysis reveals a role for macrophage migration inhibitory factor (MIF) as thiol-protein oxidoreductase. *J Mol Biol* **280**, 85-102 (1998).

138. Rosengren, E., Aman, P., Thelin, S., Hansson, C., Ahlfors, S., Björk, P., Jacobsson, L. & Rorsman, H. The macrophage migration inhibitory factor MIF is a phenylpyruvate tautomerase. *FEBS Lett* **417**, 85-88 (1997).

139. Kleemann, R., Mischke, R., Kapurniotu, A., Brunner, H. & Bernhagen, J. Specific reduction of insulin disulfides by macrophage migration inhibitory factor (MIF) with glutathione and dihydrolipoamide: potential role in cellular redox processes. *FEBS Lett* **430**, 191-196 (1998).

140. Swope, M., Sun, H.W., Blake, P.R. & Lolis, E. Direct link between cytokine activity and a catalytic site for macrophage migration inhibitory factor. *Embo j* **17**, 3534-3541 (1998).

141. Merk, M., Zierow, S., Leng, L., Das, R., Du, X., Schulte, W., Fan, J., Lue, H., Chen, Y., Xiong, H., Chagnon, F., Bernhagen, J., Lolis, E., Mor, G., Lesur, O. & Bucala, R. The D-dopachrome tautomerase (DDT) gene product is a cytokine and functional homolog of macrophage migration inhibitory factor (MIF). *Proc Natl Acad Sci U S A* **108**, E577-585 (2011).

142. Meyer-Siegler, K. & Hudson, P.B. Enhanced expression of macrophage migration inhibitory factor in prostatic adenocarcinoma metastases. *Urology* **48**, 448-452 (1996).

143. Calandra, T., Echtenacher, B., Roy, D.L., Pugin, J., Metz, C.N., Hültner, L., Heumann, D., Männel, D., Bucala, R. & Glauser, M.P. Protection from septic shock by neutralization of macrophage migration inhibitory factor. *Nat Med* **6**, 164-170 (2000).

144. Leech, M., Metz, C., Hall, P., Hutchinson, P., Gianis, K., Smith, M., Weedon, H., Holdsworth, S.R., Bucala, R. & Morand, E.F. Macrophage migration inhibitory factor in rheumatoid arthritis: evidence of proinflammatory function and regulation by glucocorticoids. *Arthritis Rheum* **42**, 1601-1608 (1999).

145. Bernhagen, J., Krohn, R., Lue, H., Gregory, J.L., Zernecke, A., Koenen, R.R., Dewor, M., Georgiev, I., Schober, A., Leng, L., Kooistra, T., Fingerle-Rowson, G., Ghezzi, P., Kleemann, R., McColl, S.R., Bucala, R., Hickey, M.J. & Weber, C. MIF is a noncognate ligand of CXC chemokine receptors in inflammatory and atherogenic cell recruitment. *Nat Med* **13**, 587-596 (2007).

146. Sauler, M., Bucala, R. & Lee, P.J. Role of macrophage migration inhibitory factor in age-related lung disease. *Am J Physiol Lung Cell Mol Physiol* **309**, L1-10 (2015).

147. Burger-Kentischer, A., Goebel, H., Seiler, R., Fraedrich, G., Schaefer, H.E., Dimmeler, S., Kleemann, R., Bernhagen, J. & Ihling, C. Expression of macrophage migration inhibitory factor in different stages of human atherosclerosis. *Circulation* **105**, 1561-1566 (2002).

148. Müller, II, Müller, K.A., Schönleber, H., Karathanos, A., Schneider, M., Jorbenadze, R., Bigalke, B., Gawaz, M. & Geisler, T. Macrophage migration inhibitory factor is enhanced in acute coronary syndromes and is associated with the inflammatory response. *PLoS One* **7**, e38376 (2012).

149. Lan, M.Y., Chang, Y.Y., Chen, W.H., Tseng, Y.L., Lin, H.S., Lai, S.L. & Liu, J.S. Association between MIF gene polymorphisms and carotid artery atherosclerosis. *Biochem Biophys Res Commun* **435**, 319-322 (2013).

150. Burger-Kentischer, A., Göbel, H., Kleemann, R., Zernecke, A., Bucala, R., Leng, L., Finkelmeier, D., Geiger, G., Schaefer, H.E., Schober, A., Weber, C., Brunner, H., Rütten, H., Ihling, C. & Bernhagen, J. Reduction of the aortic inflammatory response in spontaneous atherosclerosis by blockade of macrophage migration inhibitory factor (MIF). *Atherosclerosis* **184**, 28-38 (2006).

151. Pan, J.H., Sukhova, G.K., Yang, J.T., Wang, B., Xie, T., Fu, H., Zhang, Y., Satoskar, A.R., David, J.R., Metz, C.N., Bucala, R., Fang, K., Simon, D.I., Chapman, H.A., Libby, P. & Shi, G.P. Macrophage migration inhibitory factor deficiency impairs atherosclerosis in low-density lipoprotein receptor-deficient mice. *Circulation* **109**, 3149-3153 (2004).

152. Schmitz, C., Noels, H., El Bounkari, O., Straussfeld, E., Megens, R.T.A., Sternkopf, M., Alampour-Rajabi, S., Krammer, C., Tilstam, P.V., Gerdes, N., Bürger, C., Kapurniotu, A., Bucala, R., Jankowski, J., Weber, C. & Bernhagen, J. Mif-deficiency favors an atheroprotective autoantibody phenotype in atherosclerosis. *Faseb j* **32**, 4428-4443 (2018).

153. Schober, A., Bernhagen, J., Thiele, M., Zeiffer, U., Knarren, S., Roller, M., Bucala, R. & Weber, C. Stabilization of atherosclerotic plaques by blockade of macrophage migration inhibitory factor after vascular injury in apolipoprotein E-deficient mice. *Circulation* **109**, 380-385 (2004).

154. Amin, M.A., Haas, C.S., Zhu, K., Mansfield, P.J., Kim, M.J., Lackowski, N.P. & Koch, A.E. Migration inhibitory factor up-regulates vascular cell adhesion molecule-1 and intercellular adhesion molecule-1 via Src, PI3 kinase, and NFkappaB. *Blood* **107**, 2252-2261 (2006).

155. Baugh, J.A. & Bucala, R. Macrophage migration inhibitory factor. *Crit Care Med* **30**, S27-s35 (2002).

156. Atsumi, T., Nishihira, J., Makita, Z. & Koike, T. Enhancement of oxidised low-density lipoprotein uptake by macrophages in response to macrophage migration inhibitory factor. *Cytokine* **12**, 1553-1556 (2000).

157. Kong, Y.Z., Yu, X., Tang, J.J., Ouyang, X., Huang, X.R., Fingerle-Rowson, G., Bacher, M., Scher, L.A., Bucala, R. & Lan, H.Y. Macrophage migration inhibitory factor induces MMP-9 expression: implications for destabilization of human atherosclerotic plaques. *Atherosclerosis* **178**, 207-215 (2005).

158. Leng, L., Metz, C.N., Fang, Y., Xu, J., Donnelly, S., Baugh, J., Delohery, T., Chen, Y., Mitchell, R.A. & Bucala, R. MIF signal transduction initiated by binding to CD74. *J Exp Med* **197**, 1467-1476 (2003).

159. Mitchell, R.A., Metz, C.N., Peng, T. & Bucala, R. Sustained mitogen-activated protein kinase (MAPK) and cytoplasmic phospholipase A2 activation by macrophage migration inhibitory factor (MIF). Regulatory role in cell proliferation and glucocorticoid action. *J Biol Chem* **274**, 18100-18106 (1999).

160. Gore, Y., Starlets, D., Maharshak, N., Becker-Herman, S., Kaneyuki, U., Leng, L., Bucala, R. & Shachar, I. Macrophage migration inhibitory factor induces B cell survival by activation of a CD74-CD44 receptor complex. *J Biol Chem* **283**, 2784-2792 (2008).

161. Miller, E.J., Li, J., Leng, L., McDonald, C., Atsumi, T., Bucala, R. & Young, L.H. Macrophage migration inhibitory factor stimulates AMP-activated protein kinase in the ischaemic heart. *Nature* **451**, 578-582 (2008).

162. Lue, H., Dewor, M., Leng, L., Bucala, R. & Bernhagen, J. Activation of the JNK signalling pathway by macrophage migration inhibitory factor (MIF) and dependence on CXCR4 and CD74. *Cell Signal* **23**, 135-144 (2011).

163. Addison, C.L., Daniel, T.O., Burdick, M.D., Liu, H., Ehlert, J.E., Xue, Y.Y., Buechi, L., Walz, A., Richmond, A. & Strieter, R.M. The CXC chemokine receptor 2, CXCR2, is the putative receptor for ELR+ CXC chemokine-induced angiogenic activity. *J Immunol* **165**, 5269-5277 (2000).

164. Li, A., Dubey, S., Varney, M.L., Dave, B.J. & Singh, R.K. IL-8 directly enhanced endothelial cell survival, proliferation, and matrix metalloproteinases production and regulated angiogenesis. *J Immunol* **170**, 3369-3376 (2003).

165. Akhtar, S., Gremse, F., Kiessling, F., Weber, C. & Schober, A. CXCL12 promotes the stabilization of atherosclerotic lesions mediated by smooth muscle progenitor cells in Apoe-deficient mice. *Arterioscler Thromb Vasc Biol* **33**, 679-686 (2013).

166. Hu, X., Dai, S., Wu, W.J., Tan, W., Zhu, X., Mu, J., Guo, Y., Bolli, R. & Rokosh, G. Stromal cell derived factor-1 alpha confers protection against myocardial ischemia/reperfusion injury: role of the cardiac stromal cell derived factor-1 alpha CXCR4 axis. *Circulation* **116**, 654-663 (2007).

167. Döring, Y., Noels, H., van der Vorst, E.P.C., Neideck, C., Egea, V., Drechsler, M., Mandl, M., Pawig, L., Jansen, Y., Schröder, K., Bidzhekov, K., Megens, R.T.A., Theelen, W., Klinkhammer, B.M., Boor, P., Schurgers, L., van Gorp, R., Ries, C., Kusters, P.J.H., van der Wal, A., Hackeng, T.M., Gäbel, G., Brandes, R.P., Soehnlein, O., Lutgens, E., Vestweber, D., Teupser, D., Holdt, L.M., Rader, D.J., Saleheen, D. & Weber, C. Vascular CXCR4 Limits Atherosclerosis by Maintaining Arterial Integrity: Evidence From Mouse and Human Studies. *Circulation* **136**, 388-403 (2017).

168. Tarnowski, M., Grymula, K., Liu, R., Tarnowska, J., Drukala, J., Ratajczak, J., Mitchell, R.A., Ratajczak, M.Z. & Kucia, M. Macrophage migration inhibitory factor is secreted by rhabdomyosarcoma cells, modulates tumor metastasis by binding to CXCR4 and CXCR7 receptors and inhibits recruitment of cancer-associated fibroblasts. *Mol Cancer Res* **8**, 1328-1343 (2010).

169. Rajagopal, S., Kim, J., Ahn, S., Craig, S., Lam, C.M., Gerard, N.P., Gerard, C. & Lefkowitz, R.J. Beta-arrestin- but not G protein-mediated signaling by the "decoy" receptor CXCR7. *Proc Natl Acad Sci U S A* **107**, 628-632 (2010).

170. Alampour-Rajabi, S., El Bounkari, O., Rot, A., Müller-Newen, G., Bachelerie, F., Gawaz, M., Weber, C., Schober, A. & Bernhagen, J. MIF interacts with CXCR7 to promote receptor internalization, ERK1/2 and ZAP-70 signaling, and lymphocyte chemotaxis. *Faseb j* **29**, 4497-4511 (2015).

171. Weber, C., Kraemer, S., Drechsler, M., Lue, H., Koenen, R.R., Kapurniotu, A., Zernecke, A. & Bernhagen, J. Structural determinants of MIF functions in CXCR2-mediated inflammatory and atherogenic leukocyte recruitment. *Proc Natl Acad Sci U S A* **105**, 16278-16283 (2008).

172. Xu, L., Li, Y., Li, D., Xu, P., Tian, S., Sun, H., Liu, H. & Hou, T. Exploring the binding mechanisms of MIF to CXCR2 using theoretical approaches. *Phys Chem Chem Phys* **17**, 3370-3382 (2015).

173. Kraemer, S., Lue, H., Zernecke, A., Kapurniotu, A., Andreetto, E., Frank, R., Lennartz, B., Weber, C. & Bernhagen, J. MIF-chemokine receptor interactions in atherogenesis are dependent on an N-loop-based 2-site binding mechanism. *Faseb j* **25**, 894-906 (2011).

174. Lacy, M., Kontos, C., Brandhofer, M., Hille, K., Gröning, S., Sinitski, D., Bourilhon, P., Rosenberg, E., Krammer, C., Thavayogarajah, T., Pantouris, G., Bakou, M., Weber, C., Lolis, E., Bernhagen, J. & Kapurniotu, A. Identification of an Arg-Leu-Arg tripeptide that contributes to the binding interface between the cytokine MIF and the chemokine receptor CXCR4. *Sci Rep* **8**, 5171 (2018).

175. Rajasekaran, D., Gröning, S., Schmitz, C., Zierow, S., Drucker, N., Bakou, M., Kohl, K., Mertens, A., Lue, H., Weber, C., Xiao, A., Luker, G., Kapurniotu, A., Lolis, E. & Bernhagen, J. Macrophage Migration Inhibitory Factor-CXCR4 Receptor Interactions: EVIDENCE FOR PARTIAL ALLOSTERIC AGONISM IN COMPARISON WITH CXCL12 CHEMOKINE. *J Biol Chem* **291**, 15881-15895 (2016).

176. Krammer, C., Kontos, C., Dewor, M., Hille, K., Dalla Volta, B., El Bounkari, O., Taş, K., Sinitski, D., Brandhofer, M., Megens, R.T.A., Weber, C., Schultz, J.R., Bernhagen, J. & Kapurniotu, A. A MIF-derived cyclopeptide that inhibits MIF binding and atherogenic signaling via the chemokine receptor CXCR2. *Chembiochem* (2020).

177. Starlets, D., Gore, Y., Binsky, I., Haran, M., Harpaz, N., Shvidel, L., Becker-Herman, S., Berrebi, A. & Shachar, I. Cell-surface CD74 initiates a signaling cascade leading to cell proliferation and survival. *Blood* **107**, 4807-4816 (2006).

178. Shachar, I. & Flavell, R.A. Requirement for invariant chain in B cell maturation and function. *Science* **274**, 106-108 (1996).

179. Matza, D., Wolstein, O., Dikstein, R. & Shachar, I. Invariant chain induces B cell maturation by activating a TAF(II)105-NF-kappaB-dependent transcription program. *J Biol Chem* **276**, 27203-27206 (2001).

180. Matza, D., Kerem, A., Medvedovsky, H., Lantner, F. & Shachar, I. Invariant chain-induced B cell differentiation requires intramembrane proteolytic release of the cytosolic domain. *Immunity* **17**, 549-560 (2002).

181. Klasen, C., Ziehm, T., Huber, M., Asare, Y., Kapurniotu, A., Shachar, I., Bernhagen, J. & El Bounkari, O. LPS-mediated cell surface expression of CD74 promotes the proliferation of B cells in response to MIF. *Cell Signal* **46**, 32-42 (2018).

182. Lapter, S., Ben-David, H., Sharabi, A., Zinger, H., Telerman, A., Gordin, M., Leng, L., Bucala, R., Shachar, I. & Mozes, E. A role for the B-cell CD74/macrophage migration inhibitory factor pathway in the immunomodulation of systemic lupus erythematosus by a therapeutic tolerogenic peptide. *Immunology* **132**, 87-95 (2011).

183. Klasen, C., Ohl, K., Sternkopf, M., Shachar, I., Schmitz, C., Heussen, N., Hobeika, E., Levit-Zerdoun, E., Tenbrock, K., Reth, M., Bernhagen, J. & El Bounkari, O. MIF promotes B cell chemotaxis through the receptors CXCR4 and CD74 and ZAP-70 signaling. *J Immunol* **192**, 5273-5284 (2014).

184. Rijvers, L., Melief, M.J., van der Vuurst de Vries, R.M., Stéphant, M., van Langelaar, J., Wierenga-Wolf, A.F., Hogervorst, J.M., Geurts-Moespot, A.J., Sweep, F., Hintzen, R.Q. & van Luijn, M.M. The macrophage migration inhibitory factor pathway in human B cells is tightly controlled and dysregulated in multiple sclerosis. *Eur J Immunol* **48**, 1861-1871 (2018).

185. Bach, J.P., Rinn, B., Meyer, B., Dodel, R. & Bacher, M. Role of MIF in inflammation and tumorigenesis. *Oncology* **75**, 127-133 (2008).

186. Guda, M.R., Rashid, M.A., Asuthkar, S., Jalasutram, A., Caniglia, J.L., Tsung, A.J. & Velpula, K.K. Pleiotropic role of macrophage migration inhibitory factor in cancer. *Am J Cancer Res* **9**, 2760-2773 (2019).

187. Sinitski, D., Kontos, C., Krammer, C., Asare, Y., Kapurniotu, A. & Bernhagen, J. Macrophage Migration Inhibitory Factor (MIF)-Based Therapeutic Concepts in Atherosclerosis and Inflammation. *Thromb Haemost* **119**, 553-566 (2019).

188. Kok, T., Wasiel, A.A., Cool, R.H., Melgert, B.N., Poelarends, G.J. & Dekker, F.J. Small-molecule inhibitors of macrophage migration inhibitory factor (MIF) as an emerging class of therapeutics for immune disorders. *Drug Discov Today* **23**, 1910-1918 (2018).

189. Trivedi-Parmar, V. & Jorgensen, W.L. Advances and Insights for Small Molecule Inhibition of Macrophage Migration Inhibitory Factor. *J Med Chem* **61**, 8104-8119 (2018).

190. Ouertatani-Sakouhi, H., El-Turk, F., Fauvet, B., Cho, M.K., Pinar Karpinar, D., Le Roy, D., Dewor, M., Roger, T., Bernhagen, J., Calandra, T., Zweckstetter, M. & Lashuel, H.A. Identification and characterization of novel classes of macrophage migration inhibitory factor (MIF) inhibitors with distinct mechanisms of action. *J Biol Chem* **285**, 26581-26598 (2010).

191. Garai, J. & Lóránd, T. Macrophage migration inhibitory factor (MIF) tautomerase inhibitors as potential novel anti-inflammatory agents: current developments. *Curr Med Chem* **16**, 1091-1114 (2009).

192. Schinagl, A., Kerschbaumer, R.J., Sabarth, N., Douillard, P., Scholz, P., Voelkel, D., Hollerweger, J.C., Goettig, P., Brandstetter, H., Scheiflinger, F. & Thiele, M. Role of the Cysteine 81 Residue of Macrophage Migration Inhibitory Factor as a Molecular Redox Switch. *Biochemistry* **57**, 1523-1532 (2018).

193. Mahalingam, D., Patel, M.R., Sachdev, J.C., Hart, L.L., Halama, N., Ramanathan, R.K., Sarantopoulos, J., Völkel, D., Youssef, A., de Jong, F.A. & Tsimberidou, A.M. Phase I study of imalumab (BAX69), a fully human recombinant antioxidized macrophage migration inhibitory factor antibody in advanced solid tumours. *Br J Clin Pharmacol* **86**, 1836-1848 (2020).

194. Lubetsky, J.B., Dios, A., Han, J., Aljabari, B., Ruzsicska, B., Mitchell, R., Lolis, E. & Al-Abed, Y. The tautomerase active site of macrophage migration inhibitory factor is a potential target for discovery of novel anti-inflammatory agents. *J Biol Chem* **277**, 24976-24982 (2002).

195. Al-Abed, Y., Dabideen, D., Aljabari, B., Valster, A., Messmer, D., Ochani, M., Tanovic, M., Ochani, K., Bacher, M., Nicoletti, F., Metz, C., Pavlov, V.A., Miller, E.J. & Tracey, K.J. ISO-1 binding to the tautomerase active site of MIF inhibits its pro-inflammatory activity and increases survival in severe sepsis. *J Biol Chem* **280**, 36541-36544 (2005).

196. Rajasekaran, D., Zierow, S., Syed, M., Bucala, R., Bhandari, V. & Lolis, E.J. Targeting distinct tautomerase sites of D-DT and MIF with a single molecule for inhibition of neutrophil lung recruitment. *Faseb j* **28**, 4961-4971 (2014).

197. Pantouris, G., Syed, M.A., Fan, C., Rajasekaran, D., Cho, T.Y., Rosenberg, E.M., Jr., Bucala, R., Bhandari, V. & Lolis, E.J. An Analysis of MIF Structural Features that Control Functional Activation of CD74. *Chem Biol* **22**, 1197-1205 (2015).

198. Berkova, Z., Tao, R.H. & Samaniego, F. Milatuzumab - a promising new immunotherapeutic agent. *Expert Opin Investig Drugs* **19**, 141-149 (2010).

199. De Clercq, E. The bicyclam AMD3100 story. *Nat Rev Drug Discov* **2**, 581-587 (2003).

200. Henninot, A., Collins, J.C. & Nuss, J.M. The Current State of Peptide Drug Discovery: Back to the Future? *J Med Chem* **61**, 1382-1414 (2018).

201. Assis, D.N., Leng, L., Du, X., Zhang, C.K., Grieb, G., Merk, M., Garcia, A.B., McCrann, C., Chapiro, J., Meinhardt, A., Mizue, Y., Nikolic-Paterson, D.J., Bernhagen, J., Kaplan, M.M., Zhao, H., Boyer, J.L. & Bucala, R. The role of macrophage migration inhibitory factor in autoimmune liver disease. *Hepatology* **59**, 580-591 (2014).

202. Vandenbark, A.A., Meza-Romero, R., Benedek, G., Andrew, S., Huan, J., Chou, Y.K., Buenafe, A.C., Dahan, R., Reiter, Y., Mooney, J.L., Offner, H. & Burrows, G.G. A novel regulatory pathway for autoimmune disease: binding of partial MHC class II constructs to monocytes reduces CD74 expression and induces both specific and bystander T-cell tolerance. *J Autoimmun* **40**, 96-110 (2013).

203. Liang, X. CXCR4, inhibitors and mechanisms of action. *Chem Biol Drug Des* **72**, 97-110 (2008).

204. Ezerzer, C., Dolgin, M., Skovorodnikova, J. & Harris, N. Chemokine receptor-derived peptides as multi-target drug leads for the treatment of inflammatory diseases. *Peptides* **30**, 1296-1305 (2009).

205. Zernecke, A., Bernhagen, J. & Weber, C. Macrophage migration inhibitory factor in cardiovascular disease. *Circulation* **117**, 1594-1602 (2008).

206. Grieb, G., Merk, M., Bernhagen, J. & Bucala, R. Macrophage migration inhibitory factor (MIF): a promising biomarker. *Drug News Perspect* **23**, 257-264 (2010).

207. Bloom, J., Sun, S. & Al-Abed, Y. MIF, a controversial cytokine: a review of structural features, challenges, and opportunities for drug development. *Expert Opin Ther Targets* **20**, 1463-1475 (2016).

208. Tilstam, P.V., Qi, D., Leng, L., Young, L. & Bucala, R. MIF family cytokines in cardiovascular diseases and prospects for precision-based therapeutics. *Expert Opin Ther Targets* **21**, 671-683 (2017).

209. Geraci, F., Saha, I. & Bianchini, M. Editorial: RNA-Seq Analysis: Methods, Applications and Challenges. *Front Genet* **11**, 220 (2020).

210. Wang, Z., Gerstein, M. & Snyder, M. RNA-Seq: a revolutionary tool for transcriptomics. *Nat Rev Genet* **10**, 57-63 (2009).

211. Single-cell transcriptomics of 20 mouse organs creates a Tabula Muris. *Nature* **562**, 367-372 (2018).

212. Suntsova, M., Gaifullin, N., Allina, D., Reshetun, A., Li, X., Mendeleeva, L., Surin, V., Sergeeva, A., Spirin, P., Prassolov, V., Morgan, A., Garazha, A., Sorokin, M. & Buzdin, A. Atlas of RNA sequencing profiles for normal human tissues. *Sci Data* **6**, 36 (2019).

213. Costa, V., Aprile, M., Esposito, R. & Ciccodicola, A. RNA-Seq and human complex diseases: recent accomplishments and future perspectives. *Eur J Hum Genet* **21**, 134-142 (2013).

214. Virani, S.S., Alonso, A., Benjamin, E.J., Bittencourt, M.S., Callaway, C.W., Carson, A.P., Chamberlain, A.M., Chang, A.R., Cheng, S., Delling, F.N., Djousse, L., Elkind, M.S.V., Ferguson, J.F., Fornage, M., Khan, S.S., Kissela, B.M., Knutson, K.L., Kwan, T.W., Lackland, D.T., Lewis, T.T., Lichtman, J.H., Longenecker, C.T., Loop, M.S., Lutsey, P.L., Martin, S.S., Matsushita, K., Moran, A.E., Mussolino, M.E., Perak, A.M., Rosamond, W.D., Roth, G.A., Sampson, U.K.A., Satou, G.M., Schroeder, E.B., Shah, S.H., Shay, C.M., Spartano, N.L., Stokes, A., Tirschwell, D.L., VanWagner, L.B., Tsao, C.W., American Heart Association Council on, E., Prevention Statistics, C. & Stroke Statistics, S. Heart Disease and Stroke Statistics-2020 Update: A Report From the American Heart Association. *Circulation* **141**, e139-e596 (2020).

215. Ross, R. Atherosclerosis--an inflammatory disease. *N. Engl. J. Med.* **340**, 115-126 (1999).

216. Hansson, G.K. & Hermansson, A. The immune system in atherosclerosis. *Nat Immunol* **12**, 204-212 (2011).

217. Libby, P. Inflammation in atherosclerosis. *Nature* **420**, 868-874 (2002).

218. Charo, I.F. & Taubman, M.B. Chemokines in the pathogenesis of vascular disease. *Circ Res* **95**, 858-866 (2004).

219. Müller, I.I., Müller, K.A.L., Schönleber, H., Karathanos, A., Schneider, M., Jorbenadze, R., Bigalke, B., Gawaz, M. & Geisler, T. Macrophage migration inhibitory factor is enhanced in acute coronary syndromes and is associated with the inflammatory response. *PLoS ONE* **7**, e38376 (2012).

220. Calandra, T. & Roger, T. Macrophage migration inhibitory factor: a regulator of innate immunity. *Nat Rev Immunol* **3**, 791-800 (2003).

221. Tillmann, S., Bernhagen, J. & Noels, H. Arrest Functions of the MIF Ligand/Receptor Axes in Atherogenesis. *Frontiers in immunology* **4**, 115 (2013).

222. Baugh, J.A., Chitnis, S., Donnelly, S.C., Monteiro, J., Lin, X., Plant, B.J., Wolfe, F., Gregersen, P.K. & Bucala, R. A functional promoter polymorphism in the macrophage migration inhibitory factor (MIF) gene associated with disease severity in rheumatoid arthritis. *Genes Immun.* **3**, 170-176 (2002).

223. Adamali, H., Armstrong, M.E., McLaughlin, A.M., Cooke, G., McKone, E., Costello, C.M., Gallagher, C.G., Leng, L., Baugh, J.A., Fingerle-Rowson, G., Bucala, R.J., McLoughlin, P. & Donnelly, S.C. Macrophage migration inhibitory factor enzymatic activity, lung inflammation, and cystic fibrosis. *American journal of respiratory and critical care medicine* **186**, 162-169 (2012).

224. Wirtz, T.H., Fischer, P., Backhaus, C., Bergmann, I., Brandt, E.F., Heinrichs, D., Koenen, M.T., Schneider, K.M., Eggermann, T., Kurth, I., Stoppe, C., Bernhagen, J., Bruns, T., Fischer, J., Berg, T., Trautwein, C. & Berres, M.L. Genetic Variants in the Promoter Region of the Macrophage Migration Inhibitory Factor are Associated with the Severity of Hepatitis C Virus-Induced Liver Fibrosis. *Int J Mol Sci* **20**(2019).

225. Wirtz, T.H., Tillmann, S., Strussmann, T., Kraemer, S., Heemskerk, J.W., Grottke, O., Gawaz, M., von Hundelshausen, P. & Bernhagen, J. Platelet-derived MIF: a novel platelet chemokine with distinct recruitment properties. *Atherosclerosis* **239**, 1-10 (2015).

226. Asare, Y., Schmitt, M. & Bernhagen, J. The vascular biology of macrophage migration inhibitory factor (MIF). Expression and effects in inflammation, atherogenesis and angiogenesis. *Thromb Haemost* **109**, 391-398 (2013).

227. Head, T., Daunert, S. & Goldschmidt-Clermont, P.J. The Aging Risk and Atherosclerosis: A Fresh Look at Arterial Homeostasis. *Front Genet* **8**, 216 (2017).

228. Liberale, L., Montecucco, F., Tardif, J.C., Libby, P. & Camici, G.G. Inflamm-ageing: the role of inflammation in age-dependent cardiovascular disease. *Eur Heart J* **41**, 2974-2982 (2020).

229. Nakashima, Y., Plump, A.S., Raines, E.W., Breslow, J.L. & Ross, R. ApoE-deficient mice develop lesions of all phases of atherosclerosis throughout the arterial tree. *Arterioscler Thromb* **14**, 133-140 (1994).

230. Fox, J., Barthold, S., Davisson, M., Newcomer, C., Quimby, F. & Smith, A. *The Mouse in Biomedical Research*, (Elsevier, 2007).

231. Tyrrell, D.J. & Goldstein, D.R. Ageing and atherosclerosis: vascular intrinsic and extrinsic factors and potential role of IL-6. *Nat Rev Cardiol*, 1-11 (2020).

232. Akhavanpoor, M., Gleissner, C.A., Akhavanpoor, H., Lasitschka, F., Doesch, A.O., Katus, H.A. & Erbel, C. Adventitial tertiary lymphoid organ classification in human atherosclerosis. *Cardiovasc Pathol* **32**, 8-14 (2018).

233. Fingerle-Rowson, G., Petrenko, O., Metz, C.N., Forsthuber, T.G., Mitchell, R., Huss, R., Moll, U., Muller, W. & Bucala, R. The p53-dependent effects of macrophage migration inhibitory factor revealed by gene targeting. *Proc Natl Acad Sci U S A* **100**, 9354-9359 (2003).

234. Chen, Z., Sakuma, M., Zago, A.C., Zhang, X., Shi, C., Leng, L., Mizue, Y., Bucala, R. & Simon, D. Evidence for a role of macrophage migration inhibitory factor in vascular disease. *Arterioscler. Thromb. Vasc. Biol.* **24**, 709-714 (2004).

235. Ma, H., Wang, J., Thomas, D.P., Tong, C., Leng, L., Wang, W., Merk, M., Zierow, S., Bernhagen, J., Ren, J., Bucala, R. & Li, J. Impaired macrophage migration inhibitory factor-AMP-activated protein kinase activation and ischemic recovery in the senescent heart. *Circulation* **122**, 282-292 (2010).

236. Campbell, K.A., Lipinski, M.J., Doran, A.C., Skaflen, M.D., Fuster, V. & McNamara, C.A. Lymphocytes and the adventitial immune response in atherosclerosis. *Circ Res* **110**, 889-900 (2012).

237. Hu, D., Mohanta, S.K., Yin, C., Peng, L., Ma, Z., Srikakulapu, P., Grassia, G., MacRitchie, N., Dever, G., Gordon, P., Burton, F.L., Ialenti, A., Sabir, S.R., McInnes, I.B., Brewer, J.M., Garside, P., Weber, C., Lehmann, T., Teupser, D., Habenicht, L., Beer, M., Grabner, R., Maffia, P., Weih, F. & Habenicht, A.J. Artery Tertiary Lymphoid Organs Control Aorta Immunity and Protect against Atherosclerosis via Vascular Smooth Muscle Cell Lymphotoxin beta Receptors. *Immunity* **42**, 1100-1115 (2015).

238. Tyrrell, D.J. & Goldstein, D.R. Ageing and atherosclerosis: vascular intrinsic and extrinsic factors and potential role of IL-6. *Nat Rev Cardiol* **18**, 58-68 (2021).

239. Liu, D., Richardson, G., Benli, F.M., Park, C., de Souza, J.V., Bronowska, A.K. & Spyridopoulos, I. Inflammageing in the cardiovascular system: mechanisms, emerging targets, and novel therapeutic strategies. *Clin Sci (Lond)* **134**, 2243-2262 (2020).

240. Smykiewicz, P., Segiet, A., Keag, M. & Zera, T. Proinflammatory cytokines and ageing of the cardiovascular-renal system. *Mech Ageing Dev* **175**, 35-45 (2018).

241. Rammos, C., Hendgen-Cotta, U.B., Pohl, J., Totzeck, M., Luedike, P., Schulze, V.T., Kelm, M. & Rassaf, T. Modulation of circulating macrophage migration inhibitory factor in the elderly. *Biomed Res Int* **2014**, 582586 (2014).

242. Rammos, C., Hendgen-Cotta, U.B., Deenen, R., Pohl, J., Stock, P., Hinzmann, C., Kelm, M. & Rassaf, T. Age-related vascular gene expression profiling in mice. *Mech Ageing Dev* **135**, 15-23 (2014).

243. Trott, D.W., Henson, G.D., Ho, M.H.T., Allison, S.A., Lesniewski, L.A. & Donato, A.J. Age-related arterial immune cell infiltration in mice is attenuated by caloric restriction or voluntary exercise. *Exp Gerontol* **109**, 99-107 (2018).

244. Trott, D.W. & Fadel, P.J. Inflammation as a mediator of arterial ageing. *Exp Physiol* **104**, 1455-1471 (2019).

245. Du, W., Wong, C., Song, Y., Shen, H., Mori, D., Rotllan, N., Price, N., Dobrian, A.D., Meng, H., Kleinstein, S.H., Fernandez-Hernando, C. & Goldstein, D.R. Age-associated vascular inflammation promotes monocytosis during atherogenesis. *Aging Cell* **15**, 766-777 (2016).

246. Mitchell, R.A., Liao, H., Chesney, J., Fingerle-Rowson, G., Baugh, J., David, J. & Bucala, R. Macrophage migration inhibitory factor (MIF) sustains macrophage proinflammatory function by inhibiting p53: Regulatory role in the innate immune response. *Proc. Natl. Acad. Sci. USA* **99**, 345-350 (2002).

247. Djudjaj, S., Lue, H., Rong, S., Papasotiriou, M., Klinkhammer, B.M., Zok, S., Klaener, O., Braun, G.S., Lindenmeyer, M.T., Cohen, C.D., Bucala, R., Tittel, A.P., Kurts, C., Moeller, M.J., Floege, J., Ostendorf, T., Bernhagen, J. & Boor, P. Macrophage Migration Inhibitory Factor Mediates Proliferative GN via CD74. *J Am Soc Nephrol* **27**, 1650-1664 (2016).

248. Ohta, S., Misawa, A., Fukaya, R., Inoue, S., Kanemura, Y., Okano, H., Kawakami, Y. & Toda, M. Macrophage migration inhibitory factor (MIF) promotes cell survival and proliferation of neural stem/progenitor cells. *J Cell Sci* **125**, 3210-3220 (2012).

249. Aw, D., Hilliard, L., Nishikawa, Y., Cadman, E.T., Lawrence, R.A. & Palmer, D.B. Disorganization of the splenic microanatomy in ageing mice. *Immunology* **148**, 92-101 (2016).

250. Masters, A.R., Jellison, E.R., Puddington, L., Khanna, K.M. & Haynes, L. Attrition of T Cell Zone Fibroblastic Reticular Cell Number and Function in Aged Spleens. *Immunohorizons* **2**, 155-163 (2018).

251. Lefebvre, J.S., Maue, A.C., Eaton, S.M., Lanthier, P.A., Tighe, M. & Haynes, L. The aged microenvironment contributes to the age-related functional defects of CD4 T cells in mice. *Aging Cell* **11**, 732-740 (2012).

252. Moos, M.P., John, N., Grabner, R., Nossmann, S., Gunther, B., Vollandt, R., Funk, C.D., Kaiser, B. & Habenicht, A.J. The lamina adventitia is the major site of immune cell accumulation in standard chow-fed apolipoprotein E-deficient mice. *Arterioscler Thromb Vasc Biol* **25**, 2386-2391 (2005).

253. Stranford, S. & Ruddle, N.H. Follicular dendritic cells, conduits, lymphatic vessels, and high endothelial venules in tertiary lymphoid organs: Parallels with lymph node stroma. *Front Immunol* **3**, 350 (2012).

254. Ridker, P.M., Everett, B.M., Thuren, T., MacFadyen, J.G., Chang, W.H., Ballantyne, C., Fonseca, F., Nicolau, J., Koenig, W., Anker, S.D., Kastelein, J.J.P., Cornel, J.H., Pais, P., Pella, D., Genest, J., Cifkova, R., Lorenzatti, A., Forster, T., Kobalava, Z., Vida-Simiti, L., Flather, M., Shimokawa, H., Ogawa, H., Dellborg, M., Rossi, P.R.F., Troquay, R.P.T., Libby, P., Glynn, R.J. & Group, C.T. Antiinflammatory Therapy with Canakinumab for Atherosclerotic Disease. *N Engl J Med* **377**, 1119-1131 (2017).

255. Kontos, C., El Bounkari, O., Krammer, C., Sinitski, D., Hille, K., Zan, C., Yan, G., Wang, S., Gao, Y., Brandhofer, M., Megens, R.T.A., Hoffmann, A., Pauli, J., Asare, Y., Gerra, S., Bourilhon, P., Leng, L., Eckstein, H.H., Kempf, W.E., Pelisek, J., Gokce, O., Maegdefessel, L., Bucala, R., Dichgans, M., Weber, C., Kapurniotu, A. & Bernhagen, J. Designed CXCR4 mimic acts as a soluble chemokine receptor that blocks atherogenic inflammation by agonist-specific targeting. *Nat Commun* **11**, 5981 (2020).

256. Averdunk, L., Bernhagen, J., Fehnle, K., Surowy, H., Ludecke, H.J., Mucha, S., Meybohm, P., Wieczorek, D., Leng, L., Marx, G., Leaf, D.E., Zarbock, A., Zacharowski, K., On Behalf Of The, R.S.C., Bucala, R. & Stoppe, C. The Macrophage Migration Inhibitory Factor (MIF) Promoter Polymorphisms (rs3063368, rs755622) Predict Acute Kidney Injury and Death after Cardiac Surgery. *J Clin Med* **9**(2020).

257. Murphy, K. & Weaver, C. *Janeway's Immunobiology*, (Norton and Company, 2016).

258. Rolink, A., Grawunder, U., Winkler, T.H., Karasuyama, H. & Melchers, F. IL-2 receptor alpha chain (CD25, TAC) expression defines a crucial stage in pre-B cell development. *Int Immunol* **6**, 1257-1264 (1994).

259. Hardy, R.R., Carmack, C.E., Shinton, S.A., Kemp, J.D. & Hayakawa, K. Resolution and characterization of pro-B and pre-pro-B cell stages in normal mouse bone marrow. *J Exp Med* **173**, 1213-1225 (1991).

260. Rolink, A. & Melchers, F. B-cell development in the mouse. *Immunol Lett* **54**, 157-161 (1996).

261. Osmond, D.G. Proliferation kinetics and the lifespan of B cells in central and peripheral lymphoid organs. *Curr Opin Immunol* **3**, 179-185 (1991).

262. Tung, J.W., Mrazek, M.D., Yang, Y., Herzenberg, L.A. & Herzenberg, L.A. Phenotypically distinct B cell development pathways map to the three B cell lineages in the mouse. *Proc Natl Acad Sci U S A* **103**, 6293-6298 (2006).

263. Hystad, M.E., Myklebust, J.H., Bø, T.H., Sivertsen, E.A., Rian, E., Forfang, L., Munthe, E., Rosenwald, A., Chiorazzi, M., Jonassen, I., Staudt, L.M. & Smeland, E.B. Characterization of early stages of human B cell development by gene expression profiling. *J Immunol* **179**, 3662-3671 (2007).

264. Painter, M.W., Davis, S., Hardy, R.R., Mathis, D. & Benoist, C. Transcriptomes of the B and T lineages compared by multiplatform microarray profiling. *J Immunol* **186**, 3047-3057 (2011).

265. Lee, R., Munro, S., Knutson, T., LaRue, R., L., H.-H. & Farrar, M. Single-cell analysis of developing B cells reveals dynamic gene expression networks that govern B cell development and transformation. *biorxiv* (2020).

266. Tokoyoda, K., Egawa, T., Sugiyama, T., Choi, B.I. & Nagasawa, T. Cellular niches controlling B lymphocyte behavior within bone marrow during development. *Immunity* **20**, 707-718 (2004).

267. Nagasawa, T., Hirota, S., Tachibana, K., Takakura, N., Nishikawa, S., Kitamura, Y., Yoshida, N., Kikutani, H. & Kishimoto, T. Defects of B-cell lymphopoiesis and bone-marrow myelopoiesis in mice lacking the CXC chemokine PBSF/SDF-1. *Nature* **382**, 635-638 (1996).

268. Zou, Y.R., Kottmann, A.H., Kuroda, M., Taniuchi, I. & Littman, D.R. Function of the chemokine receptor CXCR4 in haematopoiesis and in cerebellar development. *Nature* **393**, 595-599 (1998).

269. von Freeden-Jeffry, U., Vieira, P., Lucian, L.A., McNeil, T., Burdach, S.E. & Murray, R. Lymphopenia in interleukin (IL)-7 gene-deleted mice identifies IL-7 as a nonredundant cytokine. *J Exp Med* **181**, 1519-1526 (1995).

270. Peschon, J.J., Morrissey, P.J., Grabstein, K.H., Ramsdell, F.J., Maraskovsky, E., Gliniak, B.C., Park, L.S., Ziegler, S.F., Williams, D.E., Ware, C.B., Meyer, J.D. & Davison, B.L. Early lymphocyte expansion is severely impaired in interleukin 7 receptor-deficient mice. *J Exp Med* **180**, 1955-1960 (1994).

271. Sapoznikov, A., Pewzner-Jung, Y., Kalchenko, V., Krauthgamer, R., Shachar, I. & Jung, S. Perivascular clusters of dendritic cells provide critical survival signals to B cells in bone marrow niches. *Nat Immunol* **9**, 388-395 (2008).

272. Dobin, A., Davis, C.A., Schlesinger, F., Drenkow, J., Zaleski, C., Jha, S., Batut, P., Chaisson, M. & Gingeras, T.R. STAR: ultrafast universal RNA-seq aligner. *Bioinformatics* **29**, 15-21 (2013).

273. Butler, A., Hoffman, P., Smibert, P., Papalexi, E. & Satija, R. Integrating single-cell transcriptomic data across different conditions, technologies, and species. *Nat Biotechnol* **36**, 411-420 (2018).

274. Wickham, H. *Ggplot2 : elegrant graphics for data analysis*, (Springer International Publishing, 2016).

275. Yu, G., Wang, L.G., Han, Y. & He, Q.Y. clusterProfiler: an R package for comparing biological themes among gene clusters. *Omics* **16**, 284-287 (2012).

276. Macosko, E.Z., Basu, A., Satija, R., Nemesh, J., Shekhar, K., Goldman, M., Tirosh, I., Bialas, A.R., Kamitaki, N., Martersteck, E.M., Trombetta, J.J., Weitz, D.A., Sanes, J.R., Shalek, A.K., Regev, A. & McCarroll, S.A. Highly Parallel Genome-wide Expression Profiling of Individual Cells Using Nanoliter Droplets. *Cell* **161**, 1202-1214 (2015).

277. Bowman, E.P., Campbell, J.J., Soler, D., Dong, Z., Manlongat, N., Picarella, D., Hardy, R.R. & Butcher, E.C. Developmental switches in chemokine response profiles during B cell differentiation and maturation. *J Exp Med* **191**, 1303-1318 (2000).

278. Stein, J.V. & Nombela-Arrieta, C. Chemokine control of lymphocyte trafficking: a general overview. *Immunology* **116**, 1-12 (2005).

279. Li, Y.S., Wasserman, R., Hayakawa, K. & Hardy, R.R. Identification of the earliest B lineage stage in mouse bone marrow. *Immunity* **5**, 527-535 (1996).

280. Noviski, M., Mueller, J.L., Satterthwaite, A., Garrett-Sinha, L.A., Brombacher, F. & Zikherman, J. IgM and IgD B cell receptors differentially respond to endogenous antigens and control B cell fate. *Elife* **7**(2018).

281. Allman, D., Lindsley, R.C., DeMuth, W., Rudd, K., Shinton, S.A. & Hardy, R.R. Resolution of three nonproliferative immature splenic B cell subsets reveals multiple selection points during peripheral B cell maturation. *J Immunol* **167**, 6834-6840 (2001).

282. Allman, D. & Pillai, S. Peripheral B cell subsets. *Curr Opin Immunol* **20**, 149-157 (2008).

283. Goldstein, L.D., Chen, Y.J., Wu, J., Chaudhuri, S., Hsiao, Y.C., Schneider, K., Hoi, K.H., Lin, Z., Guerrero, S., Jaiswal, B.S., Stinson, J., Antony, A., Pahuja, K.B., Seshasayee, D., Modrusan, Z., Hötzel, I. & Seshagiri, S. Massively parallel single-cell B-cell receptor sequencing enables rapid discovery of diverse antigen-reactive antibodies. *Commun Biol* **2**, 304 (2019).

284. Canzar, S., Neu, K.E., Tang, Q., Wilson, P.C. & Khan, A.A. BASIC: BCR assembly from single cells. *Bioinformatics* **33**, 425-427 (2017).

285. Rizzetto, S., Koppstein, D.N.P., Samir, J., Singh, M., Reed, J.H., Cai, C.H., Lloyd, A.R., Eltahla, A.A., Goodnow, C.C. & Luciani, F. B-cell receptor reconstruction from single-cell RNA-seq with VDJPuzzle. *Bioinformatics* **34**, 2846-2847 (2018).

286. Afik, S., Raulet, G. & Yosef, N. Reconstructing B-cell receptor sequences from short-read single-cell RNA sequencing with BRAPeS. *Life Sci Alliance* **2**(2019).

287. Lindeman, I., Emerton, G., Mamanova, L., Snir, O., Polanski, K., Qiao, S.W., Sollid, L.M., Teichmann, S.A. & Stubbington, M.J.T. BraCeR: B-cell-receptor reconstruction and clonality inference from single-cell RNA-seq. *Nat Methods* **15**, 563-565 (2018).

288. Kleiman, E., Salyakina, D., De Heusch, M., Hoek, K.L., Llanes, J.M., Castro, I., Wright, J.A., Clark, E.S., Dykxhoorn, D.M., Capobianco, E., Takeda, A., Renauld, J.C. & Khan, W.N. Distinct Transcriptomic Features are Associated with Transitional and Mature B-Cell Populations in the Mouse Spleen. *Front Immunol* **6**, 30 (2015).

289. Allman, D., Li, J. & Hardy, R.R. Commitment to the B lymphoid lineage occurs before DH-JH recombination. *J Exp Med* **189**, 735-740 (1999).

290. Aurrand-Lions, M. & Mancini, S.J.C. Murine Bone Marrow Niches from Hematopoietic Stem Cells to B Cells. *Int J Mol Sci* **19**(2018).

291. Jensen, C.T., Lang, S., Somasundaram, R., Soneji, S. & Sigvardsson, M. Identification of Stage-Specific Surface Markers in Early B Cell Development Provides Novel Tools for Identification of Progenitor Populations. *J Immunol* **197**, 1937-1944 (2016).

292. Heng, T.S. & Painter, M.W. The Immunological Genome Project: networks of gene expression in immune cells. *Nat Immunol* **9**, 1091-1094 (2008).

293. Addo, R.K., Heinrich, F., Heinz, G.A., Schulz, D., Sercan-Alp, Ö., Lehmann, K., Tran, C.L., Bardua, M., Matz, M., Löhning, M., Hauser, A.E., Kruglov, A., Chang, H.D., Durek, P., Radbruch, A. & Mashreghi, M.F. Single-cell transcriptomes of murine bone marrow stromal cells reveal niche-associated heterogeneity. *Eur J Immunol* **49**, 1372-1379 (2019).

294. Tikhonova, A.N., Dolgalev, I., Hu, H., Sivaraj, K.K., Hoxha, E., Cuesta-Domínguez, Á., Pinho, S., Akhmetzyanova, I., Gao, J., Witkowski, M., Guillamot, M., Gutkin, M.C., Zhang, Y., Marier, C., Diefenbach, C., Kousteni, S., Heguy, A., Zhong, H., Fooksman, D.R., Butler, J.M., Economides, A., Frenette, P.S., Adams, R.H., Satija, R., Tsirigos, A. & Aifantis, I. The bone marrow microenvironment at single-cell resolution. *Nature* **569**, 222-228 (2019).

295. Baccin, C., Al-Sabah, J., Velten, L., Helbling, P.M., Grünschläger, F., Hernández-Malmierca, P., Nombela-Arrieta, C., Steinmetz, L.M., Trumpp, A. & Haas, S. Combined single-cell and spatial transcriptomics reveal the molecular, cellular and spatial bone marrow niche organization. *Nat Cell Biol* **22**, 38-48 (2020).

296. Stein, M., Dütting, S., Mougiakakos, D., Bösl, M., Fritsch, K., Reimer, D., Urbanczyk, S., Steinmetz, T., Schuh, W., Bozec, A., Winkler, T.H., Jäck, H.M. & Mielenz, D. A defined metabolic state in pre B cells governs B-cell development and is counterbalanced by Swiprosin-2/EFhd1. *Cell Death Differ* **24**, 1239-1252 (2017).

297.	Heizmann, B., Kastner, P. & Chan, S. Ikaros is absolutely required for pre-B cell differentiation by attenuating IL-7 signals. *J Exp Med* **210**, 2823-2832 (2013).
298.	Park, H., Staehling, K., Tsang, M., Appleby, M.W., Brunkow, M.E., Margineantu, D., Hockenbery, D.M., Habib, T., Liggitt, H.D., Carlson, G. & Iritani, B.M. Disruption of Fnip1 reveals a metabolic checkpoint controlling B lymphocyte development. *Immunity* **36**, 769-781 (2012).
299.	Gallagher, E., Enzler, T., Matsuzawa, A., Anzelon-Mills, A., Otero, D., Holzer, R., Janssen, E., Gao, M. & Karin, M. Kinase MEKK1 is required for CD40-dependent activation of the kinases Jnk and p38, germinal center formation, B cell proliferation and antibody production. *Nat Immunol* **8**, 57-63 (2007).
300.	Nordlund, P. & Reichard, P. Ribonucleotide reductases. *Annu Rev Biochem* **75**, 681-706 (2006).
301.	Eklund, H., Uhlin, U., Färnegårdh, M., Logan, D.T. & Nordlund, P. Structure and function of the radical enzyme ribonucleotide reductase. *Prog Biophys Mol Biol* **77**, 177-268 (2001).
302.	Tanaka, H., Arakawa, H., Yamaguchi, T., Shiraishi, K., Fukuda, S., Matsui, K., Takei, Y. & Nakamura, Y. A ribonucleotide reductase gene involved in a p53-dependent cell-cycle checkpoint for DNA damage. *Nature* **404**, 42-49 (2000).
303.	Tang, H., Yang, P., Yang, X., Peng, S., Hu, X. & Bao, G. Growth factor receptor bound protein-7 regulates proliferation, cell cycle, and mitochondrial apoptosis of thyroid cancer cells via MAPK/ERK signaling. *Mol Cell Biochem* **472**, 209-218 (2020).
304.	Anderson, M.S. & Miller, J. Invariant chain can function as a chaperone protein for class II major histocompatibility complex molecules. *Proc Natl Acad Sci U S A* **89**, 2282-2286 (1992).
305.	Nagasawa, T. Microenvironmental niches in the bone marrow required for B-cell development. *Nat Rev Immunol* **6**, 107-116 (2006).

Appendix A: Publication III

The data presented as part of this section is not published yet, but a manuscript for the submission to the cardiovascular journal *Basic Research in Cardiology* is in final preparation.

Aging leads to loss of atheroprotection in *Mif*-deficient atherosclerotic mice

Christine Krammer[1], Bishan Yang[1], Sabrina Reichl[1], Verena Bolini[1] Corinna Schmitz[1,2], Heidi Noels[2,3], Aphrodite Kapurniotu[4], Christian Weber[5,6,7,3], Sarajo Mohanta[5], Jürgen Bernhagen[1,5,6,*]

[1]Chair of Vascular Biology, Institute for Stroke and Dementia Research (ISD), LMU University Hospital, Ludwig-Maximilians-Universität (LMU) München, 81377 Munich, Germany; [2]Institute for Molecular Cardiovascular Research (IMCAR), University Hospital Aachen, Rheinish-Westphalian Technical University (RWTH) Aachen University, 52074 Aachen, Germany; [3]Cardiovascular Research Institute Maastricht (CARIM), Maastricht University, 6229 Maastricht, The Netherlands; [4]Division of Peptide Biochemistry, TUM School of Life Sciences, Technische Universität München (TUM); [5]Institute for Cardiovascular Prevention, LMU University Hospital, Ludwig-Maximilians-Universität (LMU) München, 80336 Munich, Germany; [6]Munich Cluster for Systems Neurology (SyNergy), 81377 Munich, Germany; [7]Munich Heart Alliance, 80802 Munich, Germany.

* Last authorship and correspondence:
Professor Jürgen Bernhagen, PhD
Chair of Vascular Biology
Institute for Stroke and Dementia Research (ISD)
Ludwig-Maximilians-University (LMU) Munich
Feodor-Lynen-Straße 17,
81377 Munich, Germany
Tel.: 0049-89 4400 - 46151
E-Mail: juergen.bernhagen@med.uni-muenchen.de

Abstract

Atherosclerosis is a lipid-mediated chronic inflammatory condition of our arteries and the main underlying pathology of myocardial infarction and stroke. Pathogenesis is age-dependent, but the mechanistic links between disease progression, age, and atherogenic cytokines and chemokines are incompletely understood. Here, we studied the chemokine-like inflammatory cytokine macrophage migration inhibitory factor (MIF) in atherogenic *Apoe*$^{-/-}$ mice across different stages of aging and cholesterol-rich high-fat diet (HFD). MIF promotes atherosclerosis by mediating atherogenic monocyte and T-cell recruitment, amplifying lesional inflammation and suppressing atheroprotective B-cell responses. However, age-related links between atherogenesis and MIF and its role in advanced atherosclerosis in highly aged mice have not been explored. We compared effects of global *Mif*-gene-deficiency in 30-, 42-, and 48-week-old *Apoe*$^{-/-}$ mice on HFD for 24, 36, or 42 weeks, respectively, and in 52-week-old mice on a 6-week HFD. Our data reveal a regio-specific atheroprotective phenotype of *Mif*-deficiency in the 30/24-week-old group. Intriguingly, atheroprotection was lost in the highly aged 48/42- and 52/6-week-old groups, suggesting that atheroprotection by *Mif*-deletion is age-dependent. We identify a combination of mechanisms that parallel this phenotype: i) lesional atheroprotective Trem2$^+$ macrophage numbers are reduced in aged *Mif*-deficient mice; ii) *Mif*-deficiency favors formation of B-cell-rich atheroprotective stage-2 ATLOs in the 30/24-week-old group, but not at an advanced age; and iii) atheroprotective plasma anti-oxLDL-IgM antibody levels are decreased in aged *Mif*-deficient mice. Our study establishes a link between the atypical chemokine MIF and age-related changes in atherogenesis and identifies mechanisms that should be considered when developing MIF-directed approaches in advanced atherosclerosis.

Introduction

Cardiovascular diseases (CVDs) such as myocardial infarction or ischemic stroke are the most common underlying causes of mortality and incidence risk has steadily increased over the last decades. Disease pathology has been associated with multiple co-morbidities and risk factors, such as hypertension, type 2 diabetes, or metabolic syndrome that are further impaired by diet and lifestyle changes and increasingly manifest in an aging population[5,214]. Atherosclerosis is a lipid-mediated inflammatory condition of the medium and large arterial vasculature and has been recognized as the main underlying pathology of CVDs. Atherosclerosis may get initiated early in life and progressively develops over years and decades and is typically clinically symptomatic in middle and

late adulthood. Initially triggered by endothelial dysfunction and oxidized low density lipoprotein (oxLDL) uptake, lipid and inflammatory cell deposits in the arterial vessel wall lead to the formation of atheromatous plaques. Lesion formation involves oxLDL-mediated foam cell formation and abundant leukocyte infiltration, a process orchestrated by selectins and adhesion molecules upregulated on the inflamed endothelium as well as by endothelial-deposited chemokines and their receptors and integrins expressed on the infiltrating inflammatory cells. Cytokines and chemokines also amplify vascular inflammation through a variety of pathways. Together, this leads to increased intima-media thickening, wall remodeling, and limited arterial blood flow, but also eventually necrotic core formation, plaque destabilization, and thrombus formation, consequences which may result in severe adverse clinical outcomes such as myocardial infarction or stroke[215-218].

In addition to classical atherogenic chemokines such as CCL2 or CXCL1/8, atypical chemokines (ACKs) have been importantly associated with the atherogenic inflammatory cascade. Atypical chemokines have chemokine-like properties and engage in high-affinity interactions with classical chemokine receptors but lack classifying structural features of *bona fide* chemokines such as an *N*-terminal CC- or CXC-motif[114]. Macrophage migration inhibitory factor (MIF) is an evolutionarily conserved pleiotropic inflammatory cytokine and prototypical ACK with a potent proatherogenic activity spectrum. MIF is overexpressed in human carotid artery plaques[147] and circulating MIF levels have been associated with coronary artery disease (CAD), suggesting that MIF is critically involved in CVDs[187,205,219]. It is broadly expressed, but its secretion mainly occurs from immune cells including T cells and monocytes, as well as endothelial cells, smooth muscle cells (SMCs), and platelets[114,220]. MIF expression is triggered by atherogenic stimulation with inflammatory cytokines, oxLDL, or hypoxia[187,221]. A polymorphism in the CATT microsatellite repeat of the MIF promotor region is associated with MIF expression levels in several human inflammatory and autoimmune diseases and correlates with a susceptibility for carotid artery atherosclerosis (CAA)[149,222-224]. MIF induces signaling via its receptor CD74/invariant chain, but its proatherogenic activities are mainly mediated by non-cognate signaling via the CXC chemokine receptors CXCR2/4. This drives the atherogenic recruitment of monocytes, neutrophils, T cells, and platelets[145,221,225], and promotes foam cell formation, vascular chemokine and adhesion molecule expression, and arterial wall remodeling[147,153,226].

There is a wealth of evidence from *in vivo* models, suggesting a causal role of MIF in atherosclerosis. *Mif*-gene knockout in hyperlipidemic *Ldl receptor*-deficient (*Ldlr*$^{-/-}$) mice[145,151] or antibody-mediated blockade of MIF in *Apolipoprotein e*-deficient (*Apoe*$^{-/-}$)

mice that were subjected to a high-fat diet (HFD)[150,153] lead to decreased luminal monocyte adhesion, lower plaque macrophage counts, attenuated lesion formation, and increased plaque stability. More recently, Schmitz et *al.*[152] investigated *Mif*-gene deficiency in HFD-fed *Apoe*$^{-/-}$ mice and revealed a site-specific atheroprotective phenotype in the brachiocephalic artery (BCA) and abdominal aorta, but not in other regions of the vascular bed. Moreover, this study provided initial hints about a re-localization of adventitial B cells into cluster-like structures in *Mif*-deficient *Apoe*$^{-/-}$ mice, but not *Mif*-expressing *Apoe*$^{-/-}$ control mice.

Atherosclerosis is an age-dependent pathology driven by chronic inflammation, which becomes clinically symptomatic primarily in advanced stages in aged patients[227]. In fact, the tight causal connection between chronic inflammation and aging in CVDs has also been coined "inflamm-aging"[228]. In the *Apoe*$^{-/-}$ mouse model of atherosclerosis, the development of advanced atheromatous plaques similar to those in humans can be recapitulated within 12-24 weeks of HFD[229], but this and similar models don't fully mirror the advanced and late stage vessel phenotypes and clinical manifestations observed in humans, and atherogenic mice at an advanced age of >32 weeks, which would be equivalent to an age span of >50 years in humans (https://www.jax.org/research-and-faculty/research-labs/the-harrison-lab/gerontology/life-span-as-a-biomarker;[230]), have been investigated rather rarely. Furthermore, while studies on the impact of aging in atherosclerosis have identified contributing factors such as dysregulated cytokines and chemokines or vascular mitochondrial dysfunction[231], the underlying regulatory mechanisms and the details of their interplay with disease progression have remained incompletely understood. Interestingly, artery (or adventitial) tertiary lymphoid organs (ATLOs) have emerged as atherosclerosis-relevant lymphoid clusters with disease-modulating activity[81,82]. ATLOs are adventitial B- and T-lymphocyte-rich cell clusters with a lymphoid organ-like structure, which, in the *Apoe*$^{-/-}$ mouse model, are observed to develop in 52-78-week-old mice[81]. They have been suggested to especially control the B-cell response in aged atherosclerotic mice[83]. Not much is currently known about the formation and significance of ATLOs in human atherosclerotic disease[232]. Overall, these observations highlight the important link between aging and the dysregulation of the immune and inflammatory response in atherosclerosis. However, age-related effects of MIF activity or the *Mif* gene knockout in atherosclerosis have not been studied.

Here we sought to characterize age-related effects of MIF in advanced stages of atherosclerosis. *Mif*-gene deletion was studied in aged *Apoe*$^{-/-}$ mice by comparing lesion formation, leukocyte profiles and systemic inflammation between *Mif*$^{-/-}$ *Apoe*$^{-/-}$ and *Apoe*$^{-/-}$ mice that were on HFD for 24, 36 and 42 weeks, corresponding to an age of 30, 42, and

48 weeks, respectively, as well as in 52-week-old mice on HFD for 6 weeks. These age/HFD groups are hereinafter termed the: 30/24-, 42/36-, 48/42-, and 52/6-week-groups. The impact of B cells was investigated by an in-depth analysis of peri-adventitial cell clusters and antibody profiles directed against oxLDL. We confirm the regio-specific atheroprotective impact of *Mif*-deficiency in the BCA and abdominal aorta in 30-week-old *Apoe$^{-/-}$* mice on HFD for 24 weeks, i.e. the 30/24-week group. In contrast, the site-specific atheroprotective effect was lost in the 48/42-week group as well as in the 52/6-week group. This was accompanied by MIF- and age-dependent changes in plaque immune cells, peri-adventitial B-cell clusters, and atheroprotective natural IgM antibodies. Together, our study for the first time establishes a causal link between the atypical chemokine MIF and age-related changes in atherosclerotic pathology and shows that a combination of mechanisms is responsible for lost atheroprotection in *Mif*-deleted aged atherogenic *Apoe$^{-/-}$* mice. The results may be important when considering MIF-directed approaches against advanced atherosclerosis in aged individuals.

Materials and Methods

Chemicals, buffers, and miscellaneous reagents

Miscellaneous reagents were purchased from Sigma Aldrich/Merck (Darmstadt, Germany), VWR International GmbH (Darmstadt, Germany), Carl Roth GmbH (Karlsruhe, Germany), and Ratiopharm (Ulm, Germany) and were of the highest quality available.

Mice

Atherosclerosis-prone *Apolipoprotein e*-deficient (*Apoe$^{-/-}$*) mice and *Apoe$^{-/-}$Mif$^{-/-}$* mice were in the C57BL/6-J background. *Apoe$^{-/-}$* mice were received from Charles River Laboratories (Sulzfeld, Germany) and were propagated in the experimental animal husbandry of the Center for Stroke and Dementia Research (CSD). Global *Mif* gene-deficient mice (*Mif$^{-/-}$*) were generated by Dr. Fingerle-Rowson and Prof. Richard Bucala and have been reported on before[152,233]. For the generation of *Mif$^{-/-}$Apoe$^{-/-}$* mice, *Mif$^{-/-}$* mice were backcrossed with *Apoe$^{-/-}$* mice for more than 10 generations. Animal experiments were authorized by the local authorities (animal ethics approval ROB-55.2-2532.Vet_02-18-040) and were conducted in consistency with the German animal protection law. Animals were sacrificed under anesthesia with a mixture of midazolam (5 mg/ml), medetomidine and fentanyl (MMF).

Western-type high-fat diet (HFD)

Gender-matched mice (females) received a regular chow diet (SNIFF Spezialdiäten GmbH, Soest, Germany) until 6 weeks of age and then were subjected to a cholesterol-rich ('Western type') diet (HFD) containing 21.2% total fat and 0.2% cholesterol (TD88137, SNIFF Spezialdiäten GmbH, Soest, Germany) for 24, 36, or 42 weeks. Mice aged for 52 weeks received the HFD only in the last 6 weeks before the end of the experiment.

Isolation of blood, organs, and vessels

Blood collection was accomplished by cardiac puncture into ethylene diamine tetra-acetic acid (EDTA)-containing tubes (Sarstedt, Nümbrecht, Germany) and hematologic parameters were subsequently analyzed using the Scil Vet abc Plus+ Blood Analyzer (Scil Animal Car Company GmbH, Viernheim, Germany). For plasma preparation, the blood was centrifuged at 400 x g for 15 min at 4°C. Plasma samples were subsequently preserved in liquid nitrogen and kept at -80°C. The circulation was rinsed with 15 ml of perfusion solution (100 U/ml heparin, 10 mM EDTA in phosphate-buffered saline (PBS), pH 7.4) followed by 15 ml of PBS.

Cell suspensions were generated from spleen, lymph nodes (LNs) and bone marrow (BM) of femur and tibia by filtering using a 40 µm cell strainer (Corning, Sigma Aldrich/Merck). After red blood cell (RBC) lysis applying RBC lysis buffer (BioLegend, Koblenz, Germany), cells were washed in PBS and used for subsequent analysis. Different parts of the vascular bed, including the brachiocephalic artery (BCA) and the aortic root, were isolated and embedded in Tissue-Tek® O.C.T.™ compound (Sakura Finetek, Staufen, Germany). The embedded tissues were stored at -80°C until preparation of 5 µm thick serial cryosections. The whole aorta was excised, pinned onto a slide and fixed overnight in 1% paraformaldehyde (PFA) at 4°C. Afterwards, the aorta was excised from surrounding fat and *en face* preparations were generated. The adventitia was removed and the aorta pinned with the endothelium pointing upwards. The vessel was fixed again in 4% PFA overnight and then applied to subsequent analyses.

Flow cytometric analysis

Flow cytometry was applied for the investigation of the immune cell content (T cells: $CD45^+CD3e^+$, monocytes: $CD45^+CD11b^+CD115^+$, neutrophils: $CD45^+CD11b^+Ly6G^+$, B cells: $CD45^+CD19^+$) of different organs including BM, spleen, LN, and blood using a BD FACSVerse™ instrument with a 3 laser, 8 color (4-2-2) configuration (BD Bioscience, Heidelberg, Germany). The system automatically adjusts spillover values for the compensation of standard fluorochromes. Cells were stained with fluorescently-labeled antibodies directed against cell-specific surface marker for 30 min on ice in the dark (anti-mouse CD45-APC/Cy7, #103116, BioLegend; anti-mouse CD45-FITC, #FAB114F, R&D Systems, Wiesbaden-Nordenstadt, Germany; anti-mouse CD3e-FITC, #130-119-758, Miltenyi Biotech, Bergisch Gladbach, Germany; anti-mouse CD4-PE, #130-102-619, Miltenyi Biotech; anti-mouse CD8a-PE-Cy7, #25-4321-82, ThermoFisher Scientific, Darmstadt, Germany; anti-mouse CD19-PercP-Cy5.5, #115534, BioLegend; anti-mouse CD11b-FITC, #130-081-201, Miltenyi Biotech; anti-mouse CD115-PE, #12-1152-82, ThermoFisher Scientific; anti-mouse Ly6G, # 45-5931-80, ThermoFisher Scientific). The antibodies were diluted 1:100 in FACS buffer (0.5% bovine serum albumin (BSA)/PBS, pH 7.4). Afterwards, the cells were washed with FACS buffer and centrifuged for 5 min at 300 x g and 4°C and subsequently applied to FACS measurements. References for the background fluorescence were obtained by staining with respective isotype control antibodies purchased from BioLegend or R&D Systems (rat IgG2b,κ-APC/Cy7, rat IgG2b,κ-FITC, rat IgG2a,κ-PE, rat IgG2b,κ-PerCP/Cy5.5, rat IgG2a,κ-PerCP/Cy5.5, rat IgG2b,κ-PE, rat IgG2a,κ-PE/Cy7) or REA control antibodies (REA Control (I)-FITC, Miltenyi Biotech). Results were analyzed by FlowJo software (Tree star, USA) and presented as dot plots at a logarithmic scale.

Plasma anti-oxLDL antibody levels

Plasma anti-oxLDL antibody levels were measured in Nunc MaxiSorp™ 96-well plates (ThermoFisher Scientific) coated with 1 µg/ml oxLDL (ThermoFisher Scientific) diluted in carbonate buffer (34.8 mM $NaHCO_3$, 15 mM Na_2CO_3 in double-distilled (dd)H_2O). After coating for 1 h at 37°C, plates were rinsed three times with 100 µl of washing/blocking solution (2% BSA in PBS) and blocked for 1 h at 37°C. Next, 50 µl plasma diluted 1:100 in washing/blocking solution was added per well and incubated for 1 h at 37°C. The plates were rinsed another time and 50 µl of horseradish-peroxidase (HRP)-labeled antibodies against IgG (# ab6789, Abcam, Berlin, Germany) and IgM (#62-6820, Ther-

moFisher Scientific) diluted 1:500 in washing/blocking solution were added and incubated for 1 h at 37°C. Following additional washing steps, the assay was developed by adding 100 µl Pierce^{TM} 3,3',5,5'-tetramethylbenzidine (TMB) substrate solution (ThermoFisher Scientific) for 5 min and the reaction was terminated by adding 50 µl stop solution (0.5 M H_2SO_4 in ddH_2O). Measurements were performed using an EnSpire Multimode Plate Reader (PerkinElmer, Hamburg, Germany) at 450 nm.

Plaque morphometry, *en face* staining of aorta, and plaque lipids

Immunofluorescence of brachiocephalic artery

Immunohistochemistry was performed on 5 µm thick cryosections of the BCA. The sections were fixed with pre-cooled acetone at 4 °C for 6 min and air-dried at room temperature (RT) for 30 min, following rehydration in PBS for 10 min. Next, the sections were blocked for 30 min with blocking solution (5% donkey/goat serum, 1% BSA in PBS, pH 7.4). For biotin-streptavidin-based immunohistochemistry, additional blocking procedures were performed using the Avidin/Biotin blocking kit (Vector Laboratories, Burlingame, CA, USA) according to the manufacturer's guidelines. Next, the sections were incubated with the primary antibodies diluted in blocking solution at 4°C overnight. The following primary antibodies were applied: rat anti-mouse CD45R/B220-biotin (1:200, #553085, BD Biosciences), goat anti-mouse CD68 (1:100, #MCA1957GA, Bio-Rad, Puchheim, Germany), hamster anti-mouse CD3e (1:100, #553058, BD Biosciences), mouse anti-human/mouse SMA-Cy3 (1:200, #C6198, Sigma Aldrich), rat anti-mouse CD35 (1:100, #558768, BD Biosciences), rat anti-mouse PNAd (1:50, #553863, BD Biosciences), goat anti-mouse CXCL13 (1:25, #AF470, R&D Systems), rabbit anti-mouse collagen IV (1:500, #2150-1470, Bio-Rad), rat anti-mouse ER-TR7 (1:500, #ab51824, Abcam), rabbit anti-mouse Lyve1 (1:500, #DP35135P, Acris Antibody GmbH, Herford, Germany) and sheep anti-mouse Trem2 (1:50, #AF1729, R&D Systems). Afterwards, sections were rinsed in PBS and incubated for 1 h at RT with the respective secondary antibodies or Avidin-FITC (#434411, ThermoFisher Scientific) diluted in blocking solution. The following secondary antibodies were used: goat anti-rat-AF488 (1:500, #A-11006, ThermoFisher Scientific), goat anti-hamster-Cy3 (1:300, #127-165-160, Jackson ImmunoResearch, Hamburg, Germany), goat anti-rat(IgM)-Cy5 (1:500, #A21247, ThermoFisher Scientific), donkey anti-rabbit-Cy3 (1:500, #711-165-152, Jackson Immuno-Research), donkey anti-goat-AF647 (1:500, #A21447, ThermoFisher Scientific), donkey anti-rat-Cy3 (1:300, #712-166-153, Jackson ImmunoResearch), donkey anti-sheep-AF555 (1:500, ab150178, Abcam), and donkey anti-sheep-AF647 (1:500, ab150179,

Abcam). DAPI was used as nuclear counterstain. Afterwards, sections were washed and mounted with Fluoromount™ aqueous mounting medium (Sigma-Aldrich/Merck). Images were recorded with a DMi8 fluorescent microscope (Leica Microsystems, Wetzlar, Germany) and analyses were performed using ImageJ software.

Oil-Red-O staining of aortic root

For the quantification of lesion formation in the aortic root, Oil-Red-O (ORO) stainings were performed on 5 µm thick cryosections. First, the slides were air-dried for 5 min following rehydration in PBS for 2 min. Next, lipids were stained with ORO solution (0.5% in propylene glycol, Sigma Aldrich/Merck) at 37°C for 45 min. The slides were shortly washed with running tap water and nuclear counterstain was performed using hematoxylin. The slides were air-dried and mounted with Kaiser's glycerin gelatine mounting media (Carl Roth, Karlsruhe, Germany). Images were taken with the DMi8 fluorescent microscope and lesion quantification performed using ImageJ software. Per mouse, 12 serial sections with a distance of 50 µm between each other, were stained, and mean values calculated.

Oil-Red-O (en face) staining of aorta

Oil-Red-O stainings of the aorta including aortic arch as well as abdominal and thoracic aorta were performed after *en face* preparation and fixation in 4% PFA. The tissue was stained for 30 min in ORO solution (0.5% in isopropanol, Sigma Aldrich/Merck) at RT. Next, aortas were washed in 60% isopropanol until unspecific ORO-derived staining was removed from the endothelium. The aortas were rinsed briefly with running tap water before mounting in Kaiser's glycerin gelatine mounting media. Tilescan images were acquired with the DMi8 fluorescent microscope. The lesions were quantified via FlowJo software and depicted as percentage of total aortic surface.

Hematoxylin-eosin staining of brachiocephalic artery

Hematoxylin-eosin (H&E) staining was performed for lesion quantification of the BCA. The slides were dried at RT for 30 min and rehydrated with PBS for 2 min. Next, nuclei were visualized by staining with Mayer's hematoxylin solution (Sigma Aldrich/Merck) for 15 min at RT. Then, the slides were rinsed with water for 10 min before staining with

Eosin G-solution for 10 sec and dehydration by two changes of 95% ethanol, 100% eth-anol and xylene (2 min each). After air-drying, the slides were mounted using Eukitt® Quick-hardening mounting medium (Sigma Aldrich, Merck). Images were taken with the DMi8 fluorescent microscope. The lesion size was quantified using ImageJ software and is depicted as ratio of total inner vessel area. Per mouse, 12 sections with a distance of 50 µm between them were stained and the mean values calculated.

MIF mRNA expression analysis

Trizol-based RNA isolation

First, RNA was extracted from frozen tissues using a TRIzol™-based protocol. Briefly, the tissue was homogenized in 1 ml of TRIzol™ reagent (ThermoFisher Scientific) using stainless steel beads (5 mm mean diameter) and a TissueLyser LT adapter (Qiagen, Hilden, Germany) for 5 min at 50 Hz. After adding 200 µl chloroform and incubation for 3 min, the solution was centrifuged for 15 min at 12000 x g and 4°C. The RNA-containing fraction was mixed with 250 µl isopropanol and incubated for 10 min. Next, the samples were centrifuged at 10000 x g and 4°C for 10 min and the RNA pellets resuspended in 75% ethanol. After centrifugation for 5 min at 7500 x g and 4°C, the RNA was air-dried and dissolved in nuclease-free water. The RNA concentration was obtained using a NanoDrop™ One UV/Vis spectrophotometer (ThermoFisher Scientific).

Reverse transcription and quantitative real-time PCR (RT-qPCR)

To transcribe the purified RNA into single stranded cDNA, the First Strand cDNA syn-thesis kit (Thermo Fisher Scientific) was used according to the manufacturer´s protocol. Briefly, a reaction mix containing 1 µl RNase inhibitor, 2 µl dNTP mix, 2 µl reverse tran-scriptase,1 µl Oligo(dT)$_{18}$ primers and 4 µl 5 x reaction buffer was prepared and mixed with 1 µg of isolated RNA. The reverse transcription was performed in a Biometra ther-mocycler (Analytik Jena AG, Jena, Germany) with following incubation settings: 1 h at 37°C, 5 min at 70°C, cooling down to 4°C. RT-qPCR was conducted using ORA™ SEE qPCR Green ROX H Mix (HighQu, Kraichtal, Germany) and specific mouse primer pairs (Eurofins, Ebersberg, Germany). The following primers were used: *MIF forward: ACA GCA TCG GCA AGA TCG* and *MIF reverse: AGG CCA CAC AGC AGC TTA C; actin forward: GGA GGG GGT TGA GGT GTT* and *actin reverse: GTG TGC ACT TTT ATT GGT CTC AA*. PCR reactions were run in a Rotorgene Q (Qiagen). Relative mRNA levels were obtained by the ΔΔCt approach with *actin* as a housekeeping gene.

Lipid analysis

Cholesterol fluorometric assay

Cholesterol levels in plasma were measured using Cayman's Cholesterol Fluorometric Assay kit (Cayman Chemicals/ Biomol GmbH, Hamburg, Germany) according to the manufacturer's instructions. Briefly, plasma was diluted 1:2000 in cholesterol assay buffer and 50 µl of sample was administered to the wells of a 96-well plate. After initiation of the reaction with 50 µl of assay cocktail (4.745 ml cholesterol assay buffer, 150 µl cholesterol detector, 50 µl cholesterol assay HRP and 5 µl cholesterol esterase), the plates were incubated for 30 min at 37°C protected from light. Afterwards the fluorescence was measured at an excitation wavelength of 535 nm and an emission wavelength of 590 nm. Samples were measured in duplicates using an EnSpire Multimode Plate Reader (PerkinElmer). Diluted cholesterol standards with final concentrations between 2 and 20 µM were used for the quantification of cholesterol levels in the plasma.

Triglyceride calorimetric assay

Triglyceride levels in plasma were measured using Cayman's Triglyceride Calorimetric Assay kit (Cayman Chemicals/ Biomol GmbH) according to the manufacturer's instruction. Briefly,10 µl of undiluted plasma was mixed with 100 µl of pre-diluted enzyme mixture in a 96-well plate and incubated for 15 min at RT. The absorbance was measured at 540 nm using the EnSpire Multimode Plate Reader (PerkinElmer). Diluted triglyceride standards with final concentrations between 3.125 and 200 mg/dl were used for the quantification of triglyceride levels in mouse plasma.

Murine MIF ELISA

Plasma MIF levels were measured by the Mouse MIF DuoSet® ELISA (R&D Systems) according to the manufacturer's instruction. Briefly, wells of a 96-well plate were coated with 100 µl of capture antibody at a concentration of 400 ng/ml overnight at RT. After three washes with washing buffer (0.05% Tween 20 in PBS, pH 7.2), plates were blocked in 300 ml of 1x reagent diluent concentrate 2 (R&D Systems) for 1 h at RT. After additional rinsing, 100 µl of the appropriately diluted plasma sample or standard in 1x reagent diluent concentrate 2 was added into each well. Standards were prepared using the recombinant mouse MIF standard supplied with the kit using 2-fold serial dilutions. Standard concentrations ranged from 125 pg/ml to 2000 pg/ml. After incubation with samples/standards for 2 h at RT, washing was repeated, and 100 µl of detection antibody at

a final concentration of 200 ng/ml was added for 2 h at RT. Plates were rinsed three times, 100 µl of Streptavidin-HRP (1:200 dilution) added, and incubated for 20 min at RT, followed by incubation with 100 µl of TMB substrate solution (ThermoFisher Scientific) for another 20 min at RT. The reaction was terminated by adding 50 µl of stop solution (2N H_2SO_4) per well. Optical density was determined at 450 nm using an EnSpire Multimode Plate Reader (PerkinElmer). Plasma dilutions of 1:50 and 1:100 were found to be optimal for best signal/noise ratios and mean values were used for analysis.

Statistics

All statistical tests were conducted using GraphPad Prism 6.0 or 7.0 (GraphPad Software Inc.). In order to estimate the normality of the data the D'Agostino-Pearson test was performed. Two-tailed Student's T-test (parametric) or by Mann-Whitney test (non-parametric) were used as appropriate. For multiple comparisons Two-way ANOVA with Sidak´s multiple comparisons test was applied. *P*<0.05 was considered statistically significant.

Results

Site-specific atheroprotection due to *Mif*-deficiency is lost in aged *Apoe*$^{-/-}$ mice

The role of MIF in atherogenesis has previously been investigated in young and middle-aged atherogenic *Apoe*$^{-/-}$ or *Ldlr*$^{-/-}$ mice on HFD for up to 26 weeks[145,150-153,234]. However, age-dependent effects of MIF were not addressed in these studies. Here, we determined the effect of *Mif*-deficiency in 30-, 42-, and 48-week-old *Apoe*$^{-/-}$ mice that were subjected to an HFD for 24, 36 and 42 weeks, respectively, as well as in 52-week-old mice that received an HFD in the last 6 weeks, i.e. in 30/24-, 42/36-, 48/42-, and 52/6-week treatment groups.

We first compared the body weights of *Apoe*$^{-/-}$*Mif*$^{-/-}$ mice with those of *Apoe*$^{-/-}$ controls over the course of aging and HFD. Interestingly, *Mif*-deficiency appeared to affect weight gain during aging. Whereas the body weight of *Apoe*$^{-/-}$ control mice steadily increased with age and the duration of the HFD, the *Mif*-deficient animals maintained or even lost body weight over the same course (24 weeks HFD: 34.0±3.7 g; 42 weeks HFD: 32.6±3.3 g) (Table A.1). In line with these findings, *Apoe*$^{-/-}$*Mif*$^{-/-}$ mice displayed reduced body weights in comparison to the *Apoe*$^{-/-}$ controls at all time intervals and this difference almost reached significance at 42 weeks of HFD (*Apoe*$^{-/-}$*Mif*$^{-/-}$: 32.6±3.3 g; *Apoe*$^{-/-}$: 38.2±5.5 g; *P*=0.057).

Table A.1: Body weights of the *Apoe^{−/−}Mif^{−/−}* and *Apoe^{−/−}* mice after 24, 36, and 42 weeks of high-fat diet (HFD).

HFD (weeks)	*Apoe^{−/−}*			*Apoe^{−/−}Mif^{−/−}*			P value
	Weight (g)	SD[1]	n[2]	Weight (g)	SD[1]	n[2]	
24	35.4	4.8	8	34.0	3.7	6	0.961
36	37.8	6.3	7	32.1	6.0	6	0.120
42	38.2	5.5	9	32.6	3.3	8	0.057

[1]SD, standard deviation; [2]n, number of mice.

These data were paralleled by corresponding differences in lipid levels (Table A.2), and significantly decreased triglyceride levels were detected in the plasma of *Apoe^{−/−}Mif^{−/−}* mice after 42 weeks of HFD in comparison to *Apoe^{−/−}* controls (Table A.2; *Apoe^{−/−}Mif^{−/−}*: 116.9±28.9 g; *Apoe^{−/−}*: 211.4±88.2 g; *P*=0.024). Cholesterol levels in the *Apoe^{−/−}Mif^{−/−}* mice were lower both after 24 and 42 weeks of HFD in comparison to the *Apoe^{−/−}* mice. However, no statistically significant effects were obtained in this context (Table A.2).

Table A.2: Plasma triglyceride and cholesterol determinations in *Apoe^{−/−}Mif^{−/−}* and *Apoe^{−/−}* mice after 24 and 42 weeks of high-fat diet (HFD).

HFD (weeks)	Parameter	*Apoe^{−/−}*			*Apoe^{−/−}Mif^{−/−}*			P value
		Mean	SD[1]	n[2]	Mean	SD[1]	n[2]	
24	Cholesterol (mg/dl)	899.6	423.5	7	670.1	274.9	7	0.296
42		1050.4	278.3	9	806.9	186.7	8	0.197
24	Triglyceride (mg/dl)	132.8	68.6	7	134.4	59.5	6	0.999
42		211.4	88.2	7	116.9	28.9	7	0.025

[1]SD, standard deviation; [2]n, number of mice.

Also, additional blood parameters, such as total white blood cell count (WBC), red blood cells (RBC), hemoglobin (HGB), and hematocrit (HCT) did not differ between mouse strains and age groups (Table A.3).

Table A.3: Blood parameters of *Apoe$^{-/-}$Mif$^{-/-}$* and *Apoe$^{-/-}$* mice after 24 and 42 weeks of high-fat diet (HFD).

HFD	Parameter	*Apoe$^{-/-}$*			*Apoe$^{-/-}$Mif$^{-/-}$*			
		Mean	SD[1]	n[2]	Mean	SD[1]	n[2]	P value
24 weeks	WBC[3] (10^3/mm^3; 10^9/l)	3.700	1.113	5	4.100	1.220	5	>0.999
	RBC[4] (10^3/mm^3; 10^{12}/l)	4.385	1.885	6	5.498	0.971	6	>0.999
	HGB[5] (g/dl)	9.350	4.079	6	10.100	4.641	6	>0.999
	HCT[6] (%)	24.167	10.816	6	29.283	5.005	6	>0.999
	MCV[7] (μm^3; fl)	54.667	3.386	6	53.333	1.366	6	>0.999
	MCH[8] (pg)	21.283	1.539	6	20.133	2.484	6	>0.999
	MCHC[9] (g/dl)	38.950	2.061	6	37.650	3.908	6	>0.999
	MPV[10] (μm^3; fl)	5.900	0.505	6	6.200	0.316	4	>0.999
	RDW[11] (%)	13.833	0.647	6	14.700	2.268	6	>0.999
42 weeks	WBC[3] (10^3/mm^3; 10^9/l)	3.814	1.410	7	3.812	1.389	8	>0.999
	RBC[4] (10^3/mm^3; 10^{12}/l)	6.230	0.794	9	5.699	1.205	8	>0.999
	HGB[5] (g/dl)	11.844	2.210	9	12.390	2.292	11	>0.999
	HCT[6] (%)	34.350	5.334	9	27.168	8.685	11	0.6
	MCV[7] (μm^3; fl)	52.555	1.446	9	53.625	1.188	8	>0.999
	MCH[8] (pg)	18.044	1.573	9	20.569	1.166	8	>0.999
	MCHC[9] (g/dl)	34.239	3.086	9	38.138	1.502	8	>0.999
	MPV[10] (μm^3; fl)	6.400	0.240	9	5.923	1.081	11	>0.999
	RDW[11] (%)	14.172	0.602	9	14.068	0.792	8	>0.999

[1]SD, standard deviation; [2]n, number of mice; [3]WBC, white blood cells; [4]RBC, red blood cells; [5]HGB, hemoglobin; [6]HCT, hematocrit; [7]MCV, mean corpuscular/cell volume; [8]MCH, mean corpuscular/cellular hemoglobin; [9]MCH, mean corpuscular/cellular hemoglobin concentration; [10]MPV, mean platelet volume; [11]RDW, red blood cell distribution width.

We next analyzed the atherosclerotic lesions across the vascular tree. Plaque area analysis in 30-week-old mice that were on HFD for 24 weeks confirmed the intriguing regiospecific atheroprotective effect of *Mif*-gene deletion that had been previously observed[152]. *Apoe$^{-/-}$Mif$^{-/-}$* mice exhibited a significantly reduced plaque size compared to *Apoe$^{-/-}$* controls in BCA and abdominal aorta, but not in aortic root, aortic arch, and thoracic aorta (Figure A.1). Strikingly, the atheroprotective effect of *Mif*-knockout mice was lost over the time course of aging and HFD. While attenuation of plaque formation in the *Mif*-knockout genotype was still observed in the BCA and abdominal aorta after 36 weeks

of HFD, it was lost in the 48-week-old mice on HFD for 42 weeks (Figure A.1a,b,e,f,i) with an almost inverted plaque phenotype seen in abdominal aorta of the most aged animals of 48/42 weeks (Figure A.1i). The loss of the atheroprotective phenotype in *Mif*-deficient mice at a highly advanced age was further confirmed in 52/6-week mouse group. No difference in plaque size was seen in those mice, neither in aortic root, arch, and thoracic aorta, nor in brachiocephalic artery and abdominal aorta (Supplementary figure A.1a-h). Moreover, the similar outcome in the 48/42- *versus* 52/6-week models was indicative of a predominant role of aging *per se* over the duration of the HFD in an atherogenic *Apoe*$^{-/-}$ background.

MIF expression levels may decrease over the course of aging [235] and this may lead to a relative reduction in the difference of MIF levels between *Apoe*$^{-/-}$*Mif*$^{-/-}$ and *Apoe*$^{-/-}$ mice, in turn affecting the differences seen in atheroprotection at different age stages. However, quantification of MIF expression levels in liver and spleen by qPCR as well as plasma MIF determinations by MIF ELISA did not reveal any differences in MIF levels in *Apoe*$^{-/-}$ mice of the 30/24- *versus* 48/42-week groups (Supplementary figure A.2).

The comparison of plaque phenotypes across age, HFD duration and vascular bed locations led to additional interesting observations irrespective of the investigation of *Mif*-deficiency. In the BCA of *Apoe*$^{-/-}$ mice, plaque burden stagnated at approximately 80% plaque area after 24 weeks of HFD (Figure A.1b), whereas an aging/HFD duration-dependent increase was observed in aortic root, arch, and thoracic aorta (Figure A.1d,g,h).

In conclusion, the atherosclerotic lesion analysis confirmed that *Mif*-deficiency causes lesion attenuation in a regio-specific way in the relatively younger mice and showed that the atheroprotective effect of *Mif*-deletion is lost at an advanced age. Thus, aging seems to be an important contributing factor, when considering MIF-mediated effects during atherosclerotic disease progression.
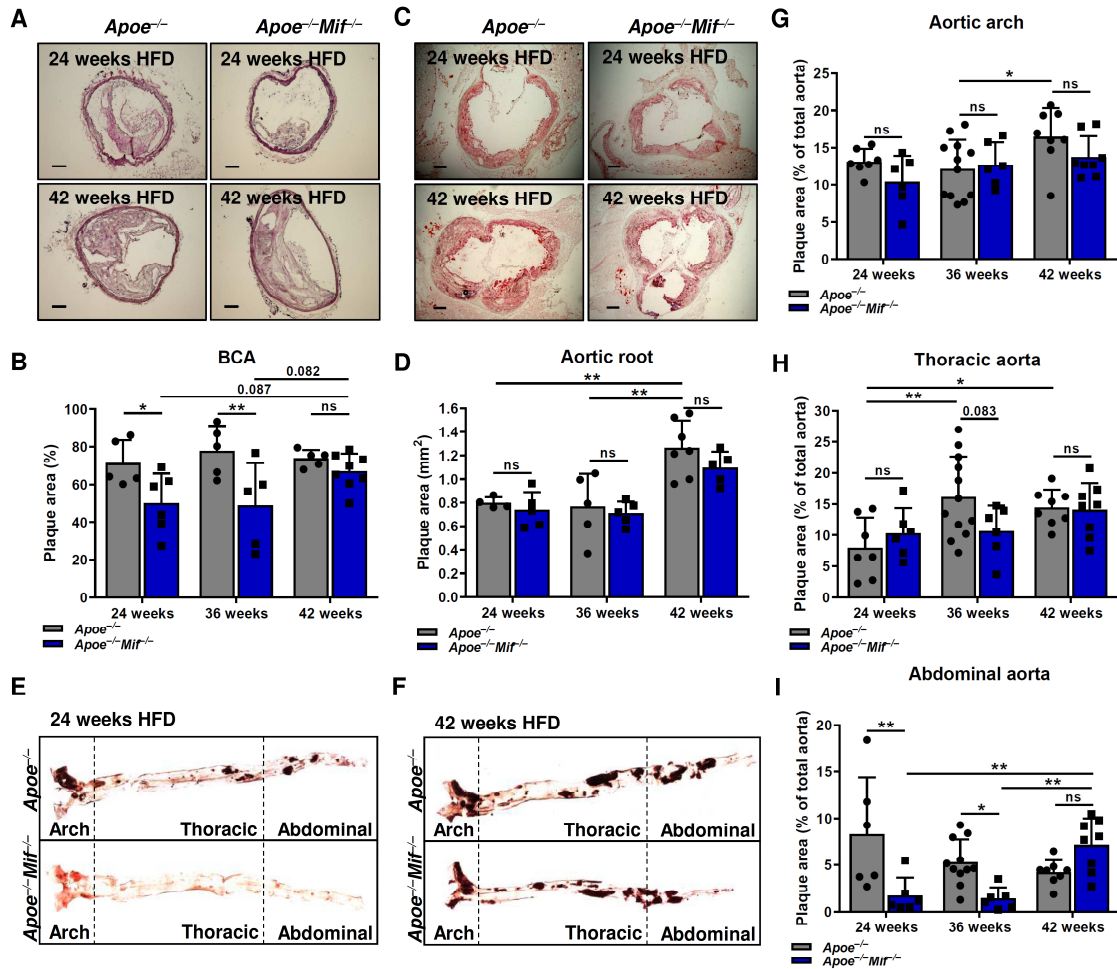
Figure A.1: Atheroprotection due to *Mif*-deficiency is lost in highly aged hyperlipidemic *Apoe*⁻/⁻ mice. Atherosclerotic plaques were quantified in brachiocephalic artery (BCA), aortic arch and root, as well as in thoracic and abdominal aorta of 30-, 42-, and 48-week-old *Apoe*⁻/⁻*Mif*⁻/⁻ mice after 24, 36, and 42 weeks of high-fat diet (HFD), respectively (blue), and compared to corresponding lesions in *Apoe*⁻/⁻ mice (grey). **A-B)** Representative images **(A)** and plaque quantification **(B)** of hematoxylin-eosin (H&E)-stained BCA sections. For each mouse, 10 serial sections with a distance of 50 µm were used for analysis. The mean plaque area is depicted as percentage of the total inner vessel area including the plaque (n=5-8, results are presented as means ± SD; scale: 100 µm). **C-D)** Representative images **(C)** and quantification **(D)** of (Oil-Red-O) ORO-stained sections of the aortic root. Serial sections were obtained as in (A-B). The mean plaque area is depicted in mm^2 (n=4-7, results are shown as means ± SD; scale: 200 µm). **E-F)** Representative images of *en face*-prepared and ORO-stained aortas after 24 **(E)** and 42 **(F)** weeks of HFD. **G-I)** Quantification of plaque area in aorta including aortic arch **(G)**, thoracic aorta **(H)** and abdominal aorta **(I)**. The plaque area is depicted as percentage of the total aortic surface (n=6-12, results presented as means ± SD). Statistics: two-way ANOVA; *, $P<0.05$; **, $P<0.01$; ns, non-significant; non-significant results with P values between 0.05 and 0.1 are provided as precise numbers; each data point corresponds to one independent mouse.

Peripheral and splenic CD4⁺ T-cell counts are changed in an age- and MIF-dependent manner

To begin to explore the mechanism underlying the identified age- and MIF-dependent plaque phenotype, we applied flow cytometry to investigate the immune cell content of spleen, blood, LNs, and BM. Cell numbers were compared for the 30/24- and 48/42-week groups between *Apoe*⁻/⁻ and *Apoe*⁻/⁻*Mif*⁻/⁻ mice. Interestingly, the most significant changes were seen for T cells. Total splenic T-cell levels were significantly reduced in

Apoe$^{-/-}$ mice over the course of aging, and a subpopulation analysis revealed that this effect was owing to a decrease in CD4$^+$ T cells, whereas CD8$^+$ T-cell numbers remained unchanged (Figure A.2a). Similarly, peripheral T-cell numbers were decreased in the highly aged 48/42-week *Apoe*$^{-/-}$ mice in comparison to the younger animals, although statistical significance was not obtained. T cells isolated from LNs or BM were unchanged between the different groups (Figure A.2b-d).

The T-cell analysis also revealed a significant influence of MIF. Splenic CD4$^+$ T-cell numbers in *Apoe*$^{-/-}$*Mif*$^{-/-}$ mice were significantly increased compared to T-cell numbers in spleens from *Apoe*$^{-/-}$ mice, both at 24 and 42 weeks of HFD, with a more pronounced difference seen at 42 weeks (Figure A.2a). This effect in the highly aged 48/42-week mice was further confirmed in the 52/6-week aging/HFD model (Supplementary figure A.1i). To further explore whether the observed increase in splenic T-cell numbers in *Apoe*$^{-/-}$*Mif*$^{-/-}$ mice could contribute to the atheroprotection phenotype in these mice, we quantified FoxP3 mRNA levels as a marker for regulatory T cells (Tregs), which are considered anti-atherogenic. Splenic FoxP3 levels were elevated in *Apoe*$^{-/-}$*Mif*$^{-/-}$ mice after 42 weeks of HFD but not in the 24-week-HFD group (Supplementary figure A.3), overall confuting a clear-cut connection between splenic Treg numbers and atheroprotection in *Mif*-deficient mice. Other mechanisms than deregulated Treg numbers seem to underly the lost atheroprotection in aged *Mif*-deficient mice. While no MIF-dependent changes were observed for T cells from LN or BM, blood CD4$^+$ T-cell numbers were lower in *Apoe*$^{-/-}$*Mif*$^{-/-}$ mice compared to *Mif*-expressing controls in the 30/24- as well as in the 52/6-week group (Figure A.2b, Supplementary Figure A.1j).

We also determined B-cell, monocyte and neutrophil counts in spleen, LN, BM and blood. While monocyte counts were not altered between age groups or as a function of MIF, some changes were seen for B cells and neutrophils such as an expansion of CD19$^+$ B cells in blood and LNs of *Apoe*$^{-/-}$*Mif*$^{-/-}$ mice at 42 weeks HFD, a decrease of LN B cells in 24-week HFD-fed *Apoe*$^{-/-}$*Mif*$^{-/-}$ mice, or an increase in BM neutrophils in 24-week HFD *Apoe*$^{-/-}$*Mif*$^{-/-}$ mice (Supplementary figure A.4). However, these changes were subtle and did not give rise to an apparent consistent pattern that could explain the observed plaque phenotype, and thus were not pursued further.

Together, the immune cell analysis in blood and peripheral lymphoid organs indicated that especially CD4$^+$ T-cell numbers in the spleen may be controlled in a MIF- and age-dependent manner, but the determined increase in FoxP3+ Treg cells in the spleens of *Mif*-deficient mice in the 48/42- but not 30/24-week group does not readily explain the age-related loss of protection phenotype.
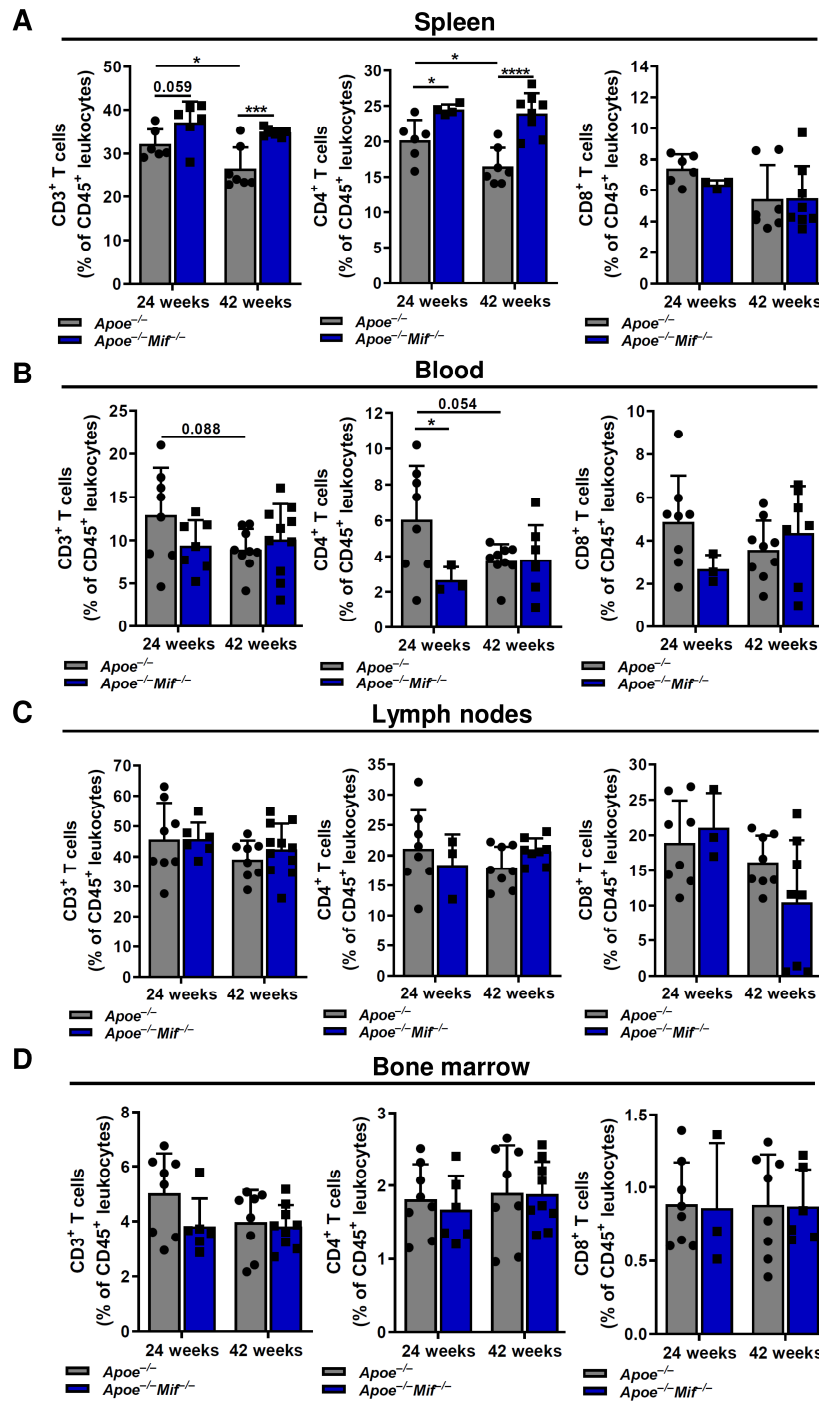
Figure A.2: CD4⁺ T-cell numbers in spleen and blood of hyperlipidemic *Apoe*⁻/⁻ mice change in a MIF-and age-dependent manner. FACS-based quantification of total CD3⁺ T cells (*left graphs*), CD4⁺ T-cell subsets (*middle graphs*), and CD8⁺ T-cell subsets (*right graphs*) in spleen **(A)**, blood **(B)**, lymph nodes **(C)**, and bone marrow **(D)** of *Apoe*⁻/⁻*Mif*⁻/⁻ mice (blue) and comparison to *Apoe*⁻/⁻ controls (grey). 30- and 48-week-old mice on HFD for 24 and 42 weeks, respectively, were examined. Bars shown represent data from n=3-8 independent mice and results are shown as means ± SD. Statistics: two-way ANOVA; *, $P<0.05$; ***, $P<0.001$; ****, $P<0.0001$, non-significant results with P values between 0.05 and 0.1 are indicated.

Lesional Trem2⁺ macrophage numbers are reduced in *Mif*-deficient *Apoe*⁻ᐟ⁻ mice during aging

For the further investigation of the loss of atheroprotection in aged *Mif*-deficient mice, we analyzed SMCs and macrophages in plaques of the BCA after 24 and 42 weeks of HFD. While the content of smooth muscle actin (SMA)⁺ SMCs was unaltered (Figure A.3a-b), we detected substantial changes in plaque macrophage numbers (Figure A.3c-d). As indicated by vessel staining with an anti-CD68 antibody, macrophage numbers in plaques of *Apoe*⁻ᐟ⁻*Mif*⁻ᐟ⁻ mice subjected to an HFD for 24 weeks were decreased compared with those of the 42-week HFD group (Figure A.3c-d). As this effect paralleled the observed loss of protection from plaque formation in *Apoe*⁻ᐟ⁻*Mif*⁻ᐟ⁻ mice between 24 and 42 weeks of HFD, we hypothesized that the age-dependent decrease in macrophages could be predominantly due to a reduction in atheroprotective macrophage subsets. To this end, single cell (sc) RNAseq analysis recently revealed an accumulation of lipid-loaded 'foamy' Trem2ʰⁱᵍʰ macrophages within atherosclerotic lesions, a previously unrecognized macrophage subtype assigned anti-inflammatory and homeostatic functions[26-28]. We therefore analyzed our plaque specimens for Trem2⁺ macrophages and found reduced Trem2 expression in cellular (DAPI⁺) plaque areas of *Mif*-deficient *Apoe*⁻ᐟ⁻ mice following 42 weeks of HFD in comparison to the 24-week HFD group (Figure A.3e-f). Although the detected lesional Trem2 signal may also represent plaque-deposited soluble Trem2 (sTrem2) in necrotic core areas, the detected plaque Trem2 positivity likely fully stems from plaque macrophages, either directly or indirectly, as non-central nervous system Trem2 expression is limited to cells of myeloid origin.

Together, the analysis of lesional immune cells suggested that the age/HFD duration-dependent loss of atheroprotection in *Apoe*⁻ᐟ⁻*Mif*⁻ᐟ⁻ mice is linked to a reduction in anti-inflammatory Trem2⁺ plaque macrophages.
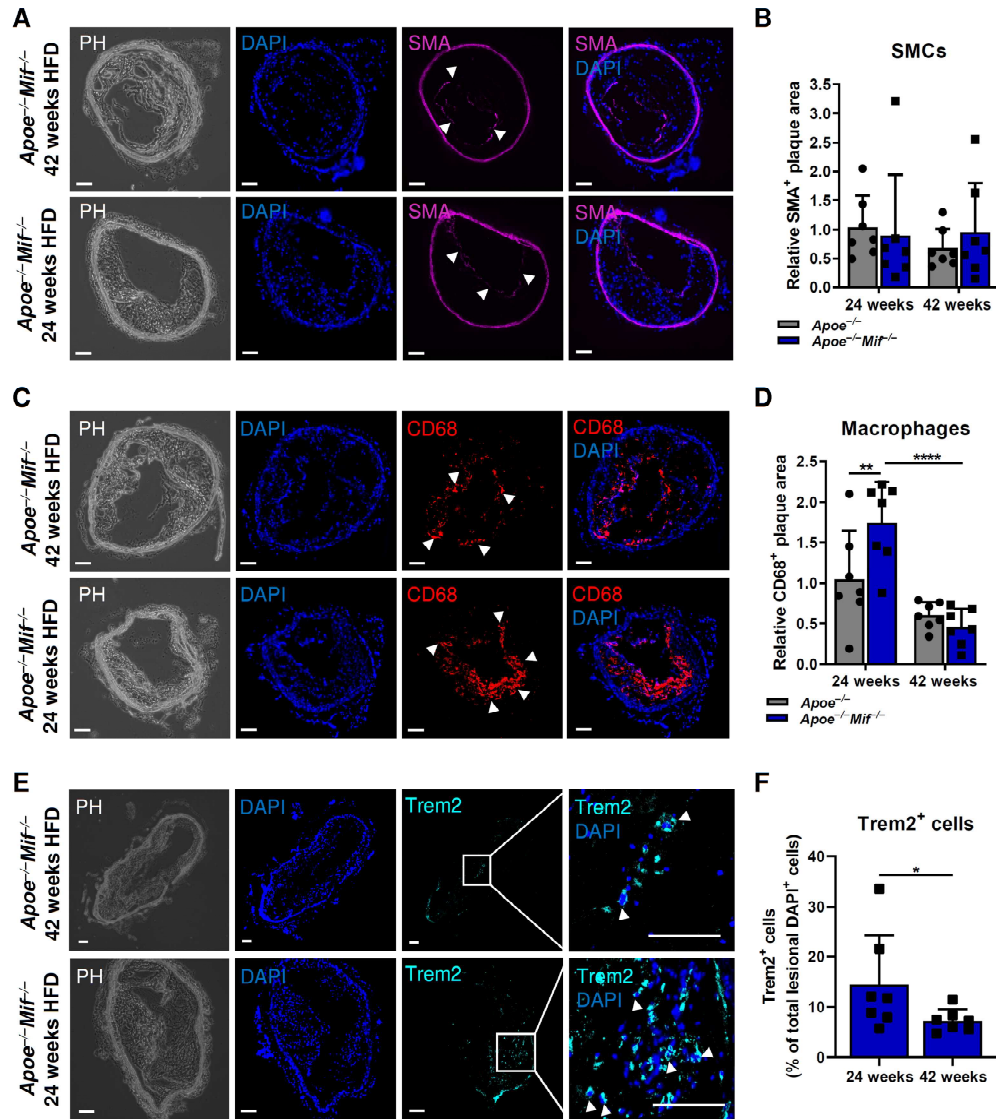
Figure A.3: Age- and MIF-dependent changes in lesional total macrophage and Trem2$^+$ macrophage numbers. Immunohistochemistry (IHC) was performed on brachiocephalic artery (BCA) sections derived from 30- and 48-week-old *Apoe$^{-/-}$Mif$^{-/-}$* (blue) and *Apoe$^{-/-}$* (grey) mice after 24 and 42 weeks of HFD, respectively. Smooth muscle cells (SMA), total macrophage content (CD68), and Trem2$^+$ macrophages were quantified in the plaque area. Nuclear counterstain was performed using DAPI. **A-B)** Representative images **(A)** and quantification **(B)** of the SMA$^+$ plaque area. 2-3 sections were analyzed per mouse and mean values normalized to values of the 30-week-old *Apoe$^{-/-}$* controls that received HFD for 24 weeks (n=7 mice; results presented as means ± SD; scale bar: 100 µm; arrows indicate the SMA$^+$ plaque area; PH=phase contrast). **C-D)** Representative images **(C)** and quantification **(D)** of the CD68$^+$ plaque area. Analysis performed as in (A-B) (n=7, results are presented as means ± SD; scale bar: 100 µm; arrows indicate the CD68$^+$ plaque area). **E-F)** Representative images **(E)** and quantification **(F)** of Trem2$^+$ cells within the plaque. Cells are indicated by an arrow in the enlarged image section. Trem2$^+$ cells were quantified manually and are depicted as percentage of total DAPI$^+$ cells in the plaque. As Trem2 expression in the lesion is limited to myeloid cells, the stained cells were considered as Trem2$^+$ macrophages. Two sections were analyzed per animal (n=7 mice; results are presented as means ± SD; scale bar: 100 µm). Statistics: two-way ANOVA; *, $P<0.05$; **, $P<0.01$; ****, $P<0.0001$; each data point corresponds to one independent mouse.

Mif-deficiency accelerates the formation of stage-2 ATLO-like B-cell clusters in _Apoe_[−/−] mice while ATLO numbers match in _Mif_-deficient and wildtype mice at advanced aging stage

While we concluded that the above-described change in plaque Trem2^{+} macrophages contributes to the age-dependent loss-of-atheroprotection phenotype in _Apoe_[−/−]_Mif_[−/−] mice, we surmised that additional MIF-driven mechanisms may be involved as well. We recently uncovered a link between MIF and B cells in atherosclerotic lesions and obtained initial hints for a regulatory function of MIF in the accumulation of peri-adventitial B cells[152]. B cells are rare in atherosclerotic lesions but are present in the adventitia and adjacent periadventitial tissue[236]. Here, we show that after 24 weeks of HFD, B cells in the (peri-)adventitial area of the BCA of _Apoe_[−/−]_Mif_[−/−] mice mostly re-organized into cluster-like structures, whereas only few of these structures were detected in age-matched _Apoe_[−/−] controls (Figure A.4a-b). This difference in cluster formation disappeared in highly aged mice that received HFD for 42 weeks, as the number of clusters increased in _Apoe_[−/−] mice at this aging stage (Figure A.4a). Thus, _Mif_-deficiency accelerates cluster formation in _Apoe_[−/−] mice in medium-aged hyperlipidemic mice, but this difference is lost towards advanced aging stages. We hypothesized that the clusters contribute to the atheroprotective effect of _Mif_-deficiency after 24 weeks of HFD and therefore characterized the nature of the B-cell-rich clusters and determined whether they represent periadventitial ATLOs. Due to their B- and T-cell-rich lymphoid organ-like structure, ATLOs can be detected analyzing the expression and distribution of specific markers, including those for lymphocytes, lymph vessels, high-endothelial venules (HEVs), and capsule components. Using anti-B220 and anti-CD3e antibodies, we determined an abundance of B and T cells, respectively, in peri-adventitial clusters of _Apoe_[−/−]_Mif_[−/−] mice (Figure A.4c). Moreover, the clusters contained lymph vessels and conduit-like structures, as evidenced by pronounced staining for Lyve-1 and ER-TR7, respectively, and contained substantial collagen type IV positivity (Figure A.4c), together suggesting that the clusters display an ATLO-like composition. Also, in accordance with the observed high B-cell content, staining for the B-cell chemokine CXCL13 was noted. However, features of mature ATLOs were absent, as indicated by lack of staining for peripheral node addressin (PNAd), a marker of HEVs, and CD35, a marker for follicular dendritic cells (FDCs) (Figure A.4c). Together, these results suggested that the prominent B-cell-rich clusters that we detected in the BCA of 24-week-HFD-fed _Apoe_[−/−]_Mif_[−/−] mice as well as in the BCA of 42-week-HFD-subjected _Apoe_[−/−]_Mif_[−/−] and _Apoe_[−/−] mice likely represent early ATLOs, often also referred to as stage-2 ATLOs[82].
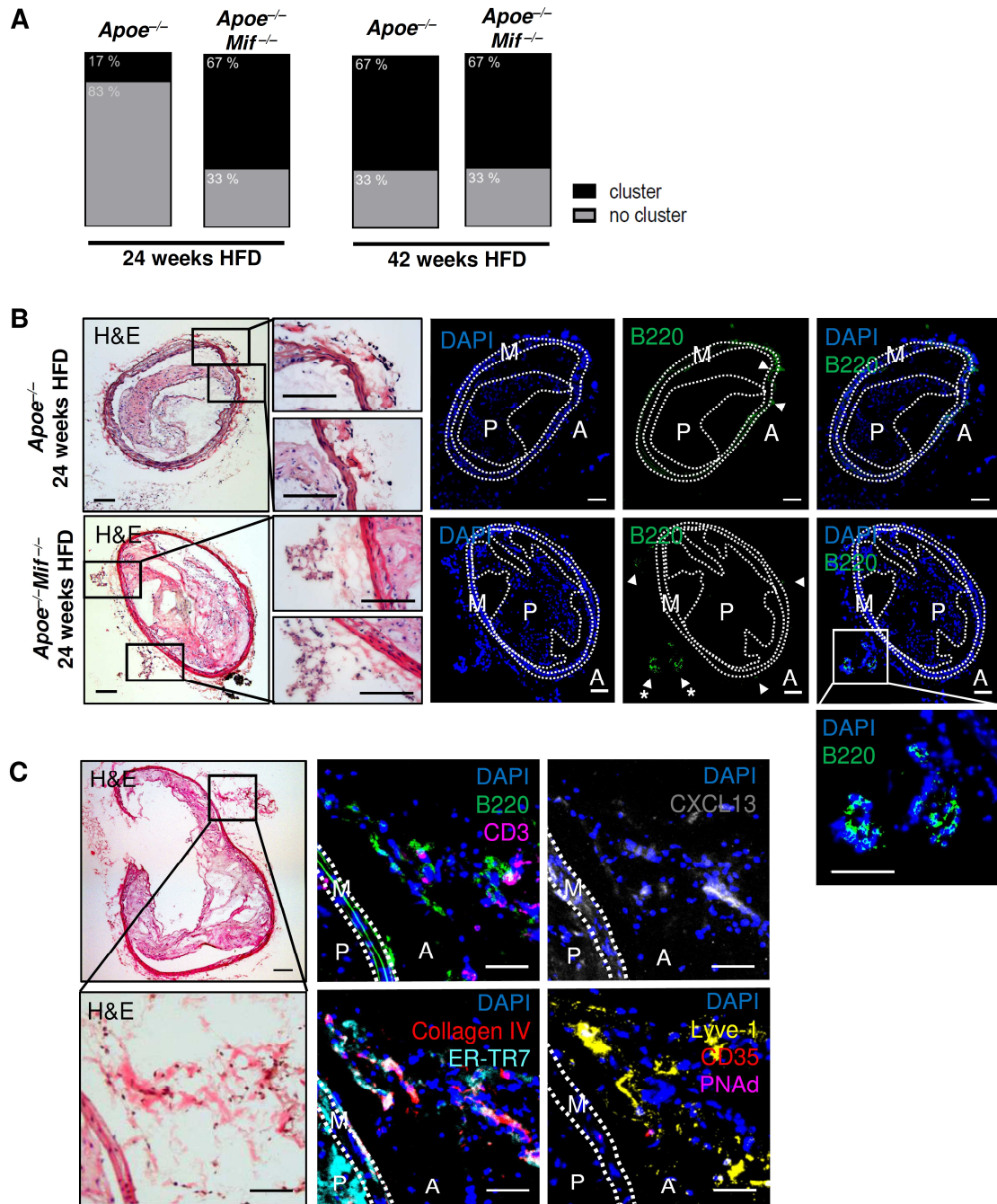
Figure A.4: *Mif*-deficiency accelerates the formation of B-cell-rich stage-2 (early) artery tertiary lymphoid organs (ATLOs). A) Quantification of the detected (peri-)adventitial B-cell clusters comparing *Apoe⁻/⁻Mif⁻/⁻* and *Apoe⁻/⁻* mice at the 30/24 and 48/42 age/HFD time intervals (n=6 mice per group). A total of 10 serial sections with a distance of 50 µm were screened for (peri-)adventitial clusters for each mouse. **B)** Representative images of the immunostainings against B220 on brachiocephalic artery (BCA) sections. Nuclear counterstain was performed using DAPI. B cells are displayed by an arrow. Arrows in combination with a star indicate B-cell clusters. A=adventitia, M=media, P=plaque, scale bar: 100 µm. **C)** Representative images of the immunostaining of the B-cell-rich clusters against ATLO-specific markers including B220 (B cells), CD3e (T cells), CXCL13 (B-cell recruitment factor), LYVE-1 (lymphatic vessel endothelial hyaluronic acid receptor 1; lymph vessels), PNAd (peripheral node addressin; high endothelial venules), CD35 (follicular dendritic cells), ER-TR7 (reticular fibers/fibroblasts), and Collagen IV (scale bar: 100 µm). Hematoxylin-eosin (H&E)-staining images are given for better orientation and visualization of the cellular clusters.

A decrease in anti-oxLDL IgM antibody titer correlates with loss of atheroprotection

While the pattern of ATLO formation across aging stages can only partially explain the loss of atheroprotection observed in highly aged *Mif*-deficient *Apoe*^{−/−} mice, the substantial increase in numbers of early ATLOs in the BCA of 24-week-HFD-subjected *Apoe*^{−/−} *Mif*^{−/−} mice could well contribute to atheroprotection seen in *Mif*-deficient mice at this age, as ATLO-derived B cells have been attributed atherogenesis-dampening properties[83,237].

To study this possibility, we analyzed the plasma levels of atherosclerosis-relevant anti-oxLDL antibody isotypes[70]. Anti-oxLDL IgM antibody levels that have been associated with atheroprotection[70] were significantly decreased after 42 weeks of HFD in *Apoe*^{−/−} *Mif*^{−/−} mice (Figure A.5a). In line with these results, titers of the anti-oxLDL IgG isotype, known to promote atherosclerosis[70], were not found to be decreased (Figure A.5b). We conclude that the observed age-dependent decrease of anti-oxLDL antibodies of the IgM isotype could contribute to the loss of atheroprotection seen in 42-week-HFD-fed *Apoe*^{−/−}*Mif*^{−/−} mice.
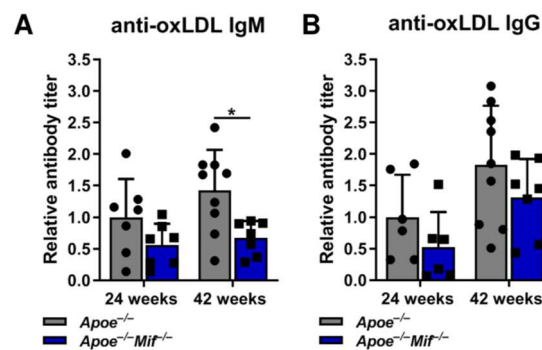
Figure A.5: *Mif*-deficiency leads to a decrease in atheroprotective anti-oxLDL IgM antibody titer in highly aged hyperlipidemic *Apoe*^{−/−} mice. Plasma antibody titer of anti-oxLDL IgM **(A)** and anti-oxLDL-IgG **(B)** antibodies in 30- and 48-week-old *Apoe*^{−/−}*Mif*^{−/−} mice (blue) *versus Apoe*^{−/−} controls (grey) on 24- and 42-week-HFD, respectively. oxLDL-coated microtiter plates were incubated with mouse plasma and HRP-labeled anti-IgM/IgG antibodies and chemiluminescent signals obtained. Values are normalized to those of the 30/24-week *Apoe*^{−/−} mouse group. Data are from n=6-9 mice and results are presented as means ± SD. Statistics: two-way ANOVA; *, $P<0.05$; each data point corresponds to one mouse.

Discussion

Macrophage migration inhibitory factor (MIF) is an inflammatory cytokine and atypical chemokine that was previously shown to promote atherogenesis by enhancing CXCR2/4-mediated leukocyte recruitment and vascular inflammation. The current study for the first time establishes a causal link between MIF and age-related changes in atherosclerotic pathology, demonstrating that regio-specific atheroprotection in *Mif*-gene-deficient atherogenic *Apoe*^{−/−} mice is lost during the course of aging and Western-type

HFD. As underlying cause, we identify a combination of mechanisms encompassing an age-dependent reduction in lesional Trem2+ macrophages, a loss in relative abundance of B-cell-rich-stage 2 ATLOs, and decreased levels of circulating anti-oxLDL IgM antibodies in *Mif*-deleted aged atherogenic *Apoe*$^{-/-}$ mice compared to *Mif*-proficient controls (Figure A.6).
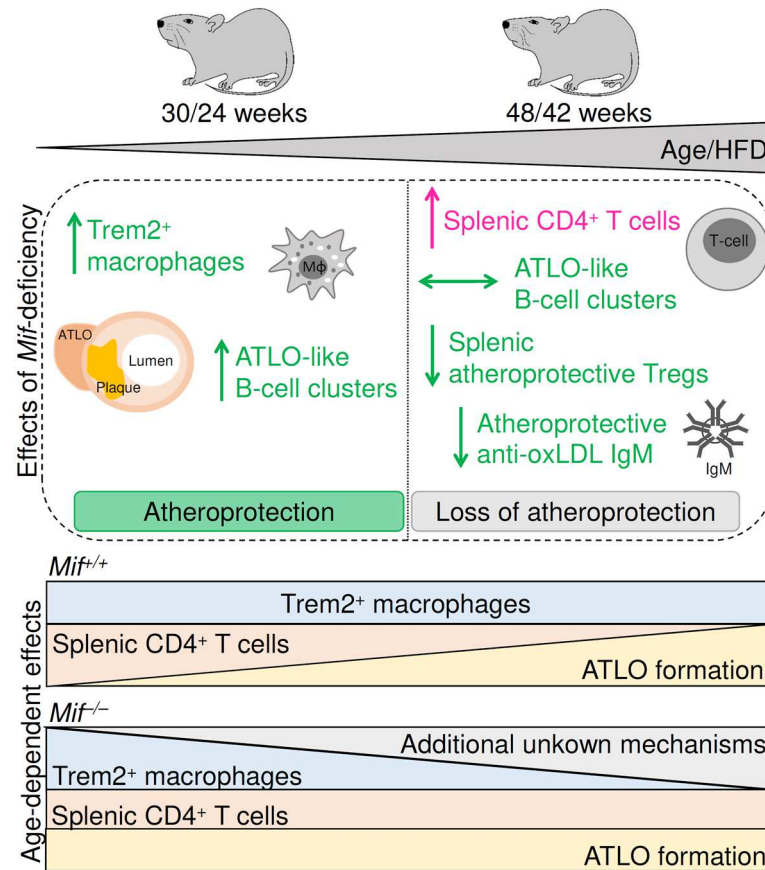

Figure A.6: Summary of age-related effects of *Mif*-deficiency in advanced atherosclerosis. The scheme summarizes the effects of global *Mif*-gene-deficiency in 30- and 48-week-old *Apoe*$^{-/-}$ mice on cholesterol-rich diet (HFD) for 24 or 42 weeks, respectively. The atheroprotective phenotype of the *Mif*-gene deletion in the 30/24-week group was associated with an increase in Trem2+ macrophages and enhanced atheroprotective ATLO-like B-cell cluster formation compared to the *Apoe*$^{-/-}$ controls. However, atheroprotection was lost in the highly aged 48/42-week group, accompanied by lowered atheroprotective anti-oxLDL IgM antibody levels and decreased splenic Treg cells in the *Mif*-deficient animals, while atheroprogressive CD4+ T-cells subsets might be increased in the spleen. Additionally, no differences in atheroprotective B-cell cluster formation between *Mif*$^{-/-}$*Apoe*$^{-/-}$ and *Apoe*$^{-/-}$ mice were observed in the highly aged animals of the 48/42-week group. Atheroprotective (green) and atheroprogressive mechanisms (magenta) are depicted.

MIF has been attributed an overall pro-inflammatory and atheroprogressive role as evidenced in various experimental models of atherosclerosis applying *Mif*-gene deficiency or antibody blockade, in line with correlations between MIF expression levels and human atherosclerotic disease[145,147,150,153,205]. However, while the specific role of the cardiac MIF/AMPK axis was examined in ischemic recovery in the senescent heart[235], the contribution of MIF to age-driven exacerbation of atherosclerotic lesion formation has not

been studied. Therefore, we analyzed the influence of *Mif*-deficiency in *Apoe*^{−/−} mice across different ages and HFD exposure intervals. *Mif*-knockout and wildtype *Apoe*^{−/−} mice were compared at an age of 30, 42, and 48 weeks, corresponding to 24, 36, and 42 weeks of HFD treatment, respectively. To further study the influence of aging *versus* duration of exposure to a cholesterol-rich HFD, a model of 52-week-old mice, in which HFD was limited to the last 6 weeks, was employed.

Deletion of the *Mif*-gene in the atherogenic *Ldlr*^{−/−} mouse model leads to protection from atherosclerotic plaque formation across the entire vascular bed, including aortic root and arch[145,151]. In contrast, protection conveyed by *Mif*-deletion in the context of the *Apoe*^{−/−} model is regio-specific and limited to the BCA and abdominal aorta[152]. The precise mechanistic causes for this background-specific difference have yet to be explored. Here, we confirm the regio-specific atheroprotective effect of *Mif*-deficiency in BCA and abdominal aorta in 30-week-old *Apoe*^{−/−} mice on HFD for 24 weeks. Strikingly, while 48-week-old *Mif*-deficient mice on HFD for 42 weeks showed significantly reduced serum triglyceride levels and a trend (P=0.057) towards reduced body weight compared to age-matched *Mif*-proficient control animals, the site-specific atheroprotective effect was found to be lost in these mice as well as in 52-week-old mice that had been on HFD for the last 6 weeks. As this ruled out major metabolic effects as an underlying cause for the observed lost atheroprotection phenotype in these highly aged in *Mif*-deficient animals, we surmised that *Mif*-deficiency delayed inflammation-mediated atherogenic processes but was no longer able to compensate for augmented inflammation in aged animals. In fact, inflammatory cytokines such as interleukin-6 (IL-6) or IL-1β have been found to be up-regulated over the course of aging and have been suggested to contribute to aging-related exacerbation of atheroprogression as both vascular extrinsic and intrinsic factors[238-240]. The correlation between the regulation of MIF expression and aging has remained unclear, but one study in humans suggests an increase in circulating MIF levels in the elderly[241], whereas age-related tissue expression of murine MIF was found to be increased in aorta[242] but decreased in cardiac tissue[235]. We determined MIF mRNA expression levels in spleen and liver and MIF protein levels in plasma in our mouse model but did not detect any differences between the 24- and 42-week-HFD groups. Thus, age-related changes in MIF expression cannot readily explain the observed loss of athero-protection in the aged *Mif*-deficient animals.

We noted a clear-cut connection between aging and MIF on macrophage numbers in the atherosclerotic lesions of the BCA. Compared to *Apoe*^{−/−} controls, *Mif*-deficient *Apoe*^{−/−} mice exhibited higher lesional macrophage counts in the 30-week-old animals after

24 weeks of HFD, but no difference was apparent in the aged 48/42-week mice. This was mainly due to a dramatic drop in lesional macrophage numbers in the *Mif*-deficient mice over the course of aging. Importantly, sub-class-specific analysis indicated that the number of Trem2^{+} macrophages significantly decreased between the 30/24 and 48/42 time points, suggesting that it could, at least partially, account for the age-dependent loss of atheroprotection in *Mif*-gene-deficient mice. Trem2^{+} macrophages were recently associated with anti-inflammatory properties and plaque regression[27,28]. Of note, arterial immune cell infiltration/content as a vascular intrinsic factor has been linked to the effects of aging on vascular inflammation and lesion formation[238,243,244]. Using an *Ldlr*^{−/−} model of atherosclerosis, it was additionally shown that aging in combination with HFD induces monocytosis and aortic macrophage accumulation[245]. How aging affects immune cell numbers specifically in the BCA of *Apoe*^{−/−} mice has not been investigated. As we did not see any significant age-dependent changes in lesional macrophage numbers in the *Apoe*^{−/−} mice, our data suggest that arterial MIF could serve as a regulator of immune cell homeostasis in the BCA over the course of aging, maintaining homeostatic macrophage sub-populations such as the Trem2^{+} subtype. *Mif*-deficiency in the vasculature might lead to an imbalance between macrophage subtypes during aging resulting in decreased Trem2^{+} macrophage counts, overall contributing to the loss of atheroprotection. However, underlying mechanisms of the decreased macrophage numbers in the *Mif*-deficient mice over the course of aging are still elusive and might be associated with an age-dependent augmentation in anti-proliferative and pro-apoptotic effects. In fact, MIF has been found to prolong macrophage survival[246] and enhances the proliferation of several cell types via its cognate receptor CD74[181,247,248]. A detailed future investigation of MIF effects on the recruitment, proliferation or survival of selective vascular wall macrophage sub-populations in the context of aging would thus be warranted.

Interestingly, we also observed an influence of MIF on T cells. Splenic CD4^{+} T-cell numbers in *Apoe*^{−/−}*Mif*^{−/−} mice were enriched both at 24 and 42 weeks of HFD compared to T-cell numbers in spleens from *Apoe*^{−/−} mice. Owing to the decrease of T-cell numbers in *Apoe*^{−/−} mice between 24 and 42 weeks of HFD, this difference was particularly pronounced at 42 weeks HFD. It is well established that aging affects the anatomy and organization of the spleen[249]. Different studies revealed a lowered abundance of splenic T-cell zones in aged C57BL/6 mice, together with a reduction in CD4^{+} T-cell recruitment and function[250,251]. We noticed that peripheral CD4^{+} T-cell counts were significantly lowered in *Mif*-deficient mice after 24 weeks of HFD as well as in the 52/6-week model of aging and hyperlipidemia. This could indicate that *Mif*-deficiency might promote T-cell egress from the periphery and favor homing to the spleen. However, the mechanism for

this scenario remains unclear and our analysis of splenic Treg numbers did not reveal an obvious connection between splenic T-cell subtypes and the observed plaque phenotype in the *Mif*-deficient animals.

We previously observed an enhanced re-organization of B cells into cluster-like structures in peri-adventitial areas in proximity to atherosclerotic plaques in the BCA of *Mif*-deficient *Apoe*^{−/−} mice[152]. Here, we show that the formation of such clusters in *Apoe*^{−/−} mice is age-dependent and that *Mif*-deficiency accelerates the formation of the clusters at 24 weeks of HFD, an effect that parallels the attenuation of lesion formation due to *Mif*-deficiency. We also noted that the increase in cluster formation in *Mif*-deficient mice compared to *Mif*-expressing controls vanished during the course of aging. The nature of these clusters had been elusive. Here, we provide evidence that these B-cell-rich clusters that form in an accelerated manner in *Mif*-deficient *Apoe*^{−/−} mice are stage-2 or early stage ATLOs. Adventitial ATLOs are typically observed in highly aged *Apoe*^{−/−} mice on chow or HFD for 52-78 weeks. ATLOs display a lymphoid-like organ structure and ATLO-based B cells are found in complex immune structures with organized T- and B-cell zones including germinal centers (GCs), lymph vessels, high-endothelial venules, and follicular dendritic cells (FDCs)[82,252]. Based on the expression of various markers, ATLOs of different maturation stages, i.e. stage 1-3, can be classified[82,253]. Moreover, ATLOs need to be differentiated from fat-associated lymphoid clusters (FALCs), which are T/B-cell accumulations that are solely found in adipose tissue[82]. Stage-1 ATLOs feature loosely arranged B cells and lymphocytes in these early ATLOs are not organized in dedicated B- and T-cell areas. They are also characterized by the expression of lymphorganogenic chemokines such as CXCL13. Stage-2 ATLOs contain individual T- and B-cell zones and emerging lymph vessels, along with conduit structures that bring the vessel wall into contact with the developing ATLO. In contrast, fully matured or stage 3 ATLOs display clearly defined T-cell zones and B-cell-rich regions. Moreover, they harbor GCs with FDCs and plasma cells (PCs) and exhibit vascular and lymphatic networks. In addition to the B- and T-cell clusters, we detected prominent cluster-associated expression of CXCL13, a vascular system including LYVE-1^{+} lymphatic vessels and appreciable collagen IV expression. However, organization of the infiltrated lymphocytes into clearly separated T- and B-cell zones as well as GC formation with FDCs that is characteristic of stage-3 ATLOs were absent[82]. Overall, the features are indicative of stage-2 ATLOs and we hypothesize that they may develop into mature stage-3 ATLOs upon further aging. As our structures only contained sparse ER-TR7 positivity, we conclude that they are distinct from secondary lymphoid organs (SLO), which would exhibit a well-structured ER-TR7^{+} encapsulation[82].

The functional role of ATLOs in atherosclerosis is incompletely understood. However, recent data revealed an atheroprotective role accompanied by activation of anti-inflammatory Treg cells within the ATLO[237]. Moreover, different B-cell subsets have been described to be present in ATLOs with B1b B cells predominating in the B-cell compartment[83]. B1 cells have been attributed atheroprotective functions by secreting natural IgM[75,76]. Based on these findings, we hypothesize that our identified stage-2 ATLOs may contribute to the atheroprotective effect in *Mif*-deficient *Apoe*^{−/−} mice that is eventually lost during aging. Accordingly, we next sought to determine if the formation of stage-2 ATLOs was accompanied by changes in the production of atheroprotective IgM *versus* atheroprogressive IgG antibodies. The mechanism by which IgG and IgM promote or attenuate atherosclerosis are mainly based on the recognition of oxidation-specific epitopes (OSEs) such as in oxLDL[70]. Atheroprotective anti-oxLDL IgM antibodies have been shown to neutralize oxLDL and inhibit its uptake by macrophages thereby suppressing foam cell formation, whereas anti-oxLDL IgG antibodies associate with oxLDL particles inducing lesional macrophage activation via Fcγ-receptors[70]. Here we noted that loss of atheroprotection in highly aged *Mif*-deficient mice correlated with significantly reduced levels of circulating atheroprotective anti-oxLDL IgM levels, whereas anti-oxLDL IgG levels remained unchanged. Overall, this finding is in line with the previously reported link between *Mif*-deficient and atheroprotective autoantibodies[152].

Our study of *Mif*-deficiency in the context of atherosclerosis and aging furthers the notion that aging affects atherogenesis in a complex manner, with cytokine/chemokine-related inflammatory mechanisms playing key roles. Considering the continuing rise of atherosclerotic patients in an aging population, the design of treatment strategies specifically tailored for elderly individuals will become important. Based on the principal success of the CANTOS trial[254] and the emerging link between inflamm'aging and atherosclerosis[228], cytokine/chemokine-directed strategies may represent promising approaches for age-tailored intervention strategies. MIF is a promising target in atherosclerosis and a variety of inhibition routes including antibody-, small molecule- and peptide-based strategies have been discussed[176,187,255]. However, age-tailored strategies have not been investigated. The preclinical data obtained in our present study confirm that MIF-based inhibition strategies may be promising in cardiovascular patients. However, the 'loss-of-atheroprotection phenotype' observed in highly aged *Mif*-deficient mice would argue that MIF-blocking strategies might be less effective in highly aged individuals. Obviously, such conclusions may be severely hampered by the well-known problems of translating data from mouse models into human disease scenarios, but clinical correlation studies in CVD patients taking into account MIF expression levels in *MIF*-low (carrying the
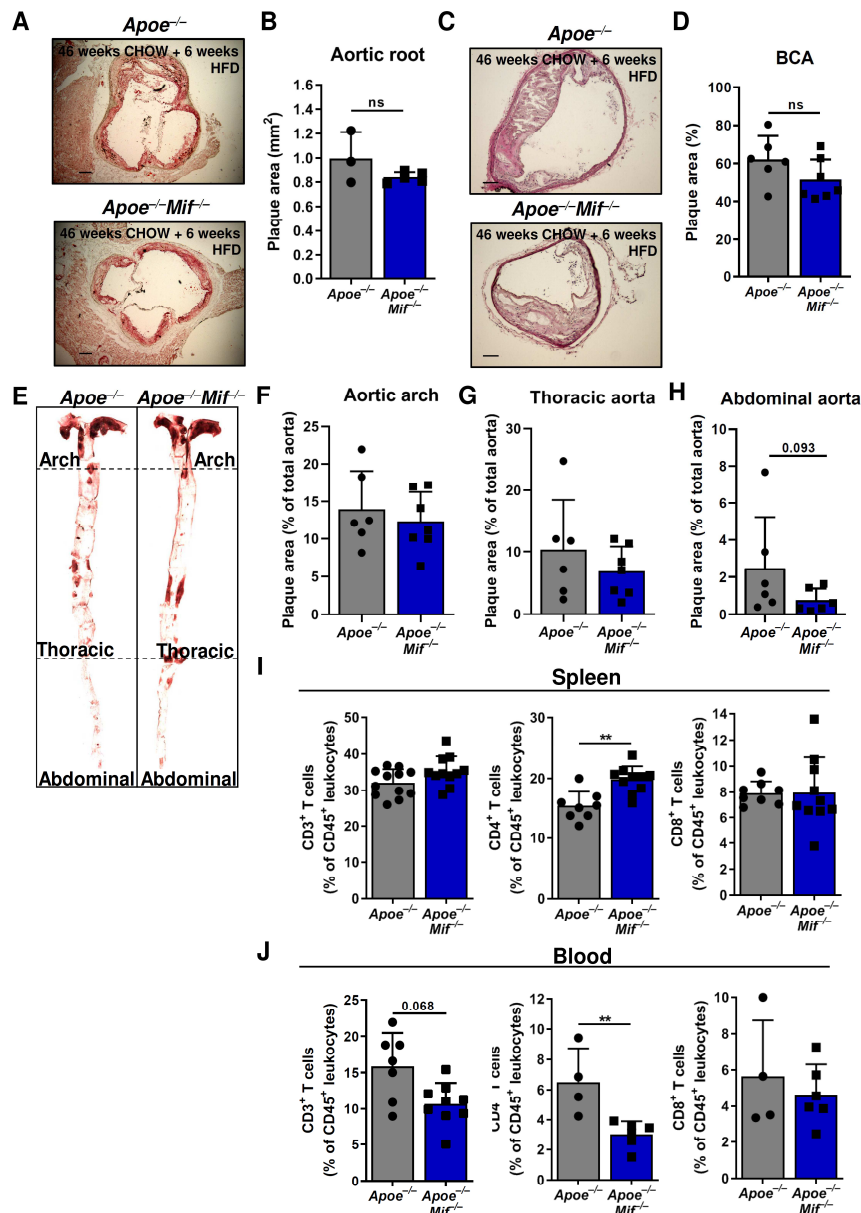
CATT5/5 or 5/6 polymorphism) *versus MIF*-high (carrying the CATT6/7 or 7/7 polymorphism) expressers[149,256] could guide such translational considerations.

In conclusion, this work unravelled a previously unknown link between *Mif*-deficiency, atheroprotection and aging in the *Apoe*$^{-/-}$ model of atherosclerosis. We show that site-specific atheroprotection in *Mif*-deficient mice is lost in highly aged animals and/or upon long-term HFD and identify a combination of mechanisms, encompassing reduced lesional Trem2+ macrophages, peri-adventitial ATLOs and decreased atheroprotective anti-oxLDL IgM antibodies, as the underlying cause of this phenotype. This needs to be considered, when devising MIF-directed targeting strategies for aged atherosclerotic patients.

Supplement

Supplementary figure A.1: *Mif*-deficiency fails to confer atheroprotection in 52-week-old *Apoe*$^{-/-}$ mice. Plaque area was quantified in brachiocephalic artery (BCA), aortic root, aortic arch, thoracic and abdominal aorta in 52-week-old *Apoe*$^{-/-}$*Mif*$^{-/-}$ mice that had been on HFD for the last 6 weeks before sacrifice (blue) and compared to corresponding *Apoe*$^{-/-}$controls (grey). **A-B)** Representative images **(A)** and quantification **(B)** of ORO-stained sections of the aortic root. For each mouse, 10 serial sections with a distance of 50 µm were used for analysis. The mean plaque area is depicted in mm^2 (n=3-5 mice per group; results are presented as means ± SD; scale bar: 200 µm). **C-D)** Representative images **(C)** and plaque quantification **(D)** of H&E-stained sections of the BCA. Serial sections were obtained as above. The mean plaque area is depicted as percentage of the total inner vessel area including the plaque (n=6-7 mice per group; results are presented as means ± SD; scale bar: 100 µm). **E)** Representative images of *en face*-prepared ORO-stained aortas. **F-H)** Quantification of the plaque are in the aorta including aortic arch **(F)**, thoracic aorta **(G)**, and abdominal aorta **(H)**. The plaque area is depicted as percentage of the total aortic surface (n=6-7 mice per group; results are presented as means ± SD). **I-J)** FACS-based quantification of total CD3$^+$ T cells **(left graphs)**, CD4$^+$ T-cell subsets **(middle graphs)**, and CD8$^+$ T-cell subsets **(right graphs)** in spleen **(I)** and blood **(J)** of *Apoe*$^{-/-}$*Mif*$^{-/-}$ mice (blue) and comparison to *Apoe*$^{-/-}$ controls (grey). 52-week-old mice on HFD for 6 weeks before sacrifice were examined (n=4-12 mice per group; results are presented as means ± SD). Statistics: Mann-Whitney Test, *, *P*<0.05, **, *P*<0.01, non-significant results with *P* values between 0.05 and 0.1 are indicated; each data point corresponds to one mouse.

91
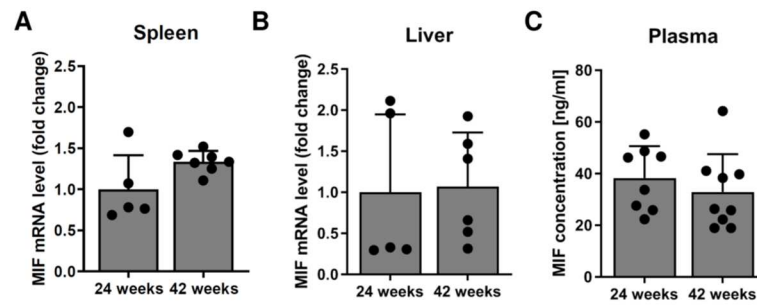
Supplementary figure A.2: MIF levels remain unchanged with increased age and duration of HFD in Apoe$^{-/-}$ mice. A-B) mRNA expression of MIF was assessed by RT-qPCR in spleen **(A)** and liver **(B)** of Apoe$^{-/-}$ mice after 24 and 42 weeks of HFD. Values were normalized to the values of the 30-week-old Apoe$^{-/-}$ controls that received HFD for 24 weeks (n=5-7 mice; results are presented as means ± SD). **C)** MIF plasma levels as measured by ELISA in Apoe$^{-/-}$ mice after 24 and 42 weeks of HFD. Values were normalized to the Apoe$^{-/-}$ controls that received HFD for 24 weeks (n=8-9 mice per group; results are presented as means ± SD). Statistics: Mann-Whitney test (no significant differences observed; each data point represents one mouse).
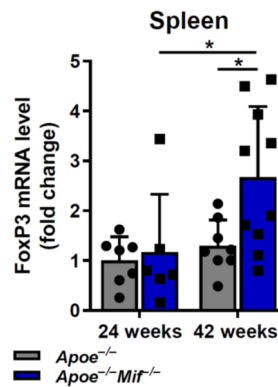
Supplementary figure A.3: Increased numbers of splenic FoxP3+ Tregs in highly aged Mif-deficient Apoe$^{-/-}$ mice. mRNA expression of FoxP3 was assessed by RT-qPCR in spleen of Apoe$^{-/-}$Mif$^{-/-}$ mice (blue) after 24 and 42 weeks of HFD and compared to the WT controls (grey). Values were normalized to the values of the 30-week-old Apoe$^{-/-}$ controls that received HFD for 24 weeks (n=6-10 mice; results are presented as means ± SD). Statistics: two-way ANOVA (each data point corresponds to one mouse).
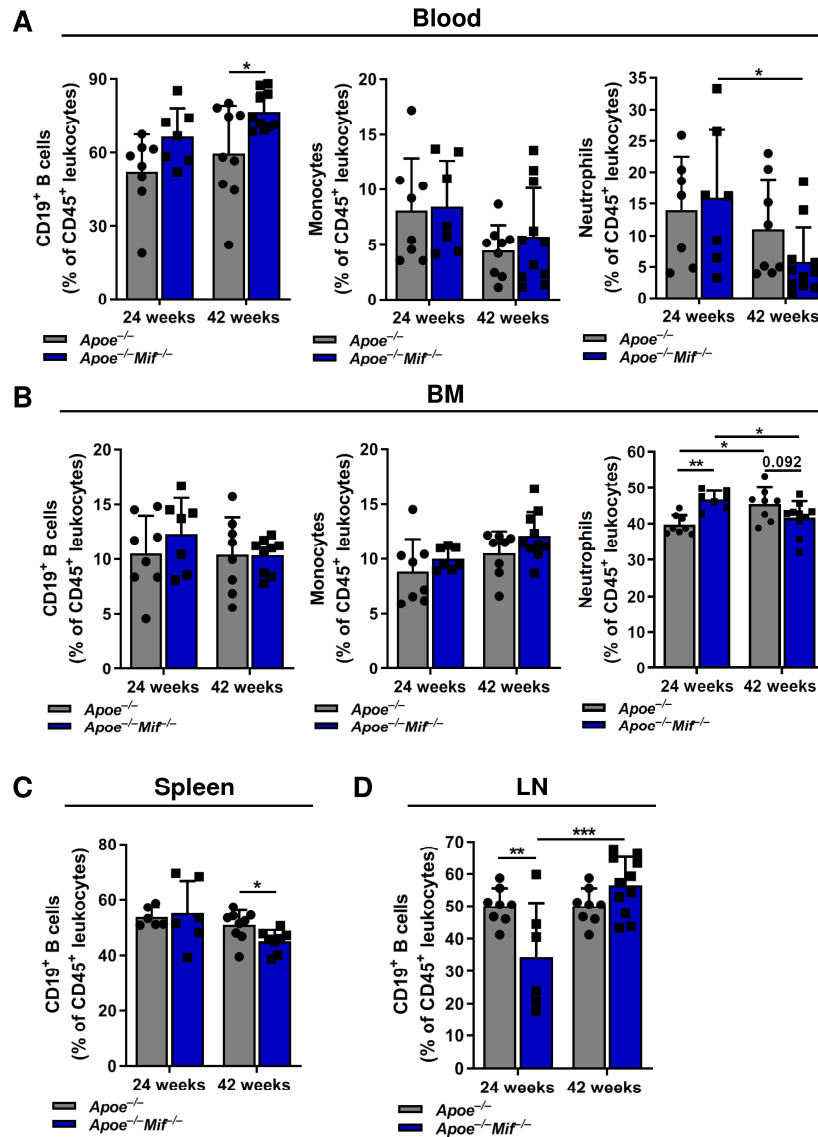
Supplementary figure A.4: FACS-based analysis of immune cell numbers in immune organs and periphery. A-D) B-cell (left graphs), monocyte (middle graphs) and neutrophil (right graphs) counts were evaluated by flow cytometry in the blood **(A)**, BM **(D)**, spleen **(C)** and LNs **(D)** of $Apoe^{-/-}Mif^{-/-}$ mice (blue) after 24 and 42 weeks of HFD and compared to the $Apoe^{-/-}$ controls. Monocyte and neutrophil counts in the spleen and LN were below 5 % and are not shown (n=6-11, results are presented as means ± SD). Statistics: two-Way ANOVA; *, $P \leq 0.05$, **, $P \leq 0.01$, ***, $P \leq 0.001$, non-significant results with P values between 0.05 and 0.1 are given as precise numbers; each data point corresponds to one independent mouse.

93

Appendix B: Publication IV

The data presented as part of this section is not published yet, but a manuscript for the submission to the developmental biology journal *Development* is in preparation.

Macrophage migration inhibitory factor (MIF) alters the transcriptomic program of bone marrow B-cell subsets to control B-cell development and function

Christine Krammer[1#], Simon Besson-Girard[2#], Fumere Usifo[2], Sabrina Reichl[1], Verena Bolini[1], Jürgen Bernhagen[1,3,4,*], Ozgun Gokce[2,3,*]

[1]Chair of Vascular Biology and [2]Systems Neuroscience group, Institute for Stroke and Dementia Research (ISD), LMU Klinikum, Ludwig-Maximilians-University (LMU), 81377 Munich, Germany; [3]Munich Cluster for Systems Neurology (SyNergy), 81377 Munich, Germany; [4]Munich Heart Alliance, 80802 Munich, Germany.

[#]contributed equally

 [*]Shared senior authorship and correspondence:

Dr. Ozgun Gokce, PhD
Systems Neuroscience Group
Institute for Stroke and Dementia Research (ISD)
Ludwig-Maximilians-University (LMU) Klinikum
Feodor-Lynen-Straße 17,
81377 Munich, Germany
Tel.: 0049-89 4400 - 46154
E-Mail: oezguen.goekce@med.uni-muenchen.de

Professor Jürgen Bernhagen, PhD
Chair of Vascular Biology
Institute for Stroke and Dementia Research (ISD)
Ludwig-Maximilians-University (LMU) Munich
Feodor-Lynen-Straße 17,
81377 Munich, Germany
Tel.: 0049-89 4400 - 46151
E-Mail: juergen.bernhagen@med.uni-muenchen.de

Abstract

Macrophage migration inhibitory factor (MIF) is an inflammatory cytokine with chemo-kine-like functions that has been implicated in innate immunity as well as chronic inflammatory conditions. It was previously shown that MIF mediates B-cell survival and recruitment, and *Mif*-deficiency was linked to a B-cell developmental block in the bone marrow (BM) of atherogenic mice. However, MIF's role in B-cell maturation is still incompletely understood and underlying molecular and functional mechanisms remain unexplored. Here, we showed that MIF mediates BM-derived B-cell chemotaxis in a subset-specific manner, suggesting a role for MIF as a BM niche factor. To characterize the contribution of MIF to the B-cell developmental cascade in depth, we performed a transcriptional analysis of B cells at defined developmental stages applying bulk RNA-sequencing (RNAseq) technology using the Smart-seq2 method. We mapped B-cell developmental trajectories and dissected changes in B-cell transcriptomic signatures and behavior in the context of *Mif*-deficiency. Our results imply that B-cell identities are maintained in *Mif*-deficient (*Mif*$^{-/-}$) mice, while the transcriptomic profile of the individual B-cell subsets significantly differs between *Mif*$^{-/-}$ and wild type (WT) mice. Gene ontology (GO)-enrichment analysis discovered pathways associated with mitosis/proliferation and adhesion to be enriched in early developmental B-cell stages in *Mif*$^{-/-}$ mice compared to WT control mice. These results were supported by functional *in vitro* data revealing an impairment in adhesion behavior of BM-derived B cells from *Mif*$^{-/-}$ mice accompanied by reduced proliferation of *Mif*-deficient pre-B-cells. Together, we provide molecular and functional insights into the role of MIF as a mediator of B-cell development and show that *Mif*-deficiency is associated with subset-specific transcriptional changes that might affect biological activities.

Introduction

B-lymphocyte maturation in the bone marrow (BM) involves sequential and strictly regulated processes that have been comprehensively described[48-50]. Arising from progenitor cells in the BM, B cells pass a series of maturation steps leading to the emergence of immature B cells representing the BM emigrants, which undergo a transition phase before they finally develop into fully maturated B cells. Mature murine B cells are divided into two subsets, namely B1 and B2 cells. B1 cells are predominating in the peritoneum and the pleural cavity, while B2 cells including marginal zone (MZB) and follicular (FOB) B cells are found in the secondary and tertiary lymphoid organs[49,80]. B cells regulate adaptive and innate immune responses and are best known for their antibody-producing

function. Additionally, B cells are important players in controlling T-cell activation, cytokine production and as key antigen-presenting cells (APCs)[257].

The investigation of stage-specific cell surface markers in combination with immunoglobulin (Ig) recombination events has revealed distinct developmental BM B-cell stages including pre–pro-, pro-, early and late pre-, as well as immature B cells. However, the marker-based classification of the subsets is inconsistent and independent strategies to discriminate between BM-derived B-cell stages have been established[50,258-262]. Together with a limited amount of available and simultaneously applicable markers, the lack of marker conformity makes the analysis of distinct developmental B-cell subsets tremendously complex and challenging. The shortage of transcriptome studies characterizing developmental B-cell subsets in mouse and humans results in an incomplete understanding of the molecular basis of B-cell maturation in the BM[263-265].

The developmental cascade is controlled at several checkpoints involving Ig rearrangements, interleukin (IL)-7- and pre-B-cell receptor (pre-BCR) signaling and CXCR4[48,51,63], but the involved regulatory network is presumed to be more complex. Thus, a dynamic microenvironment and an orchestrated niche-specific cytokine/chemokine expression landscape are crucial for B-cell homing and migration during development[63,266]. CXCL12 secreted by stromal cells has been identified as a crucial BM niche factor[266] and signaling via CXCR4 is required for B-cell maturation as evidenced by genetic deletion in mouse models[267,268]. Similarly, B-cell development is obstructed at early phases in the BM of *IL-7-* or *IL-7R*-deficient mice[269,270].

Macrophage migration inhibitory factor (MIF) is a structurally peculiar, atypical chemokine and mediator of inflammation that has been causally related to cardiovascular diseases[114,145] and has also been implicated as BM niche factor for B cells[271]. Discovered as one of the first cytokines over 50 years ago, today MIF is recognized as a functionally diverse inflammatory cytokine, which promotes atherogenesis[114,151,220]. In atherogenic mouse models, antibody-mediated neutralization or genetic knockout of MIF leads to the downregulation of important inflammatory and pro-atherogenic factors and to an athero-protective autoantibody profile[145,150-152]. MIF is semi-constitutively expressed by immune cells, endothelial cells, stromal cells and fibroblasts[220] and signaling is mediated by engagement of the CXC chemokine receptors CXCR2 and CXCR4[145] or via CD74/invariant chain[158]. Of note, CD74 has been implicated as a survival and proliferation factor involved in B-cell development[177,179]. MIF binding to a CD74/CD44 complex mediates the activation of survival pathways in B cells[160] and signaling via CXCR4/CD74 has been associated with B-cell migration[183]. However, the impact of MIF or *Mif*-gene deletion over

the B-cell developmental course is still elusive. We recently uncovered a functional cor-relation between MIF and B-cell maturation in a mouse model of atherosclerosis using hyperlipidemic *apolipoprotein E*-deficient (*Apoe*$^{-/-}$) mice[152]. While our data indicated a B-cell maturation blockade in *Mif*-gene deleted (*Mif*$^{-/-}$) mice suggesting that MIF acts as a mediator of B-cell maturation in the BM, its precise role and the underlying functional mechanisms have remained unexplored.

RNA sequencing (RNAseq) is a powerful tool to assess transcriptomic changes during development as a prerequisite to map the involved developmental routes and mechanistic pathways. Here, we provide a detailed transcriptomic characterization of B-cell developmental subsets from murine BM and spleen using RNAseq. Our data gives insight into the distinct transcriptomic signatures of B-cell stages recapitulating the developmental cascade from earliest pre–pro-B cells in the BM to mature MZB and FOB cells in the spleen. The transcriptome screen of B cells from *Mif*$^{-/-}$ mice compared to the WT controls indicates that MIF acts as a modifier of B-cell development. While *Mif*-deficiency generally maintains B-cell identities and developmental trajectories, it dramatically alters the transcriptomic signatures of B-cell subpopulations from BM and spleen with substantial effects on early stages in the BM. These results were supported by functional *in vitro* assays revealing changes in cellular pathways associated with proliferation, migration and adhesion.

Materials and Methods

Cytokines, buffers and reagents

Recombinant MIF was generated by expression in the pET11b/*E. coli* BL21/DE3 system and purification as previously described[120]. After renaturation, the purity of the protein was around 98%. Recombinant CXCL12 and CXCL13 were bought from Peprotech (Hamburg, Germany) and recombinant vascular cell adhesion molecule (VCAM-1) was obtained from R&D Systems (Wiesbaden-Nordenstadt, Germany). Miscellaneous cell culture solutions were bought from Invitrogen/Thermo Fisher Scientific (Darmstadt, Germany). Other reagents were obtained from Sigma Aldrich/Merk (Darmstadt, Germany), Carl Roth GmbH (Karlsruhe, Germany) and BioLegend (Koblenz, Germany) and were of the highest quality available.

Animals

Wild type (WT) and *Mif*-deficient (*Mif*^{−/−}) mice were on C57BL/6 background and have been reported before[145,152,158,233]. Mice were housed and bred under standardized conditions in the mouse core facility at the Center for Stroke and Dementia Research (CSD) in Munich. All animal experiments were approved by local authorities (animal ethics approval ROB-55.2-2532.Vet_02-18-040) and were conducted in consistency with the German animal protection law. Animals were sacrificed under anaesthesia with midazolam/medetomidine/fentanyl (MMF) to minimize suffering. Experiments were performed using age- (14-17 weeks) and sex-matched (female) animals.

Tissue isolation and preparation of single-cell suspensions

After sacrifice, the spleens, femurs and tibiae were harvested and stored in PBS on ice until isolation of cells. Spleens were dissociated and filtered through a 40 µm cell strainer (Corning®, Sigma Aldrich/Merck). Following lysis of red blood cells using red blood cell (RBC) lysis buffer (BioLegend), cells were washed with Magnetic cell separation (MACS) buffer (0.5% BSA and 2 mM EDTA in PBS, pH 7.2) and MZB and FOB cells pre-enriched using the Marginal Zone and Follicular B Cell Isolation kit (Miltenyi Biotech, Bergisch Gladbach, Germany) according to the manufacturer's instructions. B-cell subsets were isolated in two steps: First, cells were resuspended in 400 µl MACS buffer per 10^8 cells and non-targeted cells labeled with a cocktail of biotinylated antibodies against CD43, CD4, CD93 and Ter119 (100 µl/10^8 cells) for 5 min at 4°C. An additional 300 µl of MACS buffer per 10^8 cells was added and cell suspensions incubated with anti-biotin microbeads (200 µl/10^8 cells) for 10 min at 4°C. After washing with MACS buffer, FOB and MZB cells were enriched by depleting the magnetically labeled cells applying a LS MACS separation column (Miltenyi Biotech) and a magnetic MACS separator device (Miltenyi Biotech). Non-depleted cells were centrifuged and resuspended in 450 µl MACS buffer. In a second step, FOB cells were labeled using CD23 microbeads (50 µl/10^8 cells) for 10 min at 4°C and separated from MZB cells using a MACS separator.

BM-derived cells were collected by flushing the femur and tibia with PBS and filtering the suspension through a 40 µm cell strainer. After RBC lysis and a washing step with PBS, cells were used for subsequent analysis.

Flow cytometry and sorting of B-cell developmental subsets from BM and spleen

Isolated cells from BM or spleen were washed with FACS buffer (0.5% BSA in PBS, pH 7.4) and stained with antibodies against subset-specific surface markers for 30 min on ice protected from light. The surface marker profile of different splenic and BM B-cell subpopulations is indicated in Table B.1. The following antibodies against murine (m) epitopes were used for the sorting of B-cell developmental stages from the BM in a final dilution of 1:100 in FACS buffer: anti-mIgM-FITC (Miltenyi Biotech, #130-095-906), anti-mCD19-APC (BioLegend, #115512), anti-mCD45-APC/Cy7 (BioLegend, #103116), anti-mIgD-Vioblue (Miltenyi Biotech, #130-102-268), anti-mCD43-PE (ThermoFisher Scientific, #12-0431-81), anti-mB220-AF700 (Biolegend, #103232). In order to reduce the amount of fluorescently labeled antibodies needed for the discrimination of splenic FOB and MZB cells, these subsets were initially pre-enriched as described above allowing sorting based on only 4 different markers. The following antibodies were used for the sorting of pre-enriched FOB and MZB cells: anti-mIgM-FITC, anti-mCD21-PerCp/Cy5.5 (BioLegend, #123415), anti-mCD23-PE/Cy7 (ThermoFisher Scientific, #25-0232-81), anti-mIgD-Vioblue. Stained cells were washed with FACS buffer and pools of 50 cells were sorted using a 100 µm sorting chip and the SH800S cell sorter (Sony Biotechnology, Berlin, Germany) containing 4 lasers and 6 fluorescence detectors. Fluorescence compensation was performed using single-stained samples. Cells were sorted into wells of a 96-well plate containing 4 µl lysis buffer (0.05% Triton X-100, ERCC RNA Spike-In mix (ThermoFisher Scientific) diluted 1:24000000, 2.5 µM oligo-dT primers (Eurogentec Deutschland GmbH, Cologne, Germany), 2.5 mM dNTPs (ThermoFisher Scientific) and 1 U/µl of RNase inhibitor (Clontech, Takara Bio Europe, Saint-Germain-en-Laye, France)) and immediately frozen at -80°C.

Alternatively, especially for sorting-independent analysis or quantification purposes of B cells the BD FACSVerse™ (BD Biosciences, Heidelberg, Germany) was used in combination with the following antibodies for splenic subsets: anti-mCD45-APC/Cy7, anti-mCD19-APC, anti-mCD93-PE (ThermoFisher Scientific, #1934758), anti-mIgD-Vioblue, anti-mCD23-PE/Cy7, anti-mCD21-PerCp/Cy5.5, anti-mIgM-FITC; or BM-derived subsets: anti-mCD45-APC/Cy7, anti-mCD19-APC, anti-mB220-PE/Cy7 (BioLegend, #103222), anti-mIgD-Vioblue, anti-mIgM-PerCP-Vio700 (Miltenyi Biotech 130-106-012).

Data analysis was conducted applying FlowJo software (Tree star, USA). Cell populations were quantified as percentage of CD45$^+$ leukocytes or B220$^+$/CD19$^+$ B cells.

Table B.1: Subset-specific surface markers of splenic and BM B cells.

B-cell subset	Organ	Marker expression
Pre–pro-B cells	BM	$CD45^+CD19^-B220^+CD43^+IgM^-IgD^-$
Pro-B cells	BM	$CD45^+CD19^+B220^+CD43^+IgM^-IgD^-$
Pre-B cells	BM	$CD45^+CD19^+B220^+CD43^-IgM^-IgD^-$
Immature B cells	BM	$CD45^+CD19^+B220^+CD43^-IgM^+IgD^-$
Transitional B cells	BM	$CD45^+CD19^+B220^+CD43^-IgM^+IgD^+$
Follicular (FOB) B cells	Spleen*	$(CD45^+CD19^+CD93^-)CD21^{low}IgM^{low/high}$
Marginal Zone Precursor (MZP) B cells	Spleen*	$(CD45^+CD19^+CD93^-)CD21^+IgM^+CD23^+IgD^{high}$
Marginal Zone (MZB) B cells	Spleen*	$(CD45^+CD19^+CD93^-)CD21^+IgM^+CD23^-IgD^{low}$

*Brackets indicate that spleen suspensions were pre-enriched for MZB and FOB cells and that sorting of splenic B-cell subsets did not include the CD45, CD19 and CD93 markers.

Reverse transcription (RT) and cDNA pre-amplification

All experimental steps described in this section were performed by F. Usifo and S. Besson-Girard (Systems Neuroscience Group, ISD, Munich). Cell-containing plates were incubated for 3 min at 72°C and subsequently set on ice. For the reverse transcription (RT), a mixture of 0.14 µl H_2O, 0.95 µl SMARTScribe™ reverse transcriptase (Clontech, Takara Bio Europe) at a final concentration of 15.83 U/µl, 2 µl 5x First strand buffer (Clontech, Takara Bio Europe) at a 1.67x final dilution, 0.25 µl Recombinant RNase inhibitor (Clontech, Takara Bio Europe) at a working concentration of 1.67 U/µl, 2 µl of Betaine PCR solution (5 M, Sigma Aldrich/Merck) at a working concentration of 1.67 M, 0.5 µl of UltraPure™ Dithiothreitol (DDT) (100 mM, ThermoFisher Scientific) at a working concentration of 8.33 mM, 0.06 µL of $MgCl_2$ (1 M) at a working concentration of 0.01 M and 0.1 µl of Template-switching oligos (TSO) (100 µM, AAGCAGTGGTATCAAC-GCAGAGTACATrGrG+G) (Eurogentec Deutschland GmbH) at a working concentration of 1.67 µM was added to each well. Next, the RT reaction mixes were incubated in the thermal cycler C1000 Touch (BioRad, Feldkirchen, Germany) for 90 min at 42°C, following 10 cycles of 50°C (2 min) and 42°C (2 min), and incubation for 5 min at 70°C.

PCR-based pre-amplification of cDNA was performed by adding 15 µl of a mixture consisting of 12.5 µl KAPA HiFi Hotstart ReadyMix 2x (KAPA Biosystems Inc., Roche Diagnostics GmbH, Mannheim, Germany) at a 1.67x final dilution, 2.138 µl H_2O, 0.25 µl IS_PCR primers (10 µM, 5′-AAGCAGTGGTATCAACGCAGAGT-3) (Eurogentec) at a working concentration of 0.17 µM and 0.1125 µl Lambda exonuclease (New England

Biolabs, Frankfurt, Germany) at a working concentration of 0.038 U/µl using the thermal cycler C1000 Touch (BioRad) at the following conditions: Enzyme activation at 37°C for 30 min, initial denaturation for 3 min at 95°C, 18 cycles of denaturation (98°C for 20 sec), annealing (67°C for 15 sec) and elongation (72°C for 4 min), final elongation for 5 min at 72°C.

Afterwards the cDNA was purified by adding 18 µl of AMPure XP beads (Beckman Coulter, Munich Germany) to each well to obtain a sample to bead ratio of 1:0.7. After mixing for 2 min at 1800 rpm the solution was incubated for 5 min at RT. The plate was placed into the magnetic field of a DynaMag™-96 magnet (Thermofisher Scientific) and equilibrated for 3 min. Afterwards the beads were washed twice with 300 µl of 80% ethanol for 30 sec within the magnetic field. The beads were air-dried for 10-15 min before removing the tube from the magnetic field. After adding 20 µl of Elution buffer (Qiagen, Hilden, Germany) the sample was mixed for 2 min at 1800 rpm and placed again into the magnetic field in order to elute the cDNA from the beads.

The cDNA concentration was obtained using the Qubit DNA high sensitivity assay kits (ThermoFisher Scientific) and a Qubit 2.0 fluorometer (Life Technologies, ThermoFisher Scientific). Samples were normalized to a concentration of 160 pg/µl.

RNAseq library construction and DNA sequencing

50-cell Illumina libraries were constructed by F. Usifo and S. Besson-Girard in 96-well plates using the Illumina Nextera XT DNA sample preparation kit (Illumina, Munich, Germany) according to the manufacturer's instructions in combination with indexes provided with the Illumina Nextera XT DNA sample preparation kit.

After pooling the libraries by transferring 1 µl of each well from the 96 well plate to an eppendorf tube, samples were purified by adding 77 µl of AMPure XP beads (Beckman Coulter) at a final sample to bead ratio of 1:0.8. The complete purification procedure was performed three times as described before.

After sample purification, the 50-cell library was sequenced in paired-end mode and 150 base pairs per read with a sequencing depth of 1×10^6- 2×10^6 reads/sample using an Illumina HiSeq4000 machine. The sequencing service was provided by the *Munich Sequencing Alliance* at Helmholtz Center Munich (Munich, Germany).

Processing, quality control and normalization of scRNAseq data

All computational processes leading to the processing, quality control and normalization of the data were performed by S. Besson-Girard. The raw output from the Illumina sequencer (binary base call files) were demultiplexed with the *bcl2fastq* software from Illumina. After removal of the Nextera adapters and low-quality reads with *Trim Galore* and *Cutadapt*, alignment was made using *rnaSTAR*[272] against the GRCm38 (mm10) genome with ERCC synthetic RNA (ThermoFisher Scientific) added. Read counts were collected using the parameter *quantMode GeneCounts* of rnaSTAR and the unstranded count values. In the following, the Seurat R package was used[273]. Samples with poor quality were excluded from the dataset by using thresholds for the amounts of identified genes (minimum 2000 different genes per cell), the percentage of mitochondrial genes (maximum 8%), the percentage of ERCCs (0.4% maximum) and the number of reads on a log10 scale (between 5 to 6). We ended up with a total of 124 samples. Gene expression was normalized to 200000 counts per sample using the *NormalizeData* function. Datasets were scaled and the depth of sequencing was regressed using the *ScaleData* function and the percentage of ERCCs. The two conditions (WT and *Mif*$^{-/-}$) were then merged and analyzed using *Canonical Correlation Analysis* from the Seurat R package.

Analysis of the RNAseq data

The RNAseq data was analyzed and results were provided by S. Besson-Girard. Uniform Manifold Approximation and Reduction (UMAP) was generated with a neighborhood of 100 and a minimum distance of 0.3. All plots from the UMAP analysis were generated using Seurat's built-in functions as well as *ggplot2* in R[274]. For the identification of genes with significant changes in expression levels between *Mif*$^{-/-}$ and WT samples, the Seurat *FindAllMarkers* function from Seurat was used and *Wilcoxon rank sum* was applied on the genes showing at least 0.25-fold difference (log-scale). The *Bonferroni correction* was used for correcting the *P* value for multiple testing and we chose a cut-off of 5%. The data was visualized using heatmaps. Based on the differential gene expression (DGE) results, we used the *Bioconductor library cluster profiler*[275] and mouse genome annotations (org.Mm.eg.db: *Genome wide annotation for Mouse.* R package) to identify gene sets that were significantly enriched in each subpopulation. We used the *Benjamini-Hochberg* to correct the *P* value for multiple testing and chose a cut-off of 5%. Cell cycle analysis was performed applying a cell-cycle-related gene set from Macosko et *al.*[276] with 100 genes for G1/S phase, 113 genes for S phase, 133 genes for G2/M phase, 151 genes for M phase and 106 genes for M/G1 phase of the cell-cycle.

Transwell-based cell migration assay

The migratory potential of BM-derived B-cell subsets towards MIF or chemokines includ-ing CXCL12 and CXCL13 was assessed in a modified Boyden chamber-based chemo-taxis assay using Corning Costar Transwell chambers (6.5 mm polycarbonate-mem-brane filter with a pore size of 5.0 µm, Sigma Aldrich/Merck). Chemoattractants were diluted in a volume of 600 µl of RPMI media supplemented with 0.5% BSA and applied to the lower chamber. BM-derived cells (1×10^6 cells) were resuspended in 100 µl of sup-plemented RPMI medium and applied to the filter of the upper chamber. After incubation for 3 h at 37°C and 5% CO_2, migrated cells were collected and stained for B-cell subtype-specific surface markers as described before. Cells were analyzed using the Sony SH800S cell sorter and cell subsets quantified by FlowJo software. Migrated BM-derived B-cell subsets are depicted as percentage of CD45$^+$ leukocytes.

Vascular cell adhesion molecule (VCAM)-1 adhesion assay

For the investigation of the adhesion potential of B cells to VCAM-1, B cells were first isolated from the BM using the Pan B cell isolation kit II (Miltenyi Biotech) according to the manufacturer's instructions. Briefly, BM-derived cells were resuspended in 40 µl of MACS buffer (0.5% BSA, 2 mM EDTA in PBS, pH 7.2) per 10^7 cells and 10 µl of Pan B cell antibody cocktail (anti-CD4, anti-CD11c, anti-CD49b, anti-CD90, anti-Gr-2, anti-Ter119) were added. After incubation for 5 min at 4°C, 30 µl MACS buffer and 20 µl of anti-biotin microbeads per 10^7 cells were added. After further incubation for 10 min at 4°C, B cells were negatively selected on a LD column in a MACS separator (Miltenyi Biotech). Following isolation, B cells were incubated for 2 h at 37°C and 5% CO_2 with or without 800 ng/ml MIF in the wells of a VCAM-1 coated cell culture plate. The coating was performed at 4°C overnight using 10 µg/ml VCAM-1 following blocking with 3% BSA for 3 h at RT. Non-attached cells were removed by rinsing several times with PBS and the adherent cells were fixed with 4% paraformaldehyde (PFA). In order to distinguish between CD43$^+$ (pre–pro- and pro-) and CD43$^-$ (pre-, immature and transitional) B cells, adherent cells were stained with a PE-labeled anti-CD43 antibody (ThermoFisher Scien-tific, #12-0431-81) and DAPI-nuclear counterstain was performed. Adherent cells were counted using ImageJ.

EdU-based *in vivo* proliferation assay

The proliferative capacity of B-cell developmental subsets was assessed by measuring DNA synthesis via incorporation of 5-ethynyl-2'-deoxyuridine (EdU) (ThermoFisher Scientific) into the newly synthesized DNA. EdU was dissolved in PBS and intra-peritoneally injected at 50 mg/kg. After 14 h, the animals were sacrificed and cells were isolated from the BM. Detection of EdU was performed by a click chemistry reaction using the Click-iT™ plus flow cytometric assay kit (ThermoFisher Scientific) according to the manufacturer's instructions. Briefly, BM-derived cells were washed in PBS containing 1% BSA and stained against B-cell subset-specific surface markers for 30 min at 4°C using antibodies described before (see Table B.1). Afterwards, cells were fixed using 100 µl of Click-iT™ fixative. After incubation for 15 min at RT, cells were washed with PBS containing 1% BSA. Following cell permeabilization in 100 µl of 1x Click-iT™ permeabilization and wash reagent for 15 min at RT, the click chemistry reaction was performed by adding 500 µl Click-iT™ plus reaction cocktail containing 2% Copper protectant, 0.5% AF488-labeled picolyl azide, and 10% Reaction buffer additive in PBS and by incubation at RT for 30 min. Afterwards, the treated cells were washed in 1x Click-iT™ permeabilization and wash reagent and subsequently analyzed by flow cytometry using the BD FACSVerse™ (BD Biosciences). The Mean fluorescence intensity (MFI) was measured and normalized to the WT controls. Data analysis was conducted by FlowJo software.

Apoptosis assay

In order to estimate apoptosis of B-cell subsets, cells were derived from the BM and stained for subset-specific markers as described before. Next, the cells were incubated for 10 min at RT with FITC-labeled Annexin V (ThermoFisher Scientific) diluted 1:50 in Annexin V binding buffer (ThermoFisher Scientific). After washing the cells with Annexin V binding buffer, the Annexin V signal of the BM-derived B-cell subsets was measured via flow cytometry using the BD FACSVerse™ (BD Biosciences) and normalized to the WT controls.

Statistics

All statistical tests were conducted using GraphPad Prism 6.0 or 7.0 (GraphPad Software Inc.). For the estimation of the normality of the data the D'Agostino-Pearson test was performed. Two-tailed Student's T-test (parametric) or Mann-Whitney U test (non-parametric) were used as appropriate. In case of comparing more than two groups One-way

ANOVA (parametric) or Kruskal-Wallis test (non-parametric) were used. For multiple comparisons Two-way ANOVA with Sidak´s multiple comparisons test was performed. $P<0.05$ was considered statistically significant.

Results

MIF mediates the migration of early BM-derived B-cell subsets

In the BM, immune cells are trafficked between distinct niches where local signals regulate their differentiation and proliferation. In this context, chemokines including CXCL12 and CXCL13 are known to regulate B-cell migration subset-specifically[63,277,278]. In this study, we aimed at investigating if MIF differentially affects the migration of individual developmental B-cell stages in the BM. For this reason, we applied a transwell-based cell migration setup with BM-derived cells in the upper chamber and different chemokines (CXCL12/CXCL13) or MIF in the lower chamber (Figure B.1a). Migrated cells were collected, stained for subset-specific markers and quantified via FACS. B cells migrated towards chemokines CXCL12 and CXCL13 that were used as positive controls (Figure B.1b-c). The responsiveness towards CXCL12 increased during the B-cell developmental course and reached a maximum for the pre-B-cell population. Similarly, the migration towards CXCL13 increased from early to late B-cell stages with most significant effects on immature and transitional B-cells subsets. We performed a MIF dose-response experiment to evaluate the optimal MIF concentration for the migration of BM-derived B cells and showed that most significant effects were achieved with a concentration of 200 ng/ml (Figure B.1d). Interestingly and contrary to CXCL13, the responsiveness towards MIF was highest for early and intermediate BM-derived B-cell subpopulations (pre–pro-, pro- and pre-B cells) with significant results for pre–pro-B cells (Figure B.1b-c). In comparison to the early B-cell stages, later stages (immature and transitional B cells) did not show any migratory effect in response to MIF (Figure B.1b-c). These results indicate that MIF is involved in the migration of early BM-derived B-cell stages and might act as a niche factor during the developmental cascade by guiding and maintaining B cells within the BM.
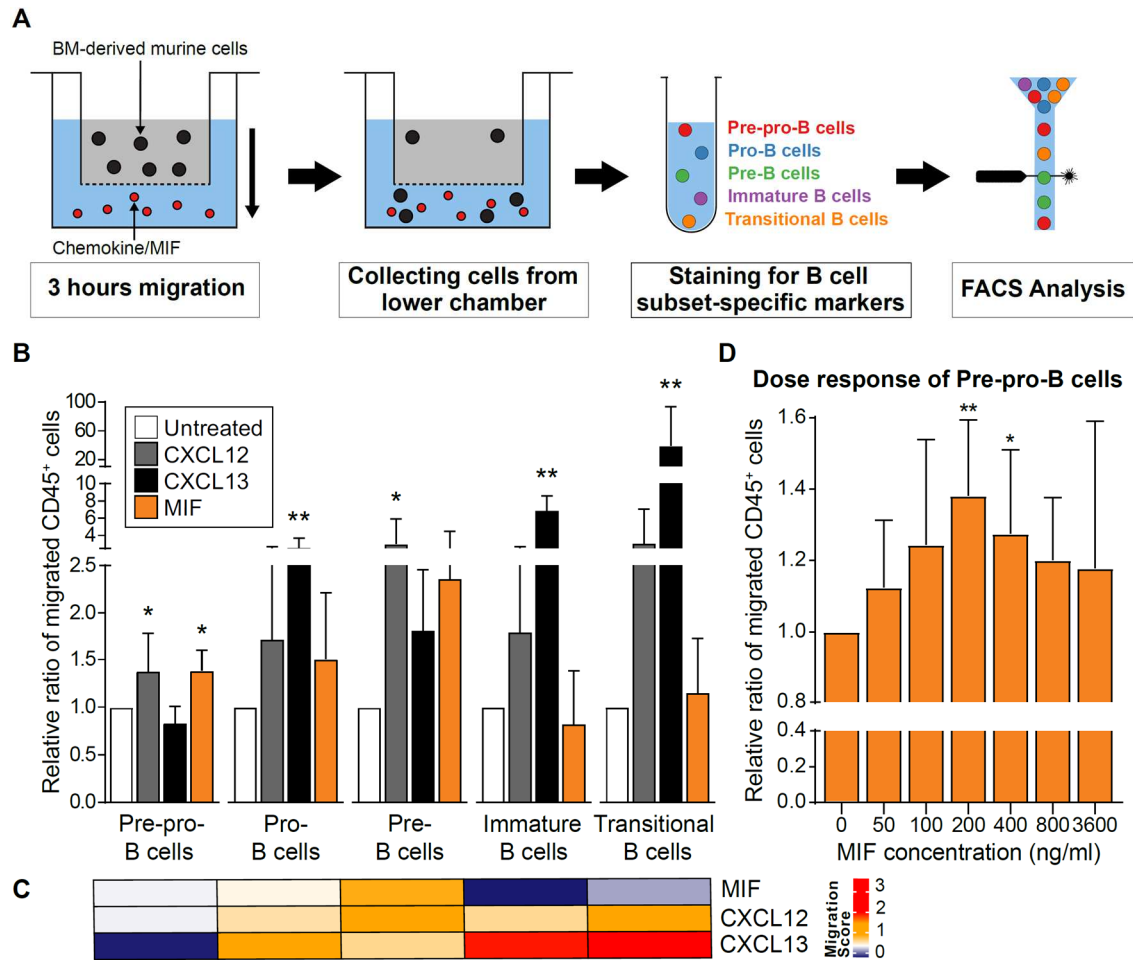
Figure B.1: MIF triggers chemotaxis of BM-derived B cells in a subset-specific way with early B-cell stages displaying highest responsiveness. A) Schematic overview of the experimental setup. Freshly isolated BM-derived cells from WT animals were applied to a transwell system and migrated towards MIF (200 ng/ml), CXCL12 (1000 ng/ml) or CXCL13 (2000 ng/ml). Migrated cells were recovered from the lower chamber, stained for subset-specific markers and inspected by flow cytometry. **B)** Quantification of migrated B-cell developmental subsets. The results show the migrated B cells as a ratio of migrated CD45+ leukocytes. The data was normalized to the untreated controls (n=5-8, results are presented as means ± SD, Kruskal Wallis test, *p<0.05, ** p<0.01). **C)** Heatmap visualizing the amount of migrated B-cell subsets towards MIF, CXCL12 and CXCL13. The results correspond to the data shown in B) to provide a better visualization of the migratory behavior of the individual B-cell stages. The scale indicates the log-values of the ratio of migrated CD45+ leukocytes from 0 (blue) to 3.5 (red). **D)** Dose-response curve of migrated pre–pro-B cells in response to MIF. Migrated B cells are depicted as a ratio of migrated CD45+ leukocytes. The data was normalized to the untreated control (n=6-7, results are presented as means ± SD, Kruskal Wallis test, *p<0.05, ** p<0.01).

B-cell developmental trajectories and identities of distinct subsets are maintained in the context of *Mif*-deficiency

To scrutinize the involvement of MIF in the B-cell developmental cascade in depth we performed a detailed transcriptome analysis of B-cell subsets derived from $Mif^{-/-}$ mice compared to the WT controls by RNAseq. For this purpose, total splenic and BM-derived cells from $Mif^{-/-}$ and WT control mice were stained for stage-specific surface antigens (Figure B.2a). To identify distinct B-cell developmental subpopulations in the BM, the

cells were analyzed according to the markers established by Hardy et *al.*[259] in combination with CD19 that was used to discriminate early B-cell stages[260,279]. Accordingly, cells were first gated into singlets (not shown) and B cells were gated as CD45+B220+ (Supplementary figure B.1a). Next, B cells were separated into CD43-negative cells including pre-, immature and transitional B cells and CD43-positive cells including pre–pro- and pro-B cells based on the expression of CD19. To distinguish CD43-negative B-cell subsets, IgM was used in combination with IgD[57,259,280]. Regarding the splenic subsets, sorting was performed after pre-enrichment (see materials and methods sections) considering the expression of CD21, CD23, IgM and IgD (Supplementary figure B.1b) according to Allman et. *al*[281,282] and Cariappa et *al.*[67]. Each B-cell subset was FACS-sorted in pools of 50 cells and further processed with a modified Smart-seq2 protocol (see materials and methods section). Based on the mean fluorescence intensity (MFI) of the sorting markers derived from the FACS-based index sorting data, t-distributed stochastic neighbor embedding (t-SNE) plots were generated demonstrating that different B-cell stages separated into well-defined clusters independently of the genotype of the mice, thereby validating our sorting strategy (Supplementary figure B.1c-d).

To check for any genotype-associated bias from the sorting markers, we analyzed the gene expression levels of those markers and found a high correlation (overall correlation 95%) between WT and *Mif*^{-/-} samples suggesting that the genotype is not introducing any bias during sorting (Supplementary figure B.1e, Supplementary table B.1). Moreover, the gene expression levels of the sorting markers were consistent with the predicted subset-specific marker expression shown in Figure B.2a and thus further verified the accuracy of the B-cell isolation. Together with the visualization of the FACS-based index sorting data (Supplementary figure B.1c-d), the results imply that B-cell identities and developmental trajectories are maintained in the context of *Mif*-deficiency.

Mif-deficiency changes the transcriptomic signature of developmental B-cell subsets

Dimensional reduction by Uniform Manifold Approximation and Projection (UMAP) arranged B cells in a hierarchical way reproducing the developmental path from the BM to the spleen. Pre–pro-, pro-, pre- and immature B cells clustered separately, suggesting that the subsets have distinct genetic features, while transitional and FOB cells, as well MZB and MZP-B cells clustered together and therefore might harbour transcriptomic similarities (Figure B.2b). UMAP visualizing the expression levels of MIF assembled *Mif*^{-/-} and WT samples into separating sub-clusters within the well-defined populations

of the B-cell subsets indicating that *Mif*-deficiency might elicit transcriptomic changes in B cells (Figure B.2c).

To estimate the impact of *Mif*-gene deletion on B-cell signatures, we performed an extended transcriptome analysis. The results are visualized by the heatmap in Figure B.2d. While the expression levels of most of the analyzed genes remained unchanged between *Mif*$^{-/-}$ and WT samples, we identified multiple differentially expressed for each B-cell subpopulation (Figure B.2d, Supplementary table B.2). Intriguingly, various genes related to mitochondrial metabolism (e.g. mt-Nd1, mt-Co1, mt-Nd4, mt-Cytb) were upregulated in the *Mif*$^{-/-}$ samples across all developmental stages. In contrast, proliferative and cell cycle-associated genes (e.g. Map3k1, Rrm2, Grb7, CD74, CD174, Rnf187, Mcm6, Dusp6) were significantly downregulated in *Mif*$^{-/-}$ samples, especially at early B-cell stages including pro- and pre-B cells (Supplementary table B.2).

In order to assign molecular functions to certain sets of genes that were differentially expressed and to better understand the underlying cellular processes, Gene ontology (GO) enrichment analysis was performed (Figure B.2e). Several GO terms were significantly enriched when comparing *Mif*$^{-/-}$ and WT samples. Regarding the BM-derived B-cell subsets, we identified gene sets related to cytoskeletal and cell adhesion pathways, as well as to cell-cycle and proliferation. Interestingly, these pathways were mainly affected in early and intermediate B-cell stages (pre–pro-, pro- and pre-B cells), but not in immature and transitional B cells. Regarding the splenic B-cell subsets, we identified GO terms of gene sets related to cell adhesion and mitochondrial metabolism to be significantly enriched (Figure B.2e).

Overall, the 50-cell RNAseq data revealed significant changes in the transcriptomic signature of *Mif*-deficient B cells from BM and spleen in a subset-dependent manner accompanied by alterations in various cellular pathways.

Figure B.2: Figure legend see next page.

Figure B.2: RNAseq reveals subset-specific differences in the transcriptomic signature of *Mif*-deficient B cells compared to the WT controls. A) Schematic overview of BM-derived and splenic B-cell stages. Subset specific markers that were used for sorting are indicated. Splenic B-cell populations were first pre-enriched to allow for the sorting based on only 4 surface markers (CD21, IgM, IgD, CD23). **B)** Uniform Manifold Approximation and Projection (UMAP) was applied to the transcriptomic dataset separating B cells into distinct developmental clusters. Each dot corresponds to a 50-cell sample (circle: WT, triangle: *Mif*−/−). **C)** UMAP-based clustering highlighting the expression levels of Mif. Each dot corresponds to a 50-cell sample (circle: WT, triangle: *Mif*−/−). The scale indicates the log-values of the normalized gene expression from 0 (blue) to 2.0 (red). **D)** Heatmap illustrating the variation in gene expression levels between *Mif*−/− and WT B-cell subpopulations. Each column represents one gene and each line corresponds to a 50-cell sample of *Mif*−/− or WT samples. The scale indicates the scaled log-values of the normalized gene expression from -2.0 (blue) to 2.0 (red). **F)** Gene ontology (GO) enrichment analysis performed on the RNAseq data of *Mif*−/− or WT B cells revealing significantly enriched GO terms. The GO terms have been grouped to related biological functions indicated at the top. GO terms (columns) are sorted by B-cell subsets (rows) and significances are indicated. The scale indicates P values from <0.01 (red) to 0.05 (black). Grey sections correspond to P values >0.05. Adjusted P value cut-off is 0.05.

Mif-deficiency affects the adhesiveness of B cells to VCAM-1

Based on the results of the GO enrichment analysis (Figure B.2e), we further aimed at a functional verification of the revealed pathways. In order to investigate the adhesive behavior of *Mif*−/− B cells in comparison to the WT-derived cells *in vitro*, an VCAM-1 adhesion assay (see materials and methods section) was conducted using isolated BM-derived B cells. MIF strongly induced the adhesion of B cells isolated from WT mice to VCAM-1 (Figure B.3a). VCAM-1 is expressed by stromal cells in the BM niche[266] and serves as the ligand of the VLA-4 integrin that is highly expressed on B cells. Strikingly, *Mif*−/− B cells significantly failed to adhere to VCAM-1 in response to MIF (Figure B.3a). We next investigated if this effect was subset-dependent. However, both, early (CD43-negative) as well as intermediate/late (CD43-positive) B-cell stages derived from the BM of *Mif*−/− mice showed significant impairments in the MIF-induced adhesion to VCAM-1 compared to the WT controls (Figure B.3b-d).
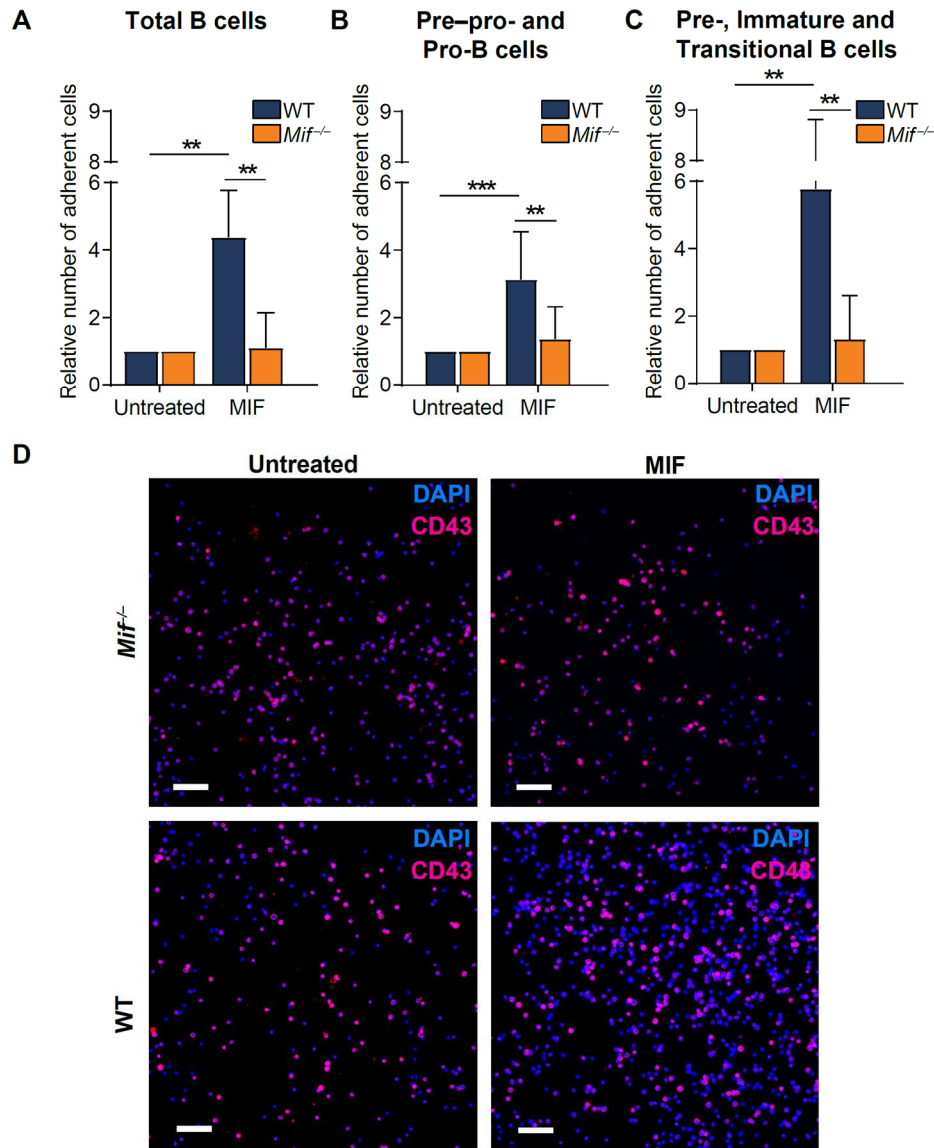
Figure B.3: *Mif*-deficiency lowers the adhesion potential of BM-derived B cells to VCAM-1. Isolated BM B-cells were added to a VCAM-1-coated cell culture plate and incubated with or without 800 ng/ml MIF. Adherent cells were fixed and DAPI nuclear counterstain was performed for the quantification of total adherent B cells. Fluorescent images (8 fields of view (FOV) per well/treatment) were recorded and cells were quantified using Image J. The results were normalized to the untreated control (n=4-6, results are presented as means ± SD, Mann-Whitney U test). **A)** Number of adherent total BM-derived B cells from *Mif*$^{-/-}$ mice (orange) and WT controls (blue) to VCAM-1. **B-C)** Attached cells were stained with a fluorescently labeled anti-CD43 antibody in order to distinguish between early (pre–pro- and pro-) **(B)** and intermediate/late (pre-, immature, and transitional) **(C)** B-cell stages. Quantification was performed as in A) (n=4-6, results are presented as means ± SD, Mann-Whitney U test). **D)** Representative images of one FOV of adherent *Mif*$^{-/-}$ B cells (top) and WT controls (bottom) after treatment with 800 ng/ml MIF (right) compared to the untreated samples (left) (scale: 100µm, blue: DAPI, magenta: CD43).

Mif-deficiency affects B-cell proliferation and mitosis in a subset-dependent manner accompanied by reduced pre-B-cell numbers

GO enrichment analysis revealed GO terms associated with proliferation and mitosis to be enriched in the samples of *Mif*^{-/-} pre-B cells (Figure B.2e). Based on these results, we were asking if *Mif*-deficiency affects B-cell numbers. Total BM-derived B220^{+} B cells were not significantly changed between *Mif*^{-/-} and WT mice (Figure B.4a). However, *Mif*-deficiency altered numbers of individual B-cell subsets, with significantly increased pre–pro- and significantly decreased pre-B-cell numbers (Figure B.4b). The cell counts of MZB, MZP-B as well as FOB cells in the spleen were unchanged upon *Mif*-deficiency (Supplementary figure B.2b, gating strategy see supplementary figure B.2a). Investigation of the expression levels of mitosis-related genes[276] revealed a significant downregulation of these genes in *Mif*-deficient pre-B cells compared to the WT controls. No significant differences in mitotic gene expression values were seen with the other developmental stages in BM and spleen (Figure B.2c).

To functionally verify potential changes in the proliferation of B cells from *Mif*^{-/-} mice compared to the WT controls and to evaluate subset-specific differences, we performed an EdU-based proliferation assay. *Mif*^{-/-} and WT mice were administered EdU, which incorporated into the DNA of dividing cells and was detected by a click chemistry reaction (protocols see methods; supplementary figure B.3k). Indeed, a reduced EdU signal was detected for *Mif*^{-/-} pre-B-cells compared to the WT controls indicating reduced proliferative capacity, although statistical significance was not obtained (Figure B.4d). This effect was absent with all other BM-derived B-cell subsets (Supplementary figure B.3a-e).

In order to rule out changes in apoptosis that could also affect B-cell numbers we performed an FACS-based Annexin V apoptosis assay comparing *Mif*-WT and *Mif*^{-/-} B cells. The Annexin V signal was similar for *Mif*^{-/-} B-cell subsets and the respective WT controls at all developmental stages (Figure B.4e, supplementary figure B.3f-j; gating strategy see supplementary figure B.3l) indicating that apoptotic pathways remain unaffected by *Mif*-deficiency.

Together with the results of the DGE analysis, revealing several proliferation-related genes to be downregulated in the *Mif*^{-/-} samples (Supplementary table B.2), these results suggest that *Mif*-deficiency impairs cell division and proliferation of B cells during their maturation, especially at early and intermediate (pre–pro-, pro- and pre-) B-cell stages.
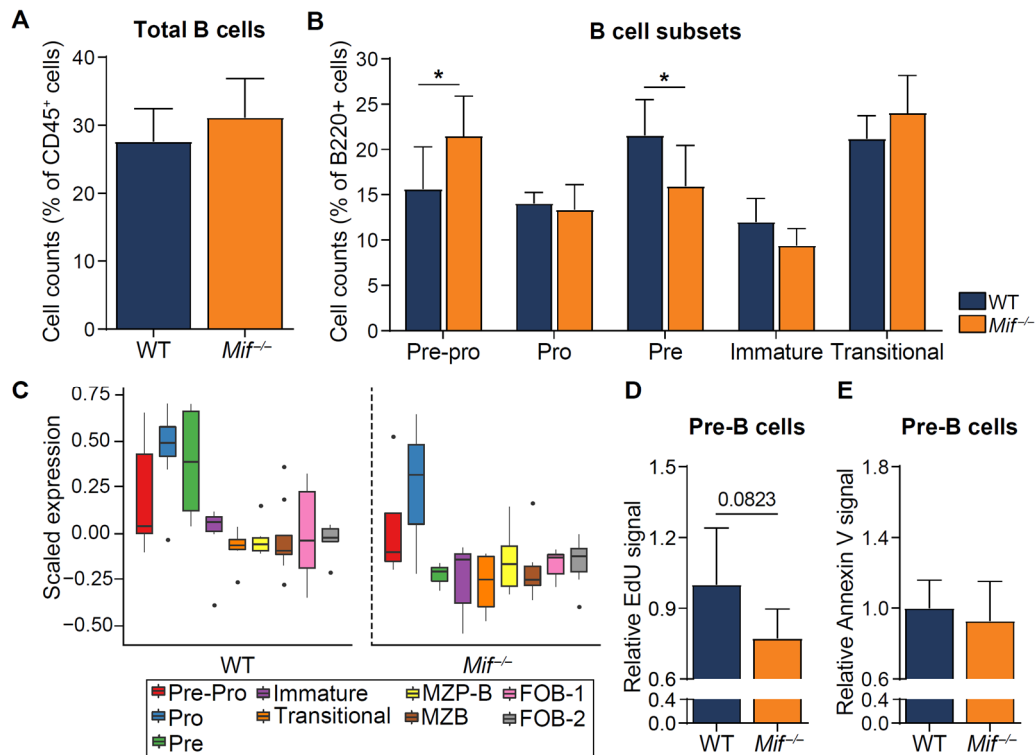
Figure B.4: *Mif*-deficiency lowers pre-B-cell counts accompanied by decreased proliferation and changes in expression levels of mitosis-related genes. A) Quantification of total BM-derived B cells from *Mif*$^{-/-}$ mice (orange) compared to WT controls (blue) based on flow cytometric analysis. Cell counts are presented as percentage of CD45$^+$ leukocytes (n=7, results are presented as means ± SD, Mann-Whitney U test). **B)** Quantification of BM-derived developmental B-cell subsets from *Mif*$^{-/-}$ mice (orange) compared to WT controls (blue) (n=7, results are presented as means ± SD, Two-Way ANOVA, *p<0.05). **C)** Average gene expression (log scale) of mitosis-related genes. The left panel shows the WT samples and the right panel corresponds to the *Mif*$^{-/-}$ samples. **D)** Proliferation of pre-B cells from *Mif*$^{-/-}$ mice (orange) in comparison to the WT controls (blue) assessed via intra-peritoneal injection of EdU (50 mg/kg). Femur and tibia were harvested and BM-derived cells isolated. DNA-incorporated EdU was FITC-labeled by a click chemistry reaction and the mean EdU-derived fluorescence intensity (MFI) of pre-B cells was measured via FACS. The results were normalized to the WT controls (n=5-6, results are presented as means ± SD, Mann-Whitney U test). **E)** The number of apoptotic cells was assessed via staining of BM-derived B-cell subsets with FITC-labeled Annexin V and analysis via FACS. The Annexin V-derived fluorescent signal of *Mif*$^{-/-}$ mice (orange) was quantified and normalized to the WT controls (blue) (n=6, results are presented as means ± SD, Mann-Whitney U test).

Discussion

Recent progress in the RNA sequencing (RNAseq) area, provided a basis for the analysis of the entire transcriptome of a single-cell in a high-throughput manner and enabled deeper insights into the cellular complexity of tissues and organs from mice and humans[210-213]. Compared to previously established microarray-based approaches, RNAseq is characterized by a broader dynamic range and larger fold changes as well as higher sensitivity with lower background[210]. A lot of effort was made in the field of BCR sequencing to capture the vast BCR repertoire providing a basis for the discovery of antibodies[283-287]. More importantly, RNAseq-based studies improved our understanding of the transcriptome of developmental B-cell subpopulations but such studies are rare and focus

mainly on mature B-cell stages[265,288]. The delay in transcriptome analysis of BM-derived B-cell subsets might be due to several limitations including non-consistent and overlapping markers[289]. The development of multicolor flow cytometry enabled the combined use of several different markers allowing for a more precise analysis and discrimination of subsets[290,291]. But still, the analysis especially of the earliest developmental stages including pre–pro-B cells is challenging as they lack Ig recombination and because of their low frequency in the BM[279]. Gene expression data from the Immunological genome project (Immgen) provided a comprehensive overview of the genes associated with the murine immune system and covers B-cell development[264,292]. Nevertheless, the transcriptional changes during B-cell development remain incompletely understood.

Recently, we discovered a link between MIF and the B-cell developmental cascade in *Apoe*$^{-/-}$ mice associated with a blockade in B-cell maturation in the BM of *Mif*-deficient mice[152]. Here, we applied comparative bulk RNAseq to better interpret the functional and molecular functions of MIF in the B-cell developmental trajectory and to thoroughly scrutinize the effects of *Mif*-deficiency on the transcriptional heterogeneity during B-cell maturation. In conjunction with experimental *in vitro* data, our results imply that MIF operates as a mediator of early B-cell maturation in the BM. *Mif*-deficiency affected the transcriptomic signature of B cells in a subset-specific way and was associated with impairments in proliferative and cell adhesion pathways in BM-derived B cells.

The BM environment is a crucial component controlling developmental pathways and the cellular complexity of BM niches has been comprehensively studied by RNAseq approaches[293-295]. B cells migrate between different niches in order to receive stage-specific signals that are needed for differentiation, survival or proliferation. Chemokines are essential for guiding the B-cell developmental stages throughout these niches as well as for the exit of transitional B cells from the BM and the migration to splenic follicles[266]. Here we revealed that B cells migrate towards distinct chemokines or MIF in a subset-dependent manner. CXCL12 has been previously described to induce the migration of pre-B cells for their escape from IL-7-rich niches to mediate the switch from proliferative signaling to differentiation[63]. In consistency with these observations, we showed that among all analyzed B-cell subsets the strongest responsiveness towards CXCL12 was seen with pre-B cells. The responsiveness to CXCL13 was robust for immature and transitional B cells, while it was comparatively low for earlier stages. Indeed, CXCL13 has been described as a chemokine driving the migration of later BM-derived B-cell stages and their homing to the spleen[277]. Interestingly and contrarily to CXCL13, we showed that MIF mediates chemotaxis of early and intermediate B-cell stages (pre–pro-, pro- and

pre-B cells), while immature and transitional B-cell stages were unresponsive. Our results suggest that MIF might serve as a BM niche factor for early and intermediate B-cell stages during B-cell maturation adding further complexity to the BM microenvironment. Accordingly, previous data provided evidence for a crucial role of MIF-secreting bone marrow resident dendritic cells for the survival of mature B cells relocated from the periphery to the BM niche[271]. However, if MIF also serves as survival and proliferation factor in the BM niche during B-cell maturation was still unknown.

To uncover mechanistic pathways explaining the fundamental relevance of MIF during B-cell development, we aimed to comprehensively scrutinize the transcriptional changes associated with *Mif*-deficiency during the development of BM-derived and splenic B cells. Our marker-based sorting strategy successfully separated B cells from BM and spleen into stage-specific clusters reproducing the developmental trajectories. Interestingly, transitional B cells from the BM and splenic FOB cells clustered together, while MZB/MZP-B cells seemed to form a separate cluster. These findings are highly congruent with RNAseq-based relationship studies revealing higher transcriptomic similarities between transitional and FOB cells than between transitional and MZB cells[288]. We showed that each developmental stage possesses characteristic transcriptomic features and that expression levels of most of the genes were not significantly changed upon *Mif*-deficiency, suggesting that B-cell identities are maintained.

Nevertheless, we uncovered several genes with expression values that significantly differed between *Mif*$^{-/-}$ and *Apoe*$^{-/-}$ mice, in particular genes related to mitochondrial metabolism and cell cycle/proliferation. Mitochondrial genes were significantly upregulated in *Mif*$^{-/-}$ B cells across all developmental stages from BM and spleen (e.g. *mt-Nd1*, *mt-Co1*, *mt-Nd4*, *mt-Cytb*). These results were accompanied by GO enrichment analysis data revealing GO terms associated with mitochondrial structure and function to be significantly enriched, suggesting that *Mif*-deficiency affects mitochondrial pathways in splenic and BM-derived B-cell subsets. By producing ATP mitochondria provide energy needed for cellular metabolism and metabolic checkpoints have been described to exist during B-cell development in the BM[296-298]. Changes in mitochondrial gene expression might lead to a dysregulation at these checkpoints leading to impairments in B-cell maturation. Further *in vitro* and *in vivo* studies focusing on the link between *Mif*-deficiency and mitochondrial gene expression during B-cell development are thus warranted.

In contrast to mitochondrial gene expression, expression levels of genes that were previously associated with proliferation and cell cycle in B cells or human cancer cell lines

were significantly downregulated in the $Mif^{-/-}$ samples, especially at early and intermediate B-cell stages in the BM (e.g. *Map3k* [299], *CD74*[177,181] *Rrm2*[300-302], *Grb7*[303], and others). Interestingly, *Rrm2* that encodes for the ribonucleotide subunit M2 involved in proliferation and DNA repair mechanisms during the cell cycle S-phase[302] was strongly downregulated in pre-B-cells. Intriguingly, the downregulation (fold change) of *Rrm2* in *Mif*-deficient pre-B cells was comparable to the fold change of *Mif* itself. Additionally, *Mif*-deficiency caused a significant decline of CD74 expression in pro-B-cells. CD74 was first described as a chaperone facilitating antigen presentation via MHC class II[304]. Further research expanded the role of CD74 to cell survival and proliferation, and as a regulator of B-cell development[177,179]. In addition, CD74 serves as a MIF receptor and signaling via CD74/CD44 has been associated with B-cell proliferation[158,160]. The downregulation of CD74 in pro-B-cells in combination with the global *Mif*-deficiency could lead to subset-specific impairments in B-cell proliferation. This hypothesis was further supported by the downregulation of mitotic genes in pre-B-cells, together with *in vitro* proliferation data and decreased pre-B-cell numbers. Of note, differentiation and proliferation of B cells are tightly regulated processes that work in synergy to ensure proper B-cell maturation[48,51]. While pre–pro-B cells with a low proliferative capacity reside next to CXCL12-expressing reticular cells, proliferating B-cell stages such as pro-B cells and large pre-B cells are localized in close proximity to IL-7-producing stromal cells[266,305].

In addition, GO enrichment analysis revealed cell adhesion pathways to be affected in *Mif*-deficient B cells. By performing a VCAM-1 adhesion assay, we aimed for the functional verification of the obtained RNAseq data. The experimental setup was based on a study of Tokoyoda et *al.* showing that the treatment with CXCL12 promotes the adhesion of pre–pro-B cells to VCAM-1 expressed by stromal cells in the BM niche, while the adhesion capacity was low for other developmental B-cell subsets[266]. Here, MIF promoted the adhesion of early (pre–pro- and pro-) B-cell stages to VCAM-1, but also of intermediate and late (pre-, immature and transitional) B cells. Due to a limited amount of simultaneously applicable markers during the IHC staining procedure leading to the analysis of mixed populations, subset-specific differences were not detected in this setting. However, much more importantly, *Mif*-deficiency almost completely abolished the adhesion of B cells to VCAM-1. Impairments in the B-cell adhesion potential could in turn alter the ability of B cells to localize to certain BM niches, where they receive critical signals for their development.

In conclusion, this work uncovered that MIF functions as a crucial mediator of B-cell development. While, B-cell identities and developmental trajectories remain unaffected

by *Mif*-gene deletion, transcriptomic signatures of B cells are changed in a subset-specific manner accompanied by impairments in cell proliferation and adhesion, critical biological processes during B-cell maturation. As defects in the B-cell developmental cascade might favor abnormalities in various immune functions potentially advancing the progression of B-cell-related inflammatory diseases, the determination of B-cell developmental mechanisms and the role of involved mediators such as MIF could help to develop novel therapeutic strategies.

Supplement

Supplementary figures
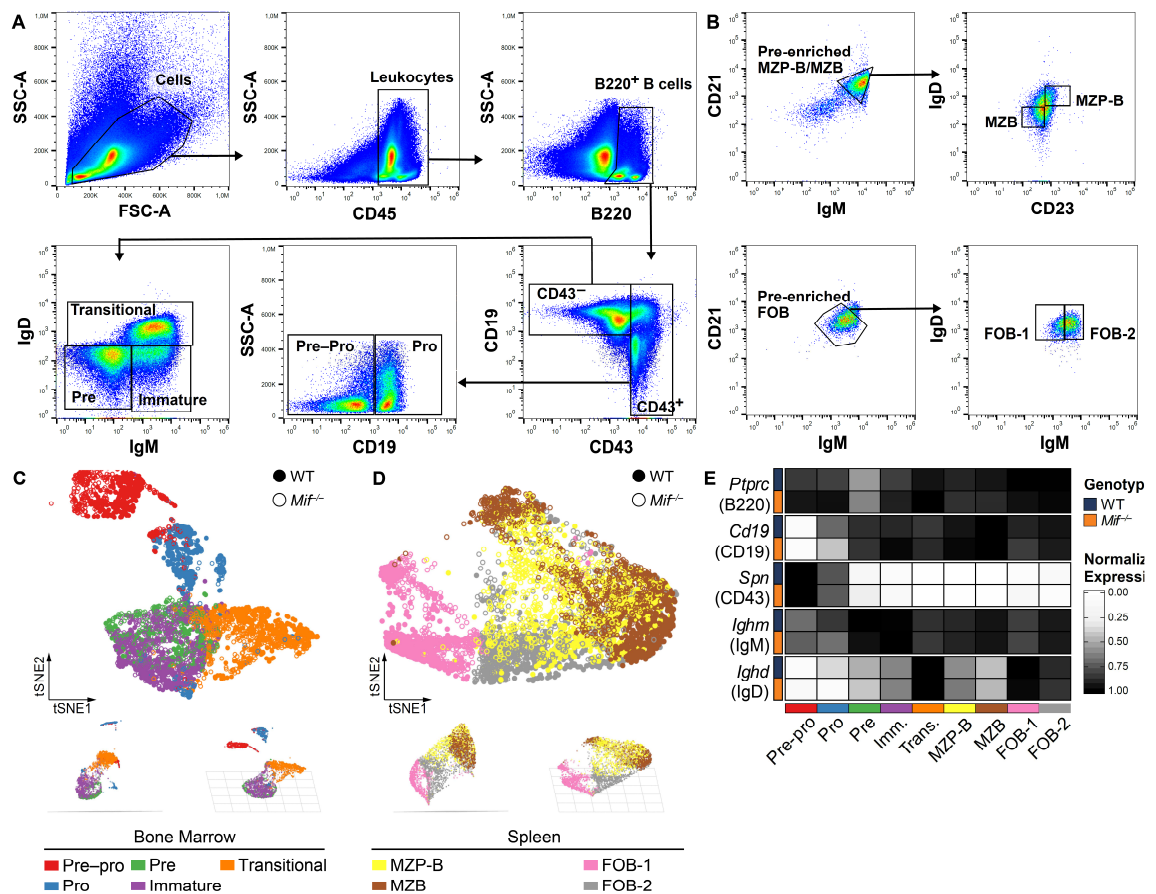
Supplementary figure B.1: Flow cytometry separates B-cell subsets from BM and spleen into distinct clusters. A) Flow cytometric gating of B-cell subpopulations from the BM using the SH800S cell sorter (Sony). Single stainings were used for compensation (SSC: Side-scatter, FSC: Forward scatter). **B)** Sorting of splenic B-cell subpopulations was performed applying four markers (IgM, CD21, CD23 and IgD) after pre-enrichment of MZB and FOB cells. **C-D)** Visualization of the FACS-derived index sorting data from BM-derived **(A)** and splenic **(B)** B-cell subsets using t-distributed stochastic neighbor embedding (t-SNE). Individual data points correspond to a single-cell (empty circle: *Mif*⁻/⁻, filled circle: WT). Rotated versions of the displayed view are shown below. **E)** Heatmap showing expression levels of the markers used for the sorting of developmental B-cell subsets. The scale indicates the normalized log-value of the gene expression from 0 (white) to 1 (black).
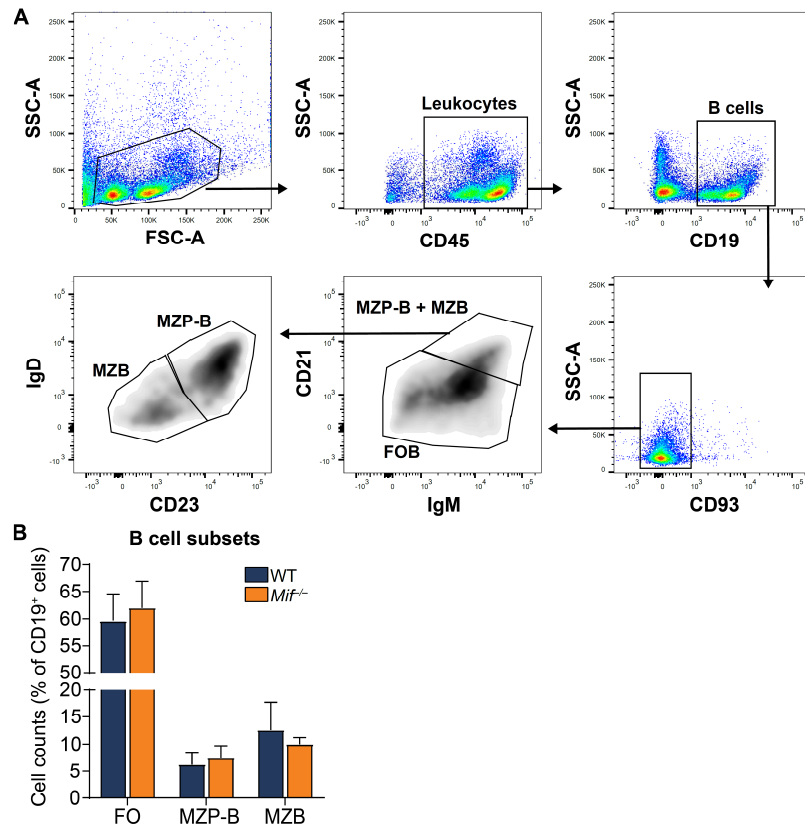
Supplementary figure B.2: Splenic B-cell counts remain unaffected in *Mif*-deficient mice. A) Flow cytometric gating of B-cell subpopulations from the spleen using the BD FACS Verse (BD Biosciences) (SSC: Side-scatter, FSC: Forward scatter). **B)** Quantification of splenic B-cell subsets from *Mif*$^{-/-}$ mice (orange) compared to the WT controls (blue) based on flow cytometric analysis using the BD FACS Verse. Cell counts are presented as a percentage of CD19$^+$ cells (n=4, results are depicted as means ± SD, Two-Way ANOVA).
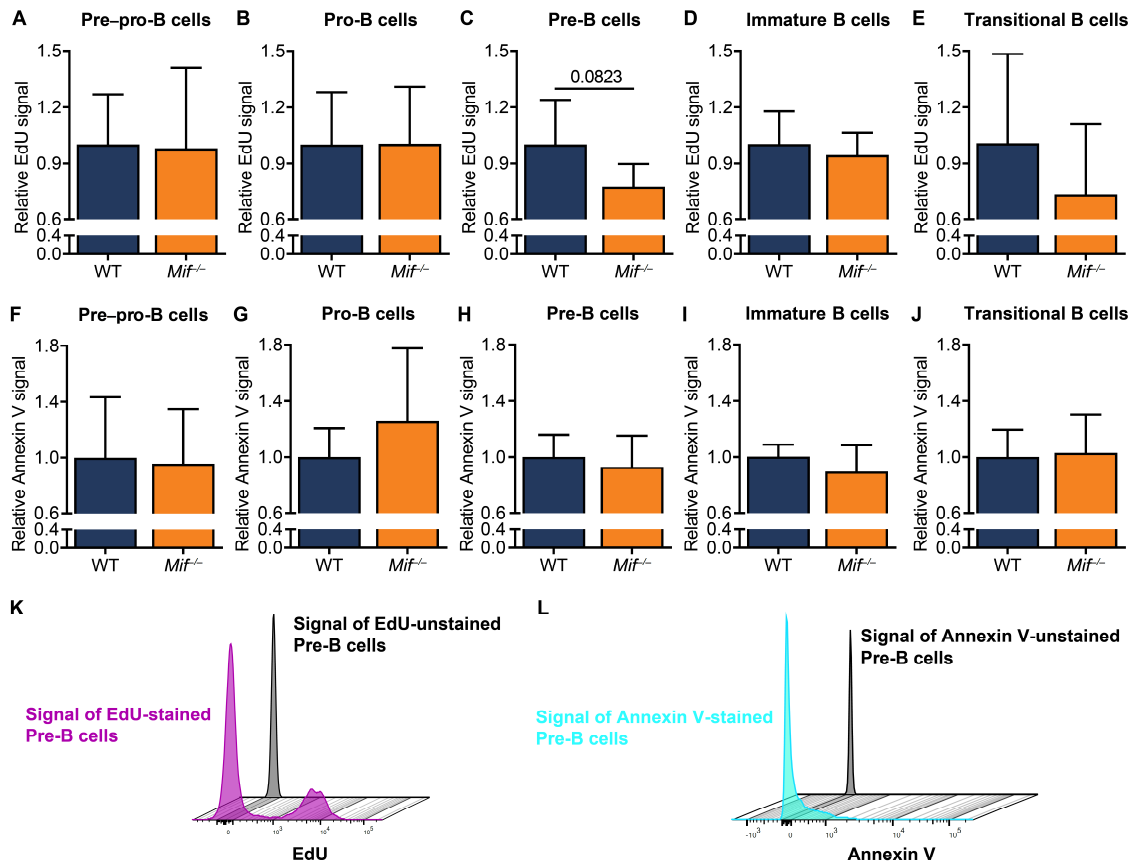
Supplementary figure B.3: Proliferation and apoptosis of pre–pro-, pro-, pre-, immature and transitional B cells remain unaffected in *Mif*-deficient mice. A-E) Proliferative potential of BM-derived B-cell subsets assessed via application of EdU. DNA-incorporated EdU was FITC-labeled by a click chemistry reaction and the EdU-derived mean fluorescence intensity (MFI) was measured by FACS analysis using the BD FACS Verse (BD Biosciences). The EDU-derived signal from *Mif*-deficient (orange) pre–pro- **(A)**, pro- **(B)**, pre- **(C)**, immature **(D)** and transitional **(E)** B cells was quantified and normalized to the WT controls (blue) (n=5-6, results are depicted as means ± SD, Mann-Whitney U test). **F-J)** Apoptosis was estimated via FITC-labeled Annexin V-staining of pre–pro- **(F)**, pro- **(G)**, pre- **(H)**, immature **(I)** and transitional **(J)** B cells and analysis by flow cytometry using the BD FACS Verse. The Annexin V-derived fluorescent signal from *Mif*−/− B cells (orange) was quantified and normalized to the WT controls (blue) (n=6, results are depicted as means ± SD, Mann-Whitney U test). **K-L)** Flow cytometric gating strategies of EdU-labeled **(K)** and Annexin V-stained **(L)** B-cell subsets from the BM using the BD FACS Verse. The MFI derived from the EdU-labeled (magenta) and Annexin V-stained subsets (cyan) was compared to the signal of respective unlabeled control cells (grey) and is shown as histograms (SSC: Side-scatter, FSC: Forward scatter).

119

Supplementary Tables

Supplementary table B.1: Expression values of the markers used for the sorting of developmental B-cell stages from BM and spleen of *Mif⁻/⁻* mice compared to the WT controls.

Subset	GT	Normalized expression (logFC)						
		Ptprc (B220)*	*Cd19* (CD19)*	*Spn* (CD43)*	*Ighm* (IgM)*	*Ighd* (IgD)*	*Cr2* (CD21)*	Fcer2a (CD23)*
Pre–pro	*Mif⁻/⁻*	2.3244	0.1167	0.7369	3.4922	0.3591	0.0245	0.0930
	WT	2.2791	0.1540	0.6868	3.2649	0.2829	0.0368	0.0056
Pro	*Mif⁻/⁻*	2.3651	1.1534	0.5413	3.2342	0.2268	0.0470	0.1668
	WT	2.2211	1.9541	0.5170	4.0349	1.3244	0.1636	0.5921
Pre	*Mif⁻/⁻*	1.5125	2.3481	0.2079	4.6150	1.5148	<0.0001	0.3583
	WT	1.4973	2.4314	0.0952	4.8158	1.7892	0.0880	0.2426
Imm.	*Mif⁻/⁻*	2.2494	2.6918	0.0653	4.8540	2.2420	0.6085	1.1739
	WT	2.2332	2.4925	0.0503	4.7783	2.2347	0.2417	0.8953
Trans.	*Mif⁻/⁻*	2.4833	2.4243	<0.0001	4.0404	3.6403	1.2933	2.3510
	WT	2.5824	2.3659	0.0061	4.1419	3.6937	1.2075	2.2725
FOB-1	*Mif⁻/⁻*	2.3596	2.2709	0.0982	3.8724	3.5506	1.6072	2.2721
	WT	2.7392	2.5092	0.0232	3.9284	3.6925	1.6191	2.3129
FOB-2	*Mif⁻/⁻*	2.4342	2.5399	0.0158	4.5098	3.0899	1.5287	2,4842
	WT	2.7278	2.6444	0.0723	4.4678	3.2587	1.6893	2,3273
MZP-B	*Mif⁻/⁻*	2.1320	2.7045	0.0088	4.3435	2.3333	2.5584	1,0070
	WT	2.4457	2.6485	<0.0001	4.2592	2.1728	2.8282	0.6586
MZB	*Mif⁻/⁻*	2.1607	2.7624	0.0024	4.5647	1.6655	2.6791	0.2734
	WT	2.5644	2.8115	<0.0001	4.5296	1.6174	3.0935	0.2520

*The gene names (italics) are indicated together with the respective protein names in brackets. GT: Genotype.

Supplementary table B.2: Expression values and adjusted *P* values of differentially expressed genes in BM-derived and splenic B-cell subsets from *Mif*$^{-/-}$ mice compared to the WT controls.

Pre–pro-B cells					
Downregulated in *Mif*$^{-/-}$			Upregulated in *Mif*$^{-/-}$		
Gene	Fold change (logFC)	Adjusted *P* value	Gene	Fold change (logFC)	Adjusted *P* value
Mif	3.5366	<0.0001	*Procr*	-1.8448	0.0189
Serpina3f	2.2553	0.0016	*Ifih1*	-1.5951	0.0074
Ptpn22	1.6254	0.0065	*Cd4*	-0.9331	0.0137
Tcp11l2	1.5981	0.0163	*Ly6a*	-0.8498	0.0007
Rnf187	0.5940	0.0096	*mt-Cytb*	-0.7252	<0.0001
			mt-Nd4	-0.5673	0.0420
			mt-Co1	-0.5527	0.0038
			Malat1	-0.5023	<0.0001
			mt-Nd1	-0.4918	<0.0001
Pro-B cells					
Downregulated in *Mif*$^{-/-}$			Upregulated in *Mif*$^{-/-}$		
Gene	Fold change (logFC)	Adjusted *P* value	Gene	Fold change (logFC)	Adjusted *P* value
Mif	4.2001	<0.0001	*Klrk1*	-1.2307	0.0031
Grb7	2.2276	0.0311	*Klrd1*	-1.1769	0.0095
Ighd	2.1883	<0.0001	*Nkg7*	-0.9837	<0.0001
Prr3	2.0955	0.0141	*Ctsw*	-0.9659	0.0138
Gstm1	2.0782	0.0019	*AW112010*	-0.8389	<0.0001
Cd38	2.0690	0.0003			
Utp4	2.0353	0.0096			
Pdk2	2.0273	0.0144			
Dnaaf5	1.9031	0.0312			
Cd74	1.8020	0.0001			
H2–Ob	1.7981	0.0045			
Iglc2	1.7791	<0.0001			
H2–DMb2	1.5024	0.0107			
Cd79a	0.9104	0.0001			
Pre-B cells					
Downregulated in *Mif*$^{-/-}$			Upregulated in *Mif*$^{-/-}$		
Gene	Fold change (logFC)	Adjusted *P* value	Gene	Fold change (logFC)	Adjusted *P* value
Rrm2	3.6371	0.0002	*Gzma*	-4,4870	<0.0001
Sqstm1	3.4227	0.0430	*Fcer1g*	-3,2122	0.0002
Mif	3.1919	0.0054	*St3gal4*	-3,0168	0.0103
Mcm6	2.8103	0.0419	*Skap1*	-2,9592	0.0250
Cops4	2.4641	0.0006	*AW112010*	-1,9800	0.0003
Dusp6	2.3234	0.0004	*Srp14*	-0,8244	0.0447
Ccng2	1.9921	0.0118	*Dnajc7*	-0,7402	0.0020
Fbxl5	1.9486	0.0057			
Gm23935	1.8707	<0.0001			
Serp1	1.6009	<0.0001			
Map3k1	1.5077	0.0033			
Lyn	1.4215	0.0027			
Capza2	1.3259	0.0036			
Litaf	1.2518	0.0447			
Actr3	1.1431	0.0196			
Ebf1	0.8959	0.0075			

Continuation of supplementary table B.2 see next page.

Immature B cells					
Downregulated in *Mif*⁻/⁻			**Upregulated in *Mif*⁻/⁻**		
Gene	**Fold change (logFC)**	**Adjusted *P* value**	**Gene**	**Fold change (logFC)**	**Adjusted *P* value**
Mif	4.0249	<0.0001	mt-Cytb	-0.6039	0.0092
Acot9	2.6456	0.0074			
Tcta	2.5306	0.0083			
Wdr18	2.5050	0.0059			
Fbxl17	2.3624	0.0445			
Stard7	2.3333	0.0008			
Anapc4	2.2884	0.0158			
Vbp1	1.4582	0.0452			
Transitional B cells					
Downregulated in *Mif*-KO			**Upregulated in *Mif*-KO**		
Gene	**Fold change (logFC)**	**Adjusted *P* value**	**Gene**	**Fold change (logFC)**	**Adjusted *P* value**
Mif	3.6453	<0.0001	*mt-Cytb*	-0.4783	<0.0001
Car2	2.4064	0.0219	*Malat1*	-0.3760	0.0227
Ercc8	2.2771	0.0196			
Ankhd1	1.2634	0.0237			
Satb1	1.0792	0.0432			
Gm23935	0.6644	0.0099			
Marginal zone precursor B cells					
Downregulated in *Mif*⁻/⁻			**Upregulated in *Mif*⁻/⁻**		
Gene	**Fold change (logFC)**	**Adjusted *P* value**	**Gene**	**Fold change (logFC)**	**Adjusted *P* value**
Mif	4.1696	<0.0001	*Gdf11*	-1.1830	<0.0001
Zfp689	1.2699	0.0156	*Gm43305*	-0.7452	0.0378
Rasgef1b	1.0107	<0.0001	*mt-Cytb*	-0.6162	<0.0001
Txnip	0.9799	<0.0001	*mt-Co1*	-0.5141	<0.0001
Stt3a	0.9451	0.0005	*Gm13340*	-0.4953	<0.0001
Tmem123	0.9324	<0.0001	*Arhgdib*	-0.3281	0.0449
Gm23935	0.9048	<0.0001			
Capza1	0.7980	0.0002			
Csde1	0.6871	0.0023			
Stk17b	0.6798	0.0006			
Rassf5	0.6624	0.0090			
Cd164	0.6089	0.0088			
Adgre5	0.5317	0.0309			

Continuation of supplementary table B.2 see next page

Marginal zone B cells					
Downregulated in *Mif*⁻/⁻			Upregulated in *Mif*⁻/⁻		
Gene	Fold change (logFC)	Adjusted *P* value	Gene	Fold change (logFC)	Adjusted *P* value
Mif	3.7341	<0.0001	*Mid1*	-1.4181	0.0038
Tmem123	1.2986	<0.0001	*Capg*	-0.5690	0.0001
Rasgef1b	1.0339	0.0002	*Rpl3*	-0.4736	0.0001
Gm47283	0.9871	0.0002	*Pfn1*	-0.3612	<0.0001
Map3k1	0.9619	0.0001	*Rplp0*	-0.3352	0.0024
Stk17b	0.8843	0.0002	*Rpl4*	-0.3169	0.0003
Txnip	0.8319	<0.0001	*Limd2*	-0.3143	0.0105
Ivns1abp	0.7576	0.0200	*Ubb*	-0.2918	0.0039
Slc28a2	0.7115	0.0053	*Cd52*	-0.2603	0.0243
Gm23935	0.6672	0.0023	*Rps19*	-0.2392	0.0414
Mbnl1	0.6379	0.0004	*Rps18*	-0.2314	0.0089
Xist	0.6194	0.0024			
Lyn	0.6169	0.0001			
Ptprc	0.4366	0.0023			
Follicular 1 B cells					
Downregulated in *Mif*⁻/⁻			Upregulated in *Mif*⁻/⁻		
Gene	Fold change (logFC)	Adjusted *P* value	Gene	Fold change (logFC)	Adjusted *P* value
Mif	4.2535	<0.0001			
Tmem123	1.3625	0.0001			
Gm23935	1.1034	0.0023			
Stk17b	1.0444	0.0375			
Serinc3	0.7568	0.0127			
Follicular 2 B cells					
Downregulated in *Mif*⁻/⁻			Upregulated in *Mif*⁻/⁻		
Gene	Fold change (logFC)	Adjusted *P* value	Gene	Fold change (logFC)	Adjusted *P* value
Mif	3.8949	<0.0001	*Ms4a4c*	-0.7023	<0.0001
Zkscan1	1.6107	0.0471	*Atp6v0e*	-0.6028	0.0387
Capza1	1.1082	0.0070	*mt-Cytb*	-0.5645	0.0001
Stk17b	1.0812	<0.0001	*Rps3a1*	-0.2947	0.0033
Gm23935	1.0104	0.0001			
Lars2	0.9986	0.0008			
Map3k1	0.9851	0.0019			
Tmem123	0.9346	<0.0001			
Cd38	0.8438	0.0097			
Serinc3	0.7242	0.0002			
Msn	0.5760	<0.0001			
CT010467	0.4470	<0.0001			

Acknowledgements